NATURE-BASED SOLUTIONS FOR COASTAL PROTECTION:

A MULTI-SCALE INVESTIGATION OF WAVE-VEGETATION INTERACTIONS

Ross Henteleff

Submitted under the supervision of

Dr. Ioan Nistor

Dr. Jacob Stolle

A thesis submitted to the University of Ottawa in partial fulfillment of the requirements for the degree of

Master of Applied Science in Civil Engineering

———————

Department of Civil Engineering
Faculty of Engineering
University of Ottawa

University of Ottawa
Ottawa, Ontario, Canada

Abstract

Nature-based solutions (NBS) are increasingly popular infrastructure protection options, particularly in coastal engineering. These systems have shown the ability to provide similar coastal protection services to traditional hard schemes while providing other ecological and economic benefits, and a capacity to adapt to changing contexts. One prominent example of coastal NBS are saltmarshes: fields of flexible or semi-flexible vegetation, which have been found to significantly reduce damage to local communities under daily and storm conditions. Scientific study of these complex, multi-faceted structures is growing in volume, but there remain many knowledge gaps in the field.

Numerical modelling is a powerful tool for investigating both large- and small-scale behaviours of saltmarshes. Numerical models provide a controlled, repeatable, and easily variable method for testing how a marsh impacts local hydrodynamic climates and how incident flow or wave conditions affect the behaviour of their constitutive vegetation. Small-scale plant behaviour is the focus of this thesis. Literature on the subject has been chiefly limited to greatly simplified vegetation modelling, reducing plants' behaviour to that of straightforward rigid cylinders. While this can be effective, it requires significant calibration to measured data and may not provide an accurate picture of the intricate flow dynamics surrounding an individual plant, let alone a full marsh system. Recently, numerical models capable of modelling flexible structures have been developed and used by researchers. However, studies applying these tools have focussed on replicating the more significant hydrodynamic effects of marshes, such as mixing or wave attenuation. By doing so, the calibration requirements of the rigid-type models remain, and the way the plants themselves are modelled loses physical meaning beyond their hydrodynamic impacts.

The work presented in this thesis aims to expand on current flexible plant modelling research by evaluating a new numerical modelling tool in the open-source software REEF3D for replicating in situ saltmarsh plant behaviour in terms of drag force and motion response to hydrodynamic forcing. Three experimental programs were designed and conducted in order to thoroughly evaluate both aspects of the model. The first, based on a flume study performed by Paul et al. (2016), tested the drag force response to regular wave action. The second, based on the work of Tschisgale & Fröhlich (2020), further investigated the drag force response using closed- and open-channel flow, as well as solitary waves. The third, based on a flume study performed with live vegetation by Markov et al. (2023), evaluated the accuracy of the motion response to irregular waves. Consistent through all three programs was an overestimation of the examined behaviour and, in the third case, persistent model breakdown. These results demonstrate that, as tested, the evaluated tool is unsuitable for this purpose. It is suggested that this is due to the foundational assumptions of the model, namely that the material of the flexible structure is of a linearly viscoelastic type, whereas a nonlinear elastic material would be more appropriate for this application. These results highlight the difficulty of numerically modelling these systems and the need for further research developing and applying practical modelling tools for marshes.

Acknowledgements

I feel immense gratitude for all that the time spent preparing this document has brought me. The sum of the opportunities and knowledge I have gained from this experience is unquantifiable. I owe this depth of experience largely to the incredible generosity of those who have helped and supported me along the way.

My thanks go first and foremost to my supervisors, Drs. Ioan Nistor and Jacob Stolle. Their effort and guidance have made me a better engineer and researcher than I would have otherwise been. Dr. Nistor's enthusiasm and belief in me as an undergraduate student with minimal experience and middling grades propelled me to where I am today. Dr. Stolle's calm and considered direction in academic and professional matters has proved invaluable throughout my time in his care. Furthermore, the opportunities they have provided me to meet others in academia and industry, from participation in exciting projects and meetings to presenting at prestigious national and international conferences, cannot be understated. I conclude this chapter a better man than I started it and with great hope for what lies ahead. For this, I am eternally grateful.

Further acknowledgement is due to Dr. Venkatachalam Sriram, whom Dr. Nistor wisely brought in at a critical juncture of this project. His suggestions regarding modelling approach and results interpretation were essential to the direction and ultimate product presented here. His extra effort to assist a student on the other side of the globe is greatly appreciated.

I express my gratitude to my fellow students whom I have met during this project, providing me with their time, advice, insight, and companionship; to Acacia Markov, Dario Sirianni, Dana Pothier, Jessica Wilson, Joseph Kim, Alexandra Forsythe, and Phillipe April-LeQuéré, my humblest thanks.

Finally, to my friends and family, I cannot hope to express my appreciation fully. The constant support of my parents is foundational to any success I have found and will have. Thank you to my partner, Lauren, for your unfailing belief in me, for providing me with any extra motivation I needed, and for your understanding and kindness. I am deeply fortunate to have you by my side. Thank you to my Opa, whose thoughtful gifts and exchanges have guided me through the challenges the last years have presented. Thank you to all my friends, particularly Benjamin and Chris, for discussing anything besides my work with me. That I have reached this point is a credit to you all. Thank you.

Table of Contents

List of Figures

List of Tables

List of Acronyms

ADCP	Acoustic Doppler Current Profiler
ADV	Acoustic Doppler Velocimeter
CCF	Closed-Channel Flow
CFD	Computational Fluid Dynamics
CSA	Canadian Standards Association
FSI	Fluid-Structure Interaction
FVM	Finite Volume Method
IBM	Immersed Boundary Method
INRS	Institut National de la Recherche Scientifique (English: National Scientific Research Institute, Quebec City, Canada)
IUCN	International Union for Conservation of Nature
JONSWAP	Joint North Sea Wave Project
LES	Large Eddy Simulation
NBS	Nature-Based Solution
NTNU	Norges Teknisk-Naturvitenskapelige Universitet (English: Norwegian University of Science and Technology, Trondheim, Norway)
OCF	Open-Channel Flow
RANS	Reynolds-Averaged Navier-Stokes
SST	Shear Stress Transport
SW	Solitary Wave
USACE	United States Army Corps of Engineers
VOF	Volume of Fluid

List of Symbols

A	Cross-sectional area of the rod (m^2)
$\underline{\underline{C}}_{\varepsilon,0}$; $\underline{\underline{C}}_{\kappa,0}$	Constitutive matrices in the Lagrangian frame of the rod
$\underline{c} = (c_t, c_{s,Y}, c_{s,Z})$	Torsion and shear correction factors
c_μ	Turbulence model constant
D	Water depth (m)
E	Young's modulus (GPa)
$\underline{f}_{ext}$	External forces on the rod
$\underline{f}$	Internal forces of the rod
G	Shear modulus (GPa)
g_i	Acceleration due to gravity (m/s^2)
H	Wave height (m)
I	Second moment of area (m^4)
k	Turbulent kinetic energy
k_s	Equivalent sand roughness (m)
k_w	Turbulent kinetic energy at the wall
$\underline{m}_{ext}$	External moments on the rod
$\underline{m}$	Internal moments of the rod
p	Pressure
P_k	Turbulent production rate
$\underline{\ddot{r}}$	Translation acceleration vector
$\underline{\underline{R}}$	Rotation matrix of the cross-sections
t	Time (s)
$u_{i,j}$	Horizontal orbital velocity in X, Y (m/s)
x	Distance in flow/wave direction (m), spatial geometric scale
Δy_p	Distance from the wall (m)

y	Distance perpendicular to flow/wave direction (m)
z	Distance along water column (m)
α	Constant = 5/9
β_k	Constant = 9/100
β	Constant = 3/40
δ_{ij}	Kronecker delta symbol
$\underline{\boldsymbol{\varepsilon}}$	Strain vector
η	Water surface excursion (m)
κ	Constant = 0.4
$\underline{\boldsymbol{\kappa}}$	Curvature vector
ν	Kinematic viscosity (m^2/s)
ν_t	Eddy viscosity (m^2/s)
ρ	Water density (kg/m^3)
ρ_s	Rod material density (kg/m^3)
σ_k	Constant = 2
σ_ω	Constant = 2
τ_w	Wall shear stress
ω	Specific turbulent dissipation

1) Introduction

1.1 Background

Coastal regions play an enormous role in our global society. They are the host to a higher population density than any other area, owing to the plethora of services they can provide, from commercial to agricultural (Wu et al., 2011; Temmerman et al., 2013). These areas have seen massive growth in the past several decades, which is projected to continue. Global seaborne trade increased almost threefold from 1990 to 2021 (Placek, 2022). While approximately one-third of the population currently lives within 100 km of the coast, this is expected to increase to one-half by the end of the decade (Bilkovic et al, 2017).

People who live by the coast have transformed the landscape to take advantage of its functionality. This modification typically takes the form of hardening, primarily done for coastal protection purposes (e.g., Bilkovic et al., 2017) or land reclamation for agricultural use (e.g., Wollenberg et al., 2018). While such changes can be effective for their primary purposes, they have been found to limit public enjoyment of coastlines, destroy natural habitats essential to local ecosystems and contribute to the erosion of adjacent, non-armoured shorelines (Zelo & Shipman, 2000; Wollenberg et al., 2018; Smith et al., 2020).

Nature-based solutions (NBS) are an increasingly popular class of infrastructure, which may be able to provide much of the function of traditional coastal infrastructure, such as wave and flood attenuation (e.g., Maza et al., 2015; Vuik et al., 2016; Schoutens et al., 2020; van Veelen et al., 2021) and erosion protection (e.g., Vousdoukas et al., 2013; Reef et al., 2018; Paul et al., 2021), as well as added ecological benefits, with fewer environmental and economic drawbacks (Temmerman et al., 2013; Wollenberg et al., 2018; Smith et al., 2020). NBS, particularly living shorelines, have increased appeal in the context of climate change and sea level rise. They have the capacity to absorb atmospheric carbon, known as “blue carbon sequestration” (Davis et al., 2015; Taillardat et al., 2018; Wollenberg et al., 2018; Burden et al., 2019), perhaps mitigating greenhouse gas emissions. Unlike static structures, such as riprap and seawalls, living systems are dynamic and adaptable. They can self-repair, limiting lifetime maintenance costs (e.g., Shepard et al., 2011; Smith et al., 2020). Especially notable is their capacity to retain incoming sediment, allowing them, in the right conditions, to accrete, potentially rising with the sea (Temmerman et al., 2013; Best et al., 2018).

These systems have seen a dramatic increase in research interest (Zhang et al., 2018) and application (Bayraktarov et al., 2015). Scientific investigations into saltmarshes, a specific and essential form of living shoreline, are performed with field, physical, and numerical modelling studies. These provide insight into different aspects of their behaviour. Field studies quantify how marshes interact with waves and currents in their natural environment (e.g., Reef et al.,

2018). Physical modelling studies investigate vegetation's behaviour in a more controlled, repeatable setting than is available in the field (e.g., Anderson & Smith, 2014). Numerical studies offer many applications not possible with either of the former options, including long-term projection modelling (e.g., Vuik et al., 2019), "marsh-scale," and extremely fine-scale flow behaviour capabilities (e.g., Marjoribanks et al., 2017), "feature-scale."

This thesis presents two studies of the latter sort, investigating the application of a numerical model to the behaviour of individual saltmarsh plants or surrogates. Numerical tools that can simulate flexible structures with hydrodynamic forcing are relatively new, with published work only existing from 2017 (Marjoribanks et al., 2017), to the author's knowledge. The existing published literature on the subject also focuses on the structures' effects on local hydrodynamics, such as mixing (Marjoribanks et al., 2017) or wave attenuation (Mattis et al., 2019). The work presented below takes a different approach, replicating the plant behaviour itself in terms of drag force and motion response to hydrodynamic forcing, thereby filling a knowledge gap in the field. It is the belief of the author that more closely replicating saltmarsh vegetation's behaviour may lead to improved understanding of how they can be implemented in coastal protection schemes.

1.2. Objectives

This thesis aims to evaluate the applicability of a new tool for modelling flexible fluid-structure interaction (FSI) to the specific case of saltmarsh vegetation. The Tschisgale & Fröhlich (2020) model, implemented in the open-source computational fluid dynamics (CFD) software REEF3D, was used for this study. Flexible FSI modelling is a burgeoning field, and an effective model could ease conducting feature-scale numerical studies into coastal vegetation. At present, such studies require significant simplification of their behaviour, typically assuming rigidity (e.g., Arunakumar et al., 2019). A functional model could be used to assess breakage conditions for saltmarsh plants, a significant concern for many coastal practitioners (Vuik et al., 2018), and analysis of fine-scale hydrodynamic behaviour surrounding vegetation. It could also be used to quantify drag force response under wave or flow action, which could contribute to improved estimation of drag coefficients for marsh-scale modelling.

REEF3D's flexible FSI module quantifies the response of the flexible structure to incident hydrodynamic conditions in two ways: 3D force and motion. Three distinct experimental programs were developed and executed to test the accuracy of the numerical structure's behaviour. The first two sets of experiments evaluated the drag force response to various hydrodynamic contexts based on studies performed by Paul et al. (2016) and Tschisgale & Fröhlich (2020), respectively. The third program assessed the motion response of the structure using a study performed by Markov et al. (2023) as a physical modelling basis. The objectives of this work are as follows.

1) Develop a validation method for numerical plant models based on physical modelling,
    a) Determine quantifiable ways plants or surrogates respond to incident hydrodynamic conditions in physical and numerical modelling contexts.

b) Find physical modelling studies that have measured plant or surrogate response which are replicable numerically.

2) Apply the validation method to the new flexible FSI module in REEF3D.
   a) Accurately replicate physical modelling studies testing flexible structure response to various hydrodynamic conditions.
   b) Compare the drag force response of the numerical plant surrogate to the physical equivalent for each of the tested hydrodynamic conditions.

3) Assess the accuracy and calibration requirements of numerical plant models in terms of plant behaviour.
   a) Investigate how the model responded relative to the physically modelled cases overall and why this was the case.
   b) Discuss potential shortcomings of the state of the art, if the model requires calibration and potential improvements that could be made for future applications.

1.3. Scope

Three numerical studies are presented in this thesis. Together, they evaluate the accuracy of a new flexible FSI module based on Tschisgale & Fröhlich (2020) and implemented in REEF3D in terms of both drag force and motion response to various hydrodynamic conditions. The first of the two drag force response tests was based on the physical modelling work of Paul et al. (2016). The second test was based on the work of Tschisgale & Fröhlich (2020). The third program, assessing the motion response, was based on the physical modelling work of Markov et al. (2023). All numerical modelling was performed on the Digital Research Alliance of Canada's Cedar supercomputer, located at Simon Fraser University in Burnaby, Canada.

This work considers the numerical replications of both vegetation surrogates in the form of plastic strips and live vegetation, specifically *Spartina alterniflora*. A broad range of hydrodynamic conditions was replicated across the three programs. The Paul et al. (2016) tests focussed on regular waves of heights between H = 0.17-0.88 m and periods ranging from T = 2.06-4.10 s in water depths of D = 1 or 2 m. The Tschisgale & Fröhlich (2020) tests used closed- and open-channel flows (CCF, OCF) with velocities ranging from U = 0.036-0.32 m/s, as well as solitary waves (SW) of heights between H = 0.009-0.058 m, sized to be of equivalent depth-averaged peak velocity, in a water depth of D = 0.16 m. The Markov et al. (2023) tests focussed on irregular waves with heights between H_{m0} = 0.10-0.20 m and wave periods of T_p = 2 s, synthesized from the JONSWAP spectra and in a water depth of D = 1.05 m. These modelling campaigns constituted a thorough assessment of the numerical tool's accuracy for the case of saltmarsh vegetation.

The scope of this study was limited by two main factors, namely model requirements and a lack of appropriate existing physical modelling studies. These are detailed as follows:

- As tested, the Tschisgale & Fröhlich (2020)-based flexible FSI model in REEF3D requires the structure to be fully submerged. This makes testing partially submerged structures not feasible.
- As tested, the Tschisgale & Fröhlich (2020)-based flexible FSI model in REEF3D requires that the structure have a strip-like geometry with a rectangular cross-section.
- Very few physical modelling studies exist quantifying either the drag or motion behaviour of saltmarsh plants or surrogates. No studies exist measuring both simultaneously for this case. Therefore, these two aspects are tested separately in the subsequent studies.
- This study models the tested plants and plant surrogates as closely to in situ as possible, to maximize the physical meaning of the results.
- The point at which results converged for grid size is related to the structure thickness. In the interest of minimizing computational cost, physical modelling studies using thick structures rather than thin are preferred.
- These studies focus on the behaviour of the flexible structure, not sediment transport, and are thus modelled with a fixed bed.

1.4. Publications

The following is a list of publications affiliated with the work presented in this thesis, for which the author is the primary contributor.

Journal Publications Under Review

1) **Henteleff, R.**; Stolle, J.; Markov, A.; Sriram, V. and Nistor, I. (2023). *An Evaluation of an Open-Source Flexible Fluid-Structure Interaction Module for Saltmarsh Vegetation Under Wave Action.* Canadian Journal of Civil Engineering, *Canadian Science Publushing.* **(Under Review).**

Conference Presentations

1) **Henteleff, R.**; Markov, A.; Stolle, J.; Sriram, V. and Nistor, I. (2022). *Flexible Fluid-Structure Interaction of a Flexible Plant Model for Nature-Based Solutions.* Oral Presentation at the 37th International Conference on Coastal Engineering (ICCE) 2022, Sydney, Australia.
2) **Henteleff, R.**; Markov, A.; Stolle, J. and Nistor, I. (2022). *Numerical Modelling of Saltmarsh Plant Behaviour.* Oral Presentation at the Nature-Based Infrastructure for Coastal Resilience and Risk Reduction Symposium (2022), Halifax, Canada.

Other Refereed Contributions Under Review

1) **Henteleff, R.**; Markov, A.; Stolle, J.; Sriram, V. and Nistor, I. (2023). *Flexible Fluid-Structure Interaction of a Flexible Plant Model for Nature-Based Solutions.* Proceedings of the 37th International Conference on Coastal Engineering (ICCE) 2022, Sydney, Australia. **(Submitted)**.

1.5. Novelty

This study is the first of its kind to attempt to model the behaviour of in situ saltmarsh plants accurately using CFD software. While previous studies have used the numerical plant(s)' hydrodynamic effect to assess the model's accuracy, this study uses the structure's behaviour, namely the drag force and motion response to incident hydrodynamic conditions for this purpose. An effective tool for this task would simplify similar studies, requiring less calibration than previous methods, and could be used to investigate fine-scale marsh plant behaviours that are difficult to quantify physically. It is also the first time that REEF3D's new flexible FSI module was tested for non-mooring structures. Using open-source software like REEF3D allows for this work to be more easily built upon in the future and for changes to the software to be implemented when necessary.

1.6. Outline of the Thesis

This thesis presents two studies conducted to meet the objectives described in Section 1.2. The remaining sections of the thesis are organized as follows:

- **Section 2.0** presents a literature review to outline the state-of-the-art of scientific investigation of living shorelines at large. The review provides an overview of field, physical and numerical studies, emphasizing those focussing on coastal vegetation. Their implementation in Canada and internationally is also discussed, along with existing design guidance.
- **Section 3.0** presents two studies discussing three experimental programs executed using REEF3D. The first section (Section 3.1) presents an investigation of the drag force response of the model, based on flume experiments conducted by Paul et al. (2016). The second section (Section 3.2) presents further testing of the drag force response based on Tschisgale & Fröhlich (2020), as well as an assessment of the motion response based on Markov et al. (2023). Both studies are presented as preprints of manuscripts submitted to the proceedings of the 37th International Conference on Coastal Engineering (submitted) and a journal to be determined (under review). The contributions of the author (RH) to each article are as follows:
    - Section 3.1: RH conceived and designed the experimental program and performed it with support from JS, and completed the data analysis with support from JS and VS. RH wrote the manuscript with inputs from JS and IN. All authors contributed to manuscript revision and final 1.4. approval.

    - Section 3.2: RH conceived and designed the experimental program and performed it with support from JS and VS, and completed the data analysis with support from JS and VS. RH wrote the manuscript with inputs from JS and IN. All authors contributed to manuscript revision and final approval.
- **Section 4.0** discusses the findings of the two studies, including potential limitations of the work. This section also presents practical application of the results and suggests future physical modelling work, as well as additions to the model within REEF3D. Finally, the uses for a fully-functional model for this application are discussed.
- **Section 5.0** summarizes the thesis, providing key conclusions from the two studies. Future work to build upon that presented herein are identified, considering the limitations discussed in Section 4.0.

2) Literature Review

2.1. Introduction

Coastal engineering is a critical and complex field, dating back as early as 3500 B.C.E. when humans first started using the sea as a means of transport (USACE, 2002). Its complexity comes from its goal: to make the sea and coasts hospitable for humans. What makes this aim difficult is that neither the ocean nor the coasts are stable. The products of coastal engineering attempt to make them so.

Nature-based solutions form a new class of infrastructure in the field of coastal engineering. They attempt to address coastal concerns, such as erosion and flooding, by imitating natural systems. They can take many forms – dynamic revetments imitate cobble beaches; artificial reefs replace their coral predecessors. Living shorelines, another example of NBS, are the focus of this literature review.

The following work first discusses the background of living shorelines, describing some of the causes of the increasing interest in such projects, as well as their fundamental principles. The state of the art is then discussed, reviewing technical studies relating to this work, first in the field, second in the lab, and third using numerical models. Examples of projects that have been implemented in Canada and internationally are also given, and current design guidelines are described. Finally, the results of these studies are discussed, focussing on the benefits and drawbacks of living shorelines and areas which need further research.

2.2. Background

Nature-based solutions generally, and living shorelines specifically, represent a departure from traditional, ‘hard’ coastal engineering infrastructure, such as sea walls, jetties, and groynes. This approach is generally associated with heavy concrete or riprap construction, which have been noted to diminish the public’s enjoyment of the coast, as well as contribute negatively to the destruction of natural habitat where they are applied and to increased erosion where it is not (Zelo and Shipman, 2000). Considering the impacts of climate change and the loss of biodiversity, these results are less acceptable than they might have been in the past.

Shepard, Crain and Beck (2011) place the origin of the rising interest in living shorelines at the occurrence of two natural disasters: the tsunami that occurred in the Indian Ocean in 2004, and Hurricane Katrina, which decimated New Orleans, USA in 2005. In both cases, the removal of coastal vegetation, the former being mangroves, the latter being saltmarshes, was thought to contribute greatly to the level of destruction caused during these events. These researchers cite a 1963 report by the US Army Corps of Engineers as an early example of studies regarding the ability of coastal vegetation to assist in coastal protection. This work was, however, not widely considered in practice. They go on to say that the scientific community’s heightened awareness

of climate change, and desire to slow or mitigate its effects, may also be contributing to the uptick in interest in preserving and restoring coastal vegetation.

The basic idea behind living shorelines as a means of coastal protection is that they can, via the friction generated by the plants, dissipate incoming wave energy, and reduce the damage waves can cause. Several factors affect their ability to perform this task. The most obvious is the sort of vegetation causing the drag. There exists a huge variety of plants that exist on coastlines, some extremely effective at attenuating incoming waves, some ineffective. Mangroves, coastal forests that exist in tropical regions of Asia and the Caribbean, can be expected to behave differently under wave action than cordgrasses of North American and European saltmarshes. Drag is typically quantified using a rigid-body assumption (e.g., Xhang & Nepf, 2021) as:

$$F_d = \frac{1}{2}\rho C_D A U^2 \quad (1)$$

where F_d is the drag force, ρ is the fluid density, C_D is the drag coefficient, A is the front-facing area of the structure and U is the fluid velocity. C_D varies greatly based on species, with values in published studies ranging from 0.0031 – 0.26 for marsh vegetation alone (Pinsky et al., 2013). A second important consideration is the water level in the marsh, how much of the plants are submerged. If the water level is low, a higher percentage of the plants are out of the water and can therefore be run into by the incoming waves, causing drag force. Fully submerged plants can also impact waves above them but may not be as effective. A third factor is the sort of waves flowing over the vegetation. Larger, faster waves are more likely to push the flora around, which in turn may affect its attenuation capabilities. This element is especially tied to the previous two considerations.

2.3. State of the Art

With interest in living shorelines growing generally, so too has academic interest. Technical studies from around the world investigate coastal vegetation from a plethora of angles. These studies can be grouped into three broad categories: field – using data collected in real saltmarshes, physical – using experimental data generated using wave flumes, and numerical – using computer models to replicate these systems. With a greater understanding than ever before, researchers and industry are coming together and applying living shorelines to help solve real coastal issues, both in Canada and internationally. Design guidelines documents are also being produced, although none are yet universally accepted.

2.3.1. Technical

2.3.1.1. Field Studies

Work in the field is both the start and end point of the study of nature-based solutions generally and living shorelines specifically. It forms the basis of the study, as their effectiveness was first noticed as they existed in nature, and the proof of concept, as restored marshes are monitored long after they are constructed (e.g., Hartmann and Stock, 2019). Field work also informs

modelling of these systems, both numerically (e.g., Vuik et al., 2016) and physically (e.g., Lei and Nepf, 2019). As such, studies involving field work are often paired with a numerical or physical model. The most common numerical model is SWAN (e.g., Vuik et al., 2016; Willemsen et al., 2020, Chakrabarti et al., 2017). Jadhav et al. (2013) paired a field study with a rigid-type physical model. Other papers present a numerical model derived from the measurements taken in the field (e.g., Foster-Martinez et al., 2018). The specifics of these modelling methods will be discussed in the Numerical Modelling section.

Pure field studies (e.g., Foster-Martinez et al., 2018; Garzon, Miesse and Ferreira, 2019; Hartmann and Stock, 2019; Reef et al., 2018) take a variety of approaches to measuring wave attenuation by vegetation. One important aspect is the sort of waves that are measured. There are two main ways to go about this found in the literature. One is longer-term, deploying wave measurement equipment over a month or more, taking the waves that occur over the study area during the period. Examples of researchers that have used this methodology include Foster-Martinez et al. (2018), Schoutens et al. (2020), and Vuik et al. (2016). This method is most useful for evaluating how these coastal protection methods perform under daily conditions, informing estimates of their long-term life span and viability, as in Vuik et al. (2016). The other sort of wave conditions investigated in the literature are those which occur during storms. These studies are shorter-term, with wave measurement devices being deployed just before a significant storm and taken out immediately afterwards, often collecting finer-resolution data. Studies of this variety include Garzon, Miesse and Ferreira (2019) and Jadhav et al. (2013). This approach works well with engineering design, which tends to focus on 'design events,' for example, a 50-year gale.

Variety in these studies comes in numerous ways. The first and most common is the plant species being focussed upon. It can reasonably be expected that different species will behave distinctly under the same wave conditions, thus, researchers have worked to quantify the species' behaviour from around the world. *Spartina alterniflora*, a cordgrass common in North America, was investigated by Jadhav et al. (2013), Reef et al. (2018) and Garzon, Miesse and Ferreira (2019). *Spartina anglica* and *Scripus maritima*, both found in Northern Europe, were studied by Vuik et al. (2016), Willemsen et al. (2020) and Hartmann & Stock (2019) and Schoutens et al. (2020). Other papers are unique in their choice of plant or plants, such as Foster-Martinez et al. (2018) looking into *Spartina foliosa* and *Salicornia pacifica*, Reef et al. (2018)'s investigation into *Puccinelia maritima* alongside the previously-mentioned *S. alterniflora* and Schoutens et al.'s 2020 study of *Schoenoplectus tabernaemontani* and *Bolboshoenus maritimus*.

Another way these studies vary is through experimental methodology, either in terms of pairing with modelling or field procedure. Studies are often conducted using one or more transects of instrumentation across one or multiple marshes (e.g. Vuik et al., 2016, Foster-Martinez et al., 2018). However, Reef et al. (2018) use a unique "field flume" technique constructed on the marsh site. The researchers built a flume facing in the main tidal direction with funnelled

openings at either end, which allowed them to collect hydrodynamic and sedimentation data with more precision than if the model was executed offsite.

Multiple studies exist which investigate the growth and development of saltmarshes. These, although not strictly within the scope of this literature review, are worth noting and contain valuable information to both the researcher and the engineer looking to implement a saltmarsh as a means of coastal protection. For example, Schoutens et al. (2020) point out that saltmarsh species tend to exist in "zones", which they suggest could make saltmarshes more effective as a means of coastal protection. This could also inform how one plants a new or restored saltmarsh. Hartmann and Stock (2019) describe the differences between constructed marshes and new, naturally formed ones. They noted that the species present in these distinct classes of marsh are somewhat different, the mean elevation is higher in the constructed marshes, and their drainage systems are less fine and longer than the new, natural marshes. Feagin et al. (2011) present the biophysical properties of common saltmarsh species. Pinsky, Guannel and Arkema (2013) undertook a broad-scale re-analysis of field data from wave attenuation studies, attempting to clarify why the results for various species and conditions are disparate. They found that most of the variation in results could be attributed to the differences in vegetation rather than the wave conditions. They also noted that, in general, wave attenuation is lower under higher Reynold's-Number flows. Failure to account for this can result in vast underestimations of wave attenuation. Finally, the researchers suggest that large areas of vegetation are required for significant wave attenuation.

2.3.1.2. Physical Modelling

Although field studies provide the most true-to-life data, they lack the control often required in a scientific context and are subject to the innate uncertainties of the natural world. Physical modelling allows for manipulation not possible in field studies. Conducted in laboratory environments, the controllable and repeatable conditions are ideal for looking into the specifics of a design, plant species, or wave condition. These work especially well in conjunction with other sorts of studies, such as field (e.g. Chakrabarti et al., 2017), or numerical (e.g. Augustin et al., 2009). To conduct an experiment in the lab, several choices must be made. Most important is what one is subjecting to waves, namely live or model vegetation. If one chooses live vegetation, difficulties with acquiring it, keeping it alive during testing, and how the testing is changing the vegetation must be considered (Lara et al., 2016). If model vegetation is chosen, the type and scale of the surrogates must be selected. One can use rigid, flexible, or combination models. Scale is often a question of available facilities, namely flume size. Whether model or live vegetation is selected, the species being investigated must be determined and either be harvested or imitated. Tested hydrodynamic conditions must also be selected. This choice is also facility-dependent, as wave generators and flumes are limited in their capabilities.

Laboratory studies using live vegetation (e.g., Rupptrecht et al., 2017; Ozeren, Wren and Wu, 2014; Lara et al., 2016; Maza et al., 2015) provide the most accurate representation of how vegetation would react to a given hydrodynamic condition in nature. However, using live

vegetation comes with difficulties that must be considered. Lara et al. (2016) describe these issues in detail, using their own experiment as an example of how one might carry out a similar set of tests. In their case, they grew one species, *P. maritima*, and collected another, *S. anglica*. They had intended on growing both. However, the results of the *S. anglica* crop were sparse, necessitating harvesting plants from the field. Ozeren, Wren and Wu (2014) collected *S. alterniflora* and *J. roemerianus* from an outdoor nursery, after measuring biophysical properties of examples in the field. Lara et al. (2016) also advise comparing grown or purchased examples to those existing in their natural habitat. This illustrates that one must be aware that a plant grown in a different context than the situation being modelled may not have the same properties. As noted by Pinsky, Guannel and Arkema (2013), plant properties are fundamental to the resulting wave attenuation, so care with accuracy in this regard is essential to good experimental results. This issue can also arise with field-collected plants. Rupptrecht et al. (2017) excavated a section of marsh containing *P. maritima* and *Elymus athericus* to conduct tests on in a wave flume and found that the flexural rigidity of both species was significantly lower in the flume than in the field, owing to the storage conditions and that the height of the *P. maritima* was significantly higher in the flume than in the field.

Model vegetation provides a more accessible, if less true-to-life, alternative to live vegetation. There are two broad categories for model types, rigid or flexible. Rigid models (e.g., Hoque, Husrin and Oumeraci, 2018; Wu and Cox, 2016; Augustin et al., 2009; Chakrabarti et al., 2017) tend to be made from wooden dowels or similar stiff cylindrical objects. The arrangement of these objects varies depending on the sort of vegetation being investigated and the specific phenomenon one is investigating. Hoque, Husrin and Oumeraci (2018) studied mangrove forests' effect on wave attenuation, arranging the cylinders in an array of varying heights, imitating the complex, above-ground root system these plants have. Yang, Irish and Weiss (2017) used a similar method to investigate patchy vegetation's effect on tsunami dynamics. Wu and Cox (2016) were interested in more typical marsh grass vegetation but wanted to know more about how the vertical variation in density exhibited by these plants affected their wave attenuation capacity. They arranged the cylinders equidistant from each other, with two densities, and varied their heights. Chakrabarti et al. (2017), Ozeren, Wren and Wu (2014) and Augustin et al. (2009) both did studies similar to that of Wu and Cox but did not vary the height of the cylinders, or in Charkrabarti et al.'s case, the density.

Flexible models are another common choice in modelling vegetation's wave attenuation capabilities (e.g., Lei and Nepf, 2018; Anderson and Smith, 2014; Paul, Bouma and Amos, 2012; Ozeren, Wren and Wu, 2014). Unlike rigid models, they move with incoming waves, providing insight into this aspect of saltmarsh vegetation's behaviour. Generally, these take two forms. Under wave action, they can behave as a cantilever, 'swaying,' or as a whip. Although natural vegetation can act in both ways (Rupptrecht et al., 2017), it is difficult to model this in practice. Because of this, researchers tend to choose a cantilever-type flexible model for marsh grass (e.g., Ozeren, Wren and Wu, 2014; Anderson and Smith, 2014) and a whip-type model for seagrass

(e.g., Paul, Bouma and Amos, 2012; Lei and Nepf, 2019). Johnson et al. (2014) present a per-species guide on what materials to use and why. A unique cantilever-type model was used to investigate how the stem, root and canopy of *Rhizophora* affect wave attenuation individually. The model was modular, with three parts representing each of the three components mentioned. These pieces could be added or subtracted depending on what was being tested.

When using models of many species of plants, scaling down becomes necessary. Most wave flumes and basins are not big enough to accommodate, for example, a full-size mangrove forest. However, the scaling of vegetation is not always as simple as geometric scaling. In the case of non-rigid plants, biophysical properties, like flexural stiffness, also need to be considered (Johnson et al., 2014). Often this is done using Froude similitude (e.g., Wu and Cox, 2016; Hoque, Husrin and Oumeraci, 2018). However, many studies attempt to forego scaling altogether, as the assumptions required to apply Froude and Reynolds scaling together in realistic wave conditions are not accurate (e.g., Ozeren, Wren and Wu, 2014; He, Chen and Jiang, 2019; Yang, Irish and Weiss, 2017). Such studies either try to match prototype conditions as best they can (e.g., Ozeren, Wren and Wu, 2014), or use a range of plant models are assumed to be a proxy for bulk vegetative conditions (e.g., He, Chen and Jiang, 2019; Yang, Irish and Weiss, 2017). If scaling is to be used, the methodology for Froude and Reynolds is provided in Johnson et al. (2014).

The other aspect of testing vegetation's wave attenuation capabilities is the hydrodynamic conditions. These can be irregular waves (e.g. Augustin, Irish and Lynett, 2009; Anderson and Smith, 2014; Ozeren, Wren and Wu, 2014), regular waves (e.g. Ozeren, Wren and Wu, 2014; He, Chen and Jiang, 2019), or a combination of waves and current (e.g. Paul, Bouma and Amos, 2012; Maza et al., 2015). This choice tends to be defined as much by available facilities as it is by research interest. Using waves and currents simultaneously simulates nature most accurately, as waves going through saltmarshes are almost always paired with a tidal current.

2.3.1.3. Numerical Modelling

The final way that wave attenuation by vegetation is investigated is by way of a numerical model. Numerical models repeatedly solve their foundational equations to replicate real-life conditions throughout the numerical domain. These tend to be software, and different software packages use different equations and have different uses. Various software packages are detailed in Table 1.

Table 2.3-1. Software features.

Software	Basic Equations	Eulerian or Lagrangian	Dimension	Scale	Phase Averaged or Resolved	Fixed or Mobile Bed	Type of Vegetation	Vegetation Handling
OpenFOAM	Navier Stokes	Both	3D	Wave	Resolved	Fixed	None	N/A
REEF 3D	Navier Stokes	Eulerian	3D	Wave	Resolved	Mobile	Rigid or flexible bodies	Rigid or flexible bodies
Delft 3D	Shallow Water	Eulerian	3D	Estuary	Averaged	Mobile	Uniform	Bed roughness/flow resistance
XBeach	Shallow Water	Both	2D	Wave group	Both	Mobile	Vertically varying	Dissipation term/drag coefficient
SWAN	Shallow Water		2D	Estuary	Averaged	Fixed	Vertically/Horizontally varying	Rigid cylinders
TELEMAC-2D	Saint Venant	Lagrangian	2D	Estuary	Averaged	Mobile	Non-submerged	Friction
SWASH	Shallow Water	Eulerian	2D	Estuary	Resolved	Fixed (suspended load)	Vertically varying	Vertical cylinders – can do more but must be modelled

Many of the models detailed in Table 1 are used throughout the literature, which has been reviewed in preparation for this review. Often, numerical models are compared with results from the other two sorts of studies. Vuik et al. (2016) and Willemsen et al. (2020) paired SWAN with field studies. XBeach was used by Garzon et al. (2019) and Bedoni et al. (2019), the latter study presenting an improvement on the model for saltmarsh edge erosion. Delft3D was used by Best et al. (2018) to model a saltmarsh undergoing sea level rise. Suzuki et al. (2019) applied SWASH to dense vegetation fields, for which inertial and porous effects are also crucial to their wave attenuation capabilities.

Numerical models are advantageous in simulating conditions or answering questions not feasibly investigable with field or physical modelling studies. One example is long-term studies, particularly those projecting into the future. Willemsen et al. (2020) and Best et al. (2018) both modelled how saltmarshes would fair into the future under a broad range of conditions. The former studied storm conditions, from daily to 1-in-10,000 years, testing with and without vegetation. The difficulty of measuring these conditions in the field is apparent, especially when considering the addition and subtraction of vegetation. This makes numerical modelling the ideal tool for such a study. The latter of the two studies, Best et al. (2018), subjected saltmarshes to sea-level rise. This is inherently a long-term problem, which the researchers modelled over 120 years and is thus also difficult to quantify with any method other than a numerical model.

2.3.2. Use of Nature-Based Solutions

2.3.2.1. In Canada

Using nature-based solutions, particularly living shorelines, for coastal defence is a small, if burgeoning, practice in Canada. Perhaps unsurprisingly, interest is most common along the coasts, especially in Nova Scotia. TransCoastal Adaptations, a partnership mainly between Saint Mary's University and environmental consultant CB-WES, works to restore marshlands through "managed dyke realignment." Much of Nova Scotia's west coast, on the Bay of Fundy, is protected by dykes. However, with climate change, they are failing more regularly than before, and it is not feasible to continue building them higher. TransCoastal Adaptations changes the alignment of dykes, and encourages the growth of marsh in the foreshore, providing added protection from overtopping and wave attack. So far, they have restored over 98 hectares of marsh, with another 338 hectares on the horizon. Another Nova Scotian organization, the Ecology Action Centre, has built example sites of living shorelines around the province and provides guidelines for site selection and construction on its website. They aim to encourage coastal landowners to consider this a viable option for their property. A landscaping company from Bridgewater, Nova Scotia, Helping Nature Heal, has carved out a niche doing this work. In British Columbia, the Green Shores Initiative aims to encourage living shorelines using tax incentives. These are mainly aimed at local governments, on the town or municipality scale, and private landowners. On the academic front, no published studies from Canada on the subject could be found, although anecdotally, there are several, including the one this document is contributing to, in progress. Furthermore, several reports on the subject of NBS have been

released recently. The Canadian Standards Association (CSA) published a report by Vouk et al. (2021) providing an overview of NBS knowledge, application, guidance, challenges and areas of potential growth for coastal and riverine contexts. The Intact Centre on Climate Adaptation, out of the University of Waterloo, published a report by Eyquem (2021) on coastal protection and integrating NBS with traditional coastal infrastructure and practices within the industry.

2.3.2.2. Internationally

Europe, particularly the Netherlands and Germany, are leaders in the realm of nature-based coastal protection schemes generally and living shorelines specifically. This can be seen in the volume of research into the topic these nations produce. Much of the software used to model coastal systems, in general, is developed by the Delft Technical University or Deltares, both from Delft in the Netherlands. Software products from these two institutions include Delft3D, SWAN, SWASH and XBeach. This goes along with an extensive library of research, for example, Vuik et al. (2016), Best et al. (2018) and Willemsen et al. (2020). Several examples of studies coming from Germany are Rupptrecht et al. (2017), Hartmann and Stock (2019) and Schoutens et al. (2020). Other European nations have contributed to the body of literature, such as the UK (e.g., Reef et al., 2018; Burdens, Garbutt and Evans, 2019) and Spain (e.g., Maza et al., 2015; Lara et al., 2016). Like the localized Canadian interest in the field, we see nations with significant coastlines having the most interest in living shorelines.

The USA is the centre of the study of living shorelines in North America. The US Army Corps of Engineers have lent their scientists and facilities extensively to the study of the topic, producing such studies as Anderson and Smith (2014), Jahdav, Chen and Smith (2013), and Bryant et al. (2019). Other American work in the field includes Foster-Martinez et al. (2018) and Garzon et al. (2019). The National Oceanic and Atmospheric Administration also contributes to living shoreline work, constructing them for coastal protection at their own facilities in Beaufort, NC, and other sites around the US. These projects are detailed thoroughly, and resources for this sort of infrastructure are provided on the NOAA website. Nearby, in and around the Caribbean, mangrove forest restoration efforts are gaining momentum, for example, in Haiti and Costa Rica.

Living shorelines are gaining global interest. Research, construction, and restoration efforts march on worldwide, and the list of research strongholds is by no means exhaustive, nor is it set in stone. Coastal protection is a pressing issue for everyone, even the landlocked nations of the world, so it is no surprise to see the variety noted above.

2.4. Design Guidelines

Design guidelines are an essential step for the widespread adoption of nature-based solutions, such as living shorelines. Their novelty is such that practitioners of coastal protection may not feel comfortable implementing, for example, a saltmarsh instead of riprap for erosion control for fear it would fail or be inadequate. The goal of a design guideline is to eliminate this hesitancy by providing methodologies that can be followed and result in an effective solution.

The most in-depth document detailing the design of nature-based solutions is Bridges et al.'s *International Guidelines on Natural and Nature-Based Features for Flood Risk Management*. A product of the USACE, it results from collaboration between international researchers in all areas related to this field. It provides a thorough discussion not only of the design of NBS, including dunes, islands, reefs and submerged vegetation along with living shorelines, but also the foundational principles of these projects, how to engage relevant stakeholders, planning and implementation, performance, benefits and costs, how to manage these projects, how to enhance their various benefits and their application to fluvial systems. The International Union for Conservation of Nature (IUCN) published a global standard outlining criteria for the effective design and execution of NBS, as well as case studies illustrating each criterion (IUCN, 2020).

Many documents exist discussing the subject of living shorelines, or those similar, from which one can put together the best practices for the design and construction of this style of infrastructure. These come from a variety of sources and cover a range of topics. Most clearly applicable is the Marine Shore Design Guidelines by Johannessen et al. (2014), which covers several shoreline-protection options, including the use of vegetation and other nature-based solutions. However, the information on how to use vegetation effectively provided in this document is not especially detailed, recommending the use of native species, care regarding the use of soil from the site, and hiring of a knowledgeable contractor. Although important, this alone does not constitute a true design guideline. The slides of a course called The Design and Construction of Living Shorelines, offered by C. Scott Hardaway Jr. and Karen A. Duhring (2010) are also available online and provide a more thorough walkthrough of how best to go about the process of living shoreline construction. However, these are also limited, especially as much is likely lost without the spoken component of the course. This document is the most detailed design guide outside of official documents, pointing out various things to consider outside of the standard wave climate parameters, such as the presence of boat traffic. It also goes through several examples, providing drawings for the various configurations a constructed marsh can take.

More common are documents relating to living shoreline construction, usually containing information pertinent to such a project but not focussing on them as their main subject, if at all. These are wide-ranging and can be grouped into a few categories, namely living dyke, large woody debris, and general erosion control. The living dyke is a concept gaining traction in British Columbia (e.g., Readshaw, 2018) and in the Netherlands (e.g., van Loon-Steensma, 2015). These projects are essentially traditional dykes, but with added vegetation covering them and/or on their foreshores. This is supposed to attenuate incoming waves and limit the erosion of the dykes. Large woody debris is used as an erosion control measure in coastal and especially riparian contexts. Large pieces of wood are placed or anchored down in eroding areas in hopes that they will capture more sediment than otherwise would be the case (B. of Reclamation, 2016). These are often paired with revegetation efforts to assist with the capture and retention of material (e.g., Zelo and Shipman, 2000). General erosion control guidelines are the most

officially sanctioned, if least applicable, set of documents for the design of living shorelines. Vegetation is a common means of erosion control for many municipal and construction projects and has thus been developed into a science (e.g., Maine Dept. of Environmental Protection, 2016). Despite the differences between a saltmarsh and, say, a newly constructed ditch, many of the same concepts apply. Such documents are beneficial given the lack of guidance on constructing saltmarshes specifically, as they provide clear instructions on soil, seeding, and other topics which cannot be found in more applicable material.

2.5. Discussion

As is shown by the sheer volume of work done studying, designing, and building living shorelines and other nature-based solutions, they have merit as infrastructure for coastal protection. Like their more traditional counterparts, they have benefits and drawbacks. Despite the wealth of research done on these systems, there are still many unknowns. Examples of this are described in this chapter.

2.5.1. Benefits

2.5.1.1. Wave Attenuation

Vegetation has been seen as an effective way to attenuate incoming wave energy, whether the waves go through or over the plants. Therefore, living shorelines could be an effective method of coastal protection. However, the plants or models used to quantify the attenuation produce different results. Studies using live vegetation in a wave flume tend to use examples of the two broad types of plants that exist in saltmarshes: tall and rigid or short and flexible (e.g., Rupptrecht et al., 2017; Maza et al., 2015; Ozeren, Wren, and Wu, 2014). These groupings extend to the model vegetation as well. In live vegetation studies, it has been found that more rigid species attenuate waves more than their flexible counterparts, at least in high wave energy conditions (Rupptrecht et al., 2017) as stiffer plants resist flow more than their flexible counterparts.

Because of the inherent differences between flexible and rigid models, several studies compare the two directly (Augustin et al., 2009; Ozeren et al., 2014). It is important to note that these studies all use both model types for the same species, namely *S. alterniflora*. Flexible models are often applied to seagrass (e.g., Paul, et al., 2012; Lei and Nepf, 2019), but these results should not be compared with those for cordgrass mimics due to the differences in vegetation and models. The flexible surrogates were, in both cases, made from rubber foam tubing, which provides a good approximation of cordgrass behaviour. In these investigations, the comparative drag's behaviour is seen to be more complicated than for rigid vegetation. Both compare the calculated drag coefficient (C_D) to the Keulegan-Carpenter number (KC). Augustin et al. (2009)'s results showed that C_D decreased with KC for both rigid and flexible plant models. Ozeren et al. (2014) found similar relationships between C_D and KC for flexible and rigid models and two live plant species, namely *S. alterniflora* and *J. roemerianus*.

2.5.1.2. Resilience to Climate Change

One appealing aspect of living shorelines and other nature-based solutions for coastal protection is their ability to adapt to changing conditions. Because they are not static structures like traditional 'hard' infrastructure, they have a certain capacity to adapt to better fit their context. This ability was modelled by Best et al. (2018), with mixed results. They found that, although after 120 years a dynamic equilibrium would be reached, the marshes would be drowned in 50-60 years in the context of sea-level rise, leaving only vegetated dykes. Although this does not bode well for the adaptation of such systems, it is important to keep in mind how multifaceted these calculations are. Sea level rise is not uniform, nor are bioaccumulation or sediment supply, all critical factors in the drowning rate. In more favourable conditions, living shorelines could be more effective for a longer term. The effects of climate change are not limited to rising sea levels. According to the Centre for Climate and Energy Solutions (accessed Jan. 2021), extreme weather events are becoming more frequent due to global warming. Living shorelines can withstand such storms better than 'hard' engineering approaches in the context of climate change, given their adaptability and relatively low cost, especially when paired with other infrastructure, such as breakwaters (Vuik et al., 2019).

Further, the use of these systems may impact climate change generally. Using more ecologically-friendly coastal protection methods such as living shorelines are part of a larger trend towards infrastructure meant, in part, to slow the effects of climate change by the absorption of atmospheric carbon and dampening the impact of storms and SLR. Although it is unlikely that a single nature-based solution project will make a significant difference, it is possible that the trend at large will.

2.5.1.3. Other Benefits

Living shorelines provide benefits beyond attenuation of waves and changing their form to suit the conditions they are in. One ecologically important function they can perform is the retainment of what is known as atmospheric, "blue" carbon. Photosynthetic processes within marshes cause a behaviour known as carbon sequestration, whereby marshes absorb and store atmospheric carbon, a greenhouse gas (Davis et al., 2015). According to Davis et al. (2015), *S. alterniflora* marshes can, via carbon sequestration, absorb up to 238 grams of carbon per square metre, per year. The rate was found to decrease with marsh age. Burden et al. (2019) modelled this phenomenon for marshes in England and found that the rate reached a steady state after about 20 years, at roughly 60% that of the initial sequestration. Similar benefits are found in other sorts of shoreline vegetation, such as mangrove forests (Taillardat et al., 2018). The opposite effect also occurs. When a marsh is destroyed, the carbon it has sequestered is rereleased into the atmosphere, thus accelerating climate change (Ramsayer, 2022).

Another benefit of living shorelines, albeit a less quantifiable one, is how they improve the area for other beings. NOAA (2020) lists improved fisheries, and thus local economy, tourism, and cleaner water as reasons they provide value beyond wave attenuation. Although these do not always fall within the realm of coastal engineering, they are important, and should be considered

along with the more typical coastal engineering factors. Methodologies for integrating such concerns into coastal decisionmaking are discussed in Sauvé et al. (2022).

2.5.2. Drawbacks

2.5.2.1. Susceptibility to Damage

Unlike more traditional heavy structures, living shorelines are more likely to be damaged under more extreme wave conditions. This has been noted as an area of concern by Garzon, Miesse and Ferreira (2019) but has only been investigated by Rupptrecht et al. (2017). This study found that, over a week of wave flume tests, 45% of the vegetation biomass was lost. However, the researchers note that if the root mat is intact, any damage to the canopy can be considered as temporary as the plants can regrow. They also quote Leonardi et al. (2016), saying that most of the damage to saltmarshes is caused by smaller, more regular storms. This result comes from a desk study and may be worth investigating in other ways.

2.5.2.2. Lack of Familiarity

The biggest obstacle to the broad-scale adaptation of nature-based solutions generally, and living shorelines specifically, is a lack of familiarity with such projects in the coastal engineering industry. Throughout the history of the field, hard infrastructure has been the only way to solve the problems typical of it. This is most clearly illustrated by the lack of their inclusion in the USACE's Coastal Engineering Manual, not including beach nourishment, as coastal structures. It is the job of researchers and practitioners in the field to push for living shorelines to be implemented in the codes and conventions of work along the coastline, which in turn raises familiarity, continuing the trend towards more ecologically sound design.

2.5.3. Research Needs

Several details of wave attenuation by vegetation warrant being explored further in a research context. One is investigating different species' capabilities in this regard. There remain many plants that have not been studied in detail, which in some cases could have significant localized interest. Another area to be explored further is the application of different numerical models to this phenomenon. Many of the models listed in Table 1 have been used to model vegetation's wave attenuation, except OpenFOAM, to the author's knowledge. Scale effects for marsh vegetation have also been studied in a limited capacity. Some attempts exist (e.g., He, Chen and Jiang, 2019), but do not scale directly using any given method, instead applying a range of sizes and assuming that the bulk conditions were accurate. More research on this subject would allow researchers with smaller facilities to more accurately model marshes physically. A third aspect of these systems that is worth studying further is how saltmarshes sustain damage under wave action. This has been investigated via a desk study and a single wave flume experiment but is worth expanding upon. Further research into marshes' survival of extreme hydrodynamic conditions and their attenuation capabilities while damaged would help inform coastal decision-makers on their effectiveness as long-term options for coastal protection.

While existing studies have applied numerical modelling tools to saltmarshes' wave attenuation capacity, they have used either areas of increased friction at larger scales or rigid cylinders at smaller scales. While these methods have been shown to be effective, they require significant calibration effort to ensure that the drag coefficient or cylinder geometry will behave like marsh vegetation and neglect critical aspects of marsh performance. The former assumes that marshes are consistent throughout, despite marsh heterogeneity having significant impact on wave damping capacity (van Loon-Steensma et al., 2016). The latter ignores the demonstrated differences in drag between rigid vegetation surrogates and live vegetation (Ozeren et al., 2014). Furthermore, the behaviour of the individual plants is neglected entirely by these approaches. The interaction of waves and flow with a canopy of flexible bodies is complex and leads to intricate hydrodynamics within and around the marsh. The behaviour of saltmarsh vegetation under wave action contributes to all the above research needs. This has recently become replicable in numerical modelling software, specifically REEF3D, with a newly added flexible fluid-structure interaction (FSI) module. To the author's knowledge, no numerical studies exist that attempt to model the behaviour of the plants numerically. Doing so would provide a way to investigate the areas of the field needing development with advanced numerical tools. This is suggested as an avenue of research in this work.

3) Numerical Modelling of Saltmarsh Plant Behaviour

3.1. Flexible FSI of a Flexible Plant Model for NBS

Preprint of an article submitted to the proceedings of the International Conference on Coastal Engineering 2022.

3.1.1. Introduction

Nature-based solutions (NBS) comprise new methods and design ideas that utilize natural systems to protect shorelines. An example of NBS, living shorelines are typically constructed or restored saltmarshes or mangroves. These engineered ecosystems can attenuate incoming waves and floods (Garzon et al., 2019a), filter water, absorb atmospheric carbon, and have the potential to accrete sediment on pace with sea-level rise, thus providing successful coastal protection along with co-benefits in the form of climate change adaptation and ecological enhancements (Short et al., 2016). However, their applicability depends on a range of factors, including wave conditions, climate, nutrient availability, among others.

Numerical modelling studies of saltmarshes tend to represent the vegetation field in two distinct ways. The first is as areas of increased friction. Examples of this approach include Chakrabarti et al. (2017) and Garzon et al. (2019b). These studies use flume- or field-calibrated drag or friction coefficient values and apply them to the vegetated area. The added drag forces replicate the effect the marsh or mangrove would have on the local hydrodynamics. The second approach is representing marshes as arrays of rigid cylinders. Studies using this method include Arunakumar et al. (2019) and Vuik et al. (2018). This approach assumes that rigid, cantilevered beams can represent plants and approximate the influence of plants on waves. The dimensions of the cylinders come primarily from fieldwork measuring the plants in question (Vuik et al., 2018). These methods can be effective with appropriate calibration but do not capture the dynamic motion characteristics of the plants.

Other studies exist modelling vegetation as fields of flexible bodies. These are relatively uncommon, given the comparatively high computational cost of this approach. Two examples are known to the authors: the work of Marjoribanks et al. (2017) and that of Mattis et al. (2019). The former investigated canopy mixing under 1D flow. The latter modelled wave attenuation capacity of saltmarsh vegetation. Neither of these studies investigated the accuracy of the plant models themselves, instead focussing on their effect on the surrounding hydrodynamics.

Though saltmarshes are relatively common, little is known about the flow within them, especially under wave action. Factors such as sheltering, the process by which plants upstream divert flow away from those immediately downstream, make the modelling of full marshes

extremely difficult and computationally expensive. Therefore, most research investigating marsh plant drag and movement has been done using individual plants.

The movement of marsh vegetation under wave action is another aspect that makes these systems challenging to model effectively. Marsh plants may sway (symmetrical motion) or move in a whip-like manner (asymmetrical) as waves pass, changing how they affect the flow at any given moment (Rupprecht et al., 2017; Ghisalberti & Nepf, 2002). By accurately replicating plants' movement, also called reconfiguration, in response to waves, the understanding of this dynamic behaviour may be improved. Furthermore, if a numerical model can be demonstrated to accurately replicate the behaviour of a saltmarsh plant or plants under a variety of conditions, the calibration requirements for future numerical modelling efforts may be lessened.

3.1.2. Objectives

This study contributes to a larger, ongoing research project which aims to develop design guideline for NBS in Canada. By expanding the understanding of the behaviour of the vegetation that makes up marshes, it is hoped that these systems can be designed and implemented more effectively by coastal zone practitioners, increase the confidence of planners and legislative bodies in their application, and encourage their use whenever feasible.

This study is a numerical investigation into the drag and reconfiguration of marsh plants under wave attack. Research by Paul et al. (2016) provides the physical modelling data for this study. An open-source computational fluid dynamics (CFD) software, REEF3D, was used to numerically model a pair of flexible plastic strips in a wave flume as a flexible body under regular wave conditions at fixed water levels. These structures were modelled exactly as tested in the physical model, limiting the necessary calibration to the parameters of the CFD model itself. The model's output was compared with the physical modelling work presented by Paul et al. (2016). The flexible fluid-structure interaction (FSI) module in REEF3D used in this study is currently under development, adding a further level of novelty to the work presented herein. The main objectives of this study are:

- Facilitate the development of a flexible FSI module for REEF3D.
- Investigate the effectiveness of this tool for a single flexible structure under wave action using published data from physical modelling work.

This study is limited to modelling saltmarsh vegetation surrogates as tested in the physical modelling study in terms of geometric and material properties. As no reconfiguration measurements were taken in the Paul et al. (2016) study, the evaluation focusses on the module's force output. This work is also limited to the small amplitude regular wave conditions tested in the original flume study. The waves tested herein are below 1 m in height and have a maximum period of just over 4 s. Long or extreme wave conditions are not tested in this study.

3.1.3. Methodology

3.1.3.1. REEF3D

REEF3D (Bihs et al., 2021) is an open-source CFD software produced by the Norwegian University of Science and Technology (NTNU). REEF3D has been used previously to model similar systems to moving marsh plants, namely the movement of aquaculture nets (Martin & Bihs, 2021a; Martin et al., 2020). The accessibility of open-source software was also appealing for this study, allowing the work to be built upon more easily. Finally, a time-averaged CFD software, as opposed to large-eddy simulation (LES), was determined to be ideal. Given the scale of vegetation or vegetation surrogates, it is expected that average conditions will be the primary driver of plant behaviour, as opposed to turbulent structures. As a primary step, the empirical turbulence models used in the CFD simulations in REEF3D were deemed sufficient for a first-order approximation of the plant motion.

REEF3D solves the Reynolds-averaged Navier-Stokes (RANS) equations using an Eulerian, or mesh-based approach to modelling the hydrodynamics. This scheme represents the modelled area as a fixed rectangular grid. The fluid movement through the grid elements is calculated per time increment, along with the associated forces. The level-set method is used to analyze the free surface of the fluid, allowing for moving surfaces to be modelled on the fixed Eulerian mesh. It works by setting the interface between the two fluids (air and water) to a zero contour of the level-set function, a signed distance function. This is then coupled with a convection function to resolve the flow field (Bihs et al., 2018). The RANS are further simplified by assuming the incompressibility of the fluids (Bihs et al., 2018).

The developers of REEF3D recommend using the k-ω turbulence model, specifically its shear-stress transport (SST) formulation (Martin et al., 2020; Miquel et al., 2018). This option is unique because it uses a k-ω model within the boundary layer but switches to a k-ε model in the free stream, making it applicable in a broad range of conditions. REEF3D accounts for solid boundaries using Schlichting's rough wall law (Bihs et al., 2018). This flexibility in the turbulence model has led to it producing the most robust and reliable results for a range of cases (Bihs et al., 2018).

3.1.3.2. Fluid-Structure Interaction Modelling

The flexible FSI module currently being implemented in REEF3D is based on the method developed by Tschisgale & Fröhlich (2020). A detailed description of how the model is used within REEF3D can be found in Martin & Bihs (2021b). Plants are simplified as long, thin strips governed by the Cosserat rod equations using a Lagrangian, or particle-based, framework (Tschisgale & Fröhlich, 2020). The specific formulation of the Cosserat rod equations used in this model is the 'geometrically exact' option, which accounts for the rigid body motion and typical deformations of cantilevered rods. The cross-section of the structure is assumed to remain rigid during the deformation of the rod (Tschisgale & Fröhlich, 2020). In this application, the Lagrangian framework is applied to the flexible structure by modelling it as a set number of particles, or markers, which are fixed together and move in relation to one another. The

difference between Lagrangian and Eulerian representations is illustrated in **Figure 3.1-1**. Continuous direct forcing is applied to model the interactions between these strips and the surrounding fluid.

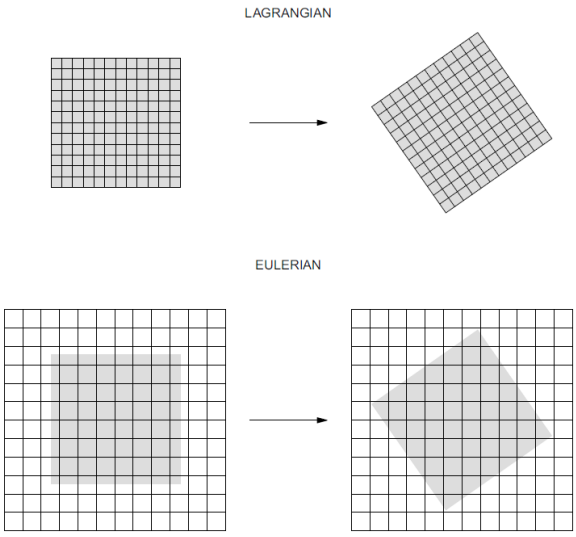

Figure 3.1-1. Lagrangian (top) and Eulerian (bottom) modelling frameworks.

This model assumes that the structures are completely submerged in fluid, with both the water and structure having constant material properties. The structures are assumed to be long and slender, making their longitudinal extension much larger than their cross-section. This allows the thickness to be approximated as zero within the fluid, making the structure coincide entirely with the fluid within the coupling model, while the Cosserat rod equations are still solved for the three-dimensional structure. Due to fluid loads, local deformations and internal strains are assumed to be small (Tschisgale & Fröhlich, 2020). External moments acting on the structure are assumed to be negligible due to the slender geometry of the strips (T. Martin, pers. comm., December 14, 2021). The model allows the structure's location in x, y and z to be varied, as well as its length (L), width (W), thickness (t), density (ρ), Young's modulus (E), its second moments of area in x, y and z (I_x, I_y, I_z), and its Poisson ratio (ν).

3.1.3.3. Physical Modelling

To validate the effectiveness of this model for plants under wave action, data from Paul et al. (2016) on plant reconfiguration and drag under wave action was used. In this study, four different iterations of surrogate and live marsh vegetation were subjected to waves in a flume, with the drag on the structures being measured continuously during testing. The hydrodynamic conditions used were regular waves with periods ranging from 2.07-4.10 s and amplitudes between 0.17-0.89 m. The still water level during testing was 1 or 2 m. Each test lasted long enough for 11 fully-developed waves to pass over the plant surrogates. The drag force of the structure and horizontal orbital velocity at 15 cm above the platform in line with the strips were

measured continuously during testing. The plastic strips were attached to a drag sensor via a metal bar, the effect of which was removed in post-processing. The experimental setup, with the numerical domain highlighted, can be seen in **Figure 3.1-2**.

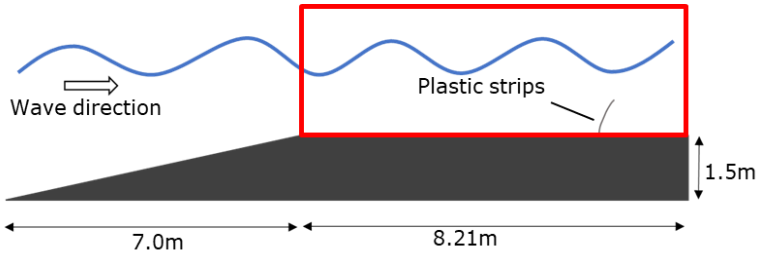

Figure 3.1-2. Physical modelling setup of Paul et al. (2016) with numerical domain highlighted in red.

The structure tested by Paul et al. (2016) used for validation in this study was a pair of model plant stems. The geometric and material properties of the stem can be found in Table 3.1-1. Both velocity and drag force are presented as average peak values per wave, referred to henceforth as "average."

Table 3.1-1. Geometric and material properties of the model step (Paul et al., 2016)

Property	**Value**
Length	L = 0.25 m
Width	W = 5.5 mm
Thickness	t = 4 mm
Density	$\rho = 1.24$ g/cm^3
Elastic Modulus	E = 3.44 GPa

The Paul et al. (2016) study was determined to be an ideal case study for the present numerical work for the following three reasons:

1. *Strip thickness*. Only one of the four tested strip configurations is modelled numerically, namely 2-strip x 4mm-thickness. REEF3D's flexible FSI module has been found to require grid sizes equal to the flexible body thickness. Grid size is the primary driver of required computational power for modelling, so the grid size is ideally maximized.

2. *Strip geometry*. REEF3D's flexible FSI module assumes the flexible bodies to be rectangular prisms when standing upright. This is the case in those tested in the Paul et al. study, thus minimizing inaccuracies and reducing potential error related to the structures' geometry.

3. *Tested hydrodynamic conditions*. The study used regular waves as part of its testing, which is ideal for numerical efforts due to its simplicity. Furthermore, only the first 11

fully developed waves were considered for the regular wave tests, limiting the experimental time that needs to be modelled. In both cases, this lowers the required computational effort for running simulations.

3.1.4. Results

3.1.4.1. Calibration

The model's sensitivity to grid size was investigated by running tests using identical wave and structure conditions with cell sizes of 0.5, 1, 2 and 3 times the thickness of the flexible body *t* (2, 4, 8 and 12mm, respectively). Beyond grid size, the results' sensitivity to the number of elements, or Lagrangian markers, for the plant structures must be analyzed. Drag force is influenced significantly by the number of elements into which the structure is divided; the movement of the structure comes from the inter-element boundaries acting as hinges. Element counts from 5-7 were tested. Results from this work are presented in Figures 3-3 and 3-4, showing the drag force over a single wave cycle for the above grid sizes and element counts, respectively.

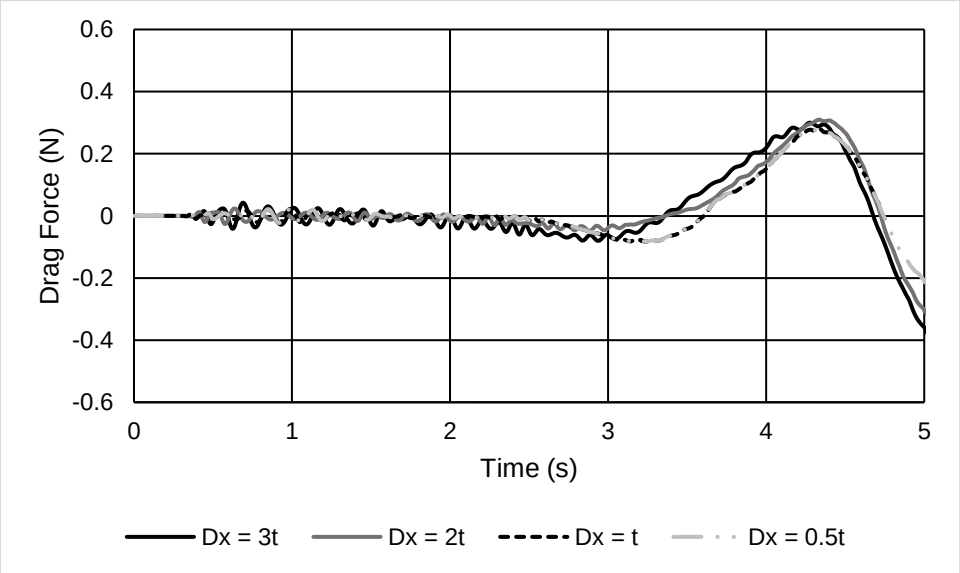

Figure 3.1-3. Drag force for various grid sizes.

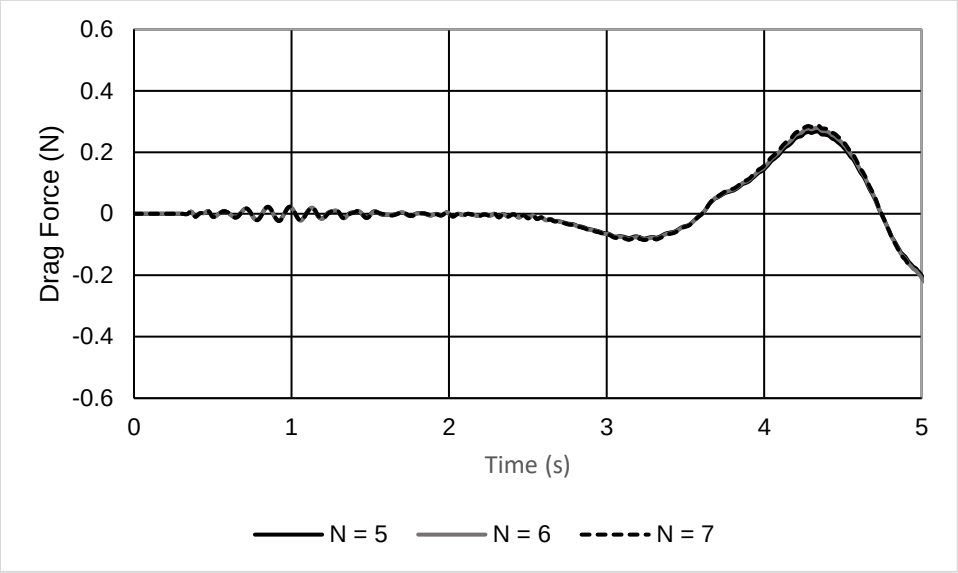

Figure 3.1-4. Drag force for various element counts.

The model's output converges for cell sizes smaller than 4mm, equal to the strip thickness, and element counts greater than 6. These values were therefore used for the simulations going forward.

3.1.4.2. Validation

The model was validated by numerically replicating the physical modelling results of Paul et al. (2016). The structure was modelled in REEF3D precisely as described in the flume study. Two plastic strips were placed 7.15 m from the start of the domain, 5 cm apart, with the physical and geometric properties described in Table 1. The average horizontal orbital velocity and drag force were compared to the physical modelling values. These are presented in Figures 3-5 and 3-6.

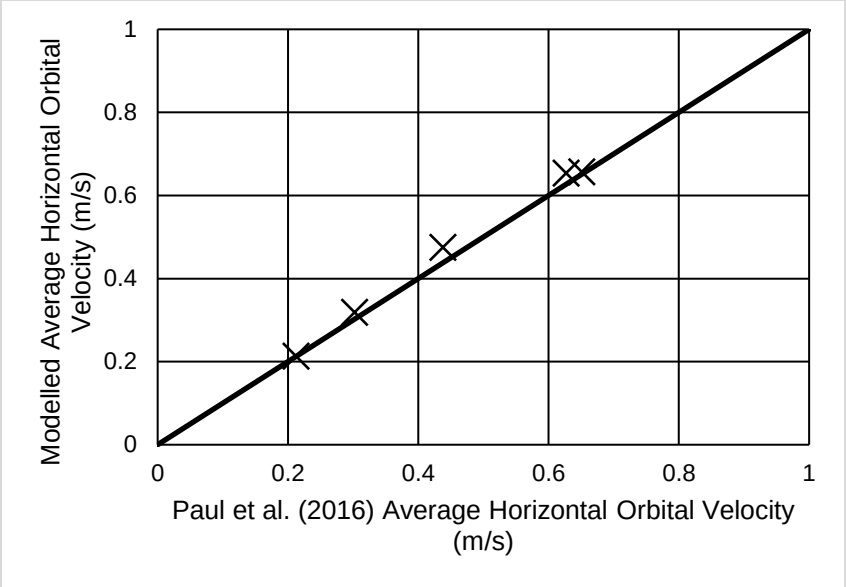

Figure 3.1-5. Modelled vs. measured average velocity.

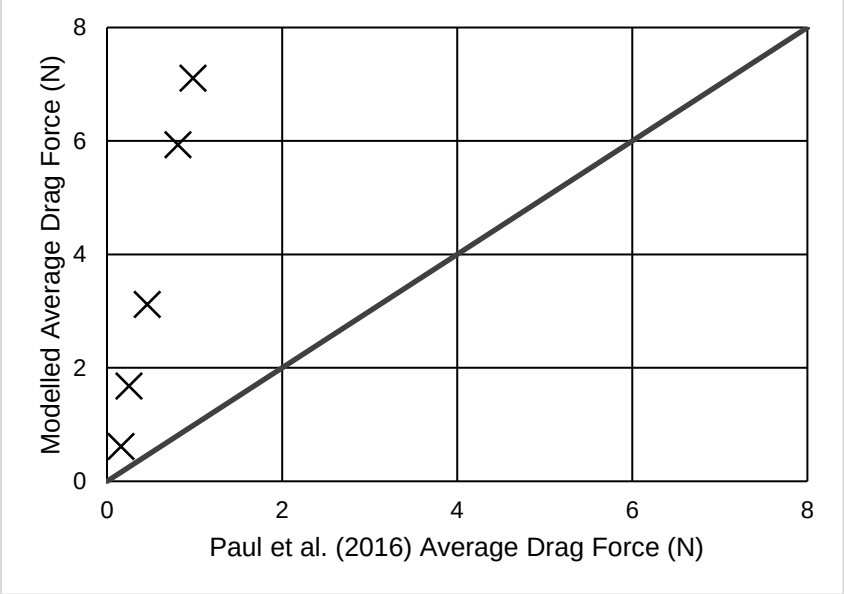

Figure 3.1-6. Modelled vs. measured average drag force.

The model is shown to replicate the hydrodynamic conditions well, but the drag force results are consistently overestimated. The meaning of these findings and how they may be used in future works are discussed below.

3.1.5. Discussion & Next Steps

The new flexible FSI module currently being implemented in REEF3D has been shown to consistently overestimate the drag force response of flexible bodies under wave action under in-situ conditions. It is also seen to overestimate the drag more as the wave height and period increase rather than the force being overestimated by a constant value. If the latter were the case,

a calibration value could be suggested, and the model may be effectively applied to the current case. However, this is not possible because the drag force response becomes increasingly overestimated with more extreme hydrodynamic conditions.

These results indicate that the module may not be able to model saltmarsh vegetation effectively. The overestimation behaviour shown above suggests that the failure is due to the module and its foundational assumptions rather than an issue with the modelling presented herein. The problematic assumption might be the model used for the structure's behaviour, i.e., the geometrically exact Cosserat rod model, or the material the structure is assumed to be made of, i.e., Kelvin-Voigt linear viscoelastic material. To determine the root cause of the issue, this needs to be investigated further. Furthermore, this study is limited to investigating the force response of the flexible FSI module. The motion response of the structure is also output, which should be investigated. Continued exploration of the software's drag force response and motion response constitute the next steps in evaluating REEF3D's new flexible FSI module's efficacy for the modelling of saltmarsh vegetation. The current results also suggest that the theoretical underpinnings of the tool should be examined in more detail.

3.1.6. Conclusions

This work tests the new flexible FSI module in the open-source CFD software REEF3D's applicability to saltmarsh vegetation under wave action in the greater context of NBS for coastal protection. Based on the physical modelling work of Paul et al. (2016), the module consistently overestimated the drag force response of plastic vegetation surrogates. While this suggests that this tool is unsuitable for this use, more work needs to be done before this can be stated with certainty. This will take the form of continued investigation into the drag force response of modelled flexible vegetation elements, exploration of the motion response, and further examination of the theoretical foundation of the FSI module.

3.1.7. Link to Section 3.2

The study presented above investigated the drag force response of the flexible FSI module newly implemented in REEF3D to a single set of wave conditions. This is built upon in the following section, wherein the drag force response to CCF, OCF and SW hydrodynamic conditions is investigated based on the work of Tschisgale & Fröhlich (2020). The motion response under irregular wave conditions is also tested using a series of experiments conducted using live vegetation at the INRS.

3.2. An Evaluation of an Open-Source Flexible FSI Module for Saltmarsh Vegetation Under Wave Action

Preprint of an article submitted to the Canadian Journal of Civil Engineering, Canadian Science Publishing.

3.2.1. Introduction

Nature-based solutions (NBS) are an increasingly important part of coastal protection schemes that attempt to emulate some of the behaviours of natural systems. NBS have been demonstrated to effectively replicate much of the function of more traditional, “grey” coastal infrastructure, such as seawalls or riprap (e.g., Bridges et al., 2021; Borsje et al., 2011), while aligning with the growing push for a more environmentally friendly built environment and, in some cases, enhancing local ecology. One common example of coastal NBS are saltmarshes. These fields of vegetation are appealing to coastal practitioners and legislators due to their ability to attenuate incoming waves and floods (e.g., van Veelen et al., 2021; Schoutens et al., 2020; Vuik et al., 2019) and limit erosion (e.g., Paul et al., 2021; Reef et al., 2018). Beyond these more engineering-focussed benefits, these systems can create additional value for their surroundings. Saltmarshes have been noted to provide ecosystem services such as water filtration and fishery improvement (e.g., Hartmann & Stock, 2019; Borsje et al., 2011) and absorb atmospheric carbon, known as “blue carbon sequestration” (e.g., Burden et al., 2019; Davis et al., 2015). They have also shown the ability to accrete by trapping the incoming sediments (Best et al., 2018), with the potential to keep pace with sea level rise and climate change.

Due to their composition, saltmarshes are difficult to accurately model numerically, and their behaviour and impact on the surrounding environment cannot be captured completely at a single spatial scale. Depending on the study's objectives, two main approaches can be used to model saltmarshes. Macro-scale modelling is commonly used to examine how a saltmarsh impacts the surrounding area in terms of flood and erosion risk (e.g., Vuik et al., 2018, Chakrabarti et al., 2017) on the scale of tens of meters to kilometres. Typically, the marsh is simplified as an area of increased bed roughness calibrated to local marsh conditions (i.e., plant species, plant density, hydrodynamic climate, etc.). This allows the model to use relatively large grid sizes and thus be computationally efficient while maintaining high accuracy. However, this method is calibration-intensive, requiring the drag coefficient to be computed using field data from the marsh being modelled (e.g., Vuik et al., 2018; Chakrabarti et al., 2017). The calculation of calibrated surface roughness usually involves the average plant height, diameter, and density and often considers a target species. The macro-scale approach omits micro-scale behaviours of marsh and flow interactions. The marsh is often simplified as uniform, despite natural marshes containing many species and a high degree of spatial variability.

Micro-scale modelling is the other approach for numerical simulations of saltmarsh vegetation and is the one used in the present study. This approach modulates the plant behaviour and turbulent scale between the plants for the given flow conditions. While this methodology is more computationally demanding, mainly to resolve the small scales, it can provide valuable insight into the micro-scale behaviour of saltmarshes, contributing to a greater understanding of their effects on the macro-scale. Micro-scale modelling of NBS has been performed in a variety of ways and for a diversity of reasons. Based on the requirement, the plant can be modelled as rigid structure or as a flexible structure. Mei et al. (2011) investigated the tsunami attenuation capability of coastal forests using a rigid cylinder or cylinders in a finite element method based model. Kim et al. (2015) studied the flow and bed morphodynamics within river vegetation under 1D flow using a large eddy-simulation (LES) model. Maza et al. (2015) modelled tsunami waves’ propagation through mangrove forests using IHFOAM. Marjoribanks et al. (2017) simulated canopy mixing within canopies of semi-rigid terrestrial and highly flexible aquatic vegetation under 1D flow using a coupled LES-biomechanical model. Chella et al. (2019)

simulated the force of breaking waves on vertical rigid cylinders using the Reynolds-Averaged Navier-Stoked (RANS)-based computational fluid dynamics software REEF3D. Arunakumar et al. (2019) modelled regular wave attenuation of saltmarshes using a rigid cylinder array, also with REEF3D. Le Minor et al. (2019) studied the hydraulics and sediment dynamics around a single rigid mangrove seedling using the finite volume method (FVM)-based software OpenFOAM. Anjum & Tanaka (2019) investigated the velocity distribution among coastal vegetation using arrays of rigid cylinders of uniform or varied height using the FVM-based software FLUENT. Hari Ram et al. (2023) modelled wave-vegetation interaction in shallow water using IITM-RANS3D. The above studies assume the vegetation as rigid cylinders. However, real vegetation has some degree of flexibility.

Modelling the behaviour of flexible structures was only recently possible due to their complexity and the associated computational cost. Mattis et al. (2019) studied the irregular wave attenuation capability of *Spartina alterniflora* using a canopy of flexible cylinders in an LES model. Amina & Tanaka (2022) studied the effect of coastal forests on the depth of flow by subjecting arrays of rigid cylinders to 1D flow in a volume of fluid (VOF) model with Reynolds-Averaged Navier-Stokes (RANS) turbulence modelling. Tschisgale & Fröhlich (2020) proposed a numerical model for slender flexible structures immersed in water. They used an immersed boundary method (IBM) coupled to a Cosserat rod model structure using continuous direct forcing. The authors also test their model on several cases, including a flexible structure in the wake of an immobile obstacle in laminar flow, a single flexible rod in uniform cross flow conditions and flow through an artificial canopy. They found success in all tested cases. This is the model implemented in REEF3D for its flexible FSI module. Based on a physical modelling study performed by Paul et al. (2016), Henteleff et al. (2023) found that this flexible FSI module overestimated the drag force response of flexible plant surrogates under wave action. This behaviour is further investigated herein using a simplified case based on results published in Tschisgale & Fröhlich (2020). The performance of the motion response of the flexible FSI module is also evaluated using a dataset generated by a physical modelling campaign conducted by Markov et al. (2023) at the Institut National de la Recherche Scientifique (INRS), Quebec City, Canada, in 2021, in which live *S. alterniflora* plants in a wave flume were subjected to irregular wave conditions.

This study aims to comprehensively evaluate Tschisgale & Fröhlich's (2020) model for flexible vegetation in the newly added flexible FSI module in REEF3D and its applicability within the context of saltmarsh plants and NBS. Rather than using the strip's hydrodynamic effects, such as wave attenuation as in Mattis et al. (2019), to evaluate the accuracy of the simulations, the strip's behaviour is used in terms of drag force and motion response and the behaviour is quantified. To the authors' knowledge, no physical modelling studies quantified both the force and motion response of saltmarsh vegetation simultaneously, thus these two aspects are assessed independently in the present numerical model study.

This work aims to test how effectively one can the model the plant physical behaviour numerically. Therefore, the plant surrogates are numerically modelled as closely as possible to those in-situ condition in terms of their geometric and material properties. This study focusses on low-velocity flows, ranging from 0.036 – 0.32 m/s. This is in keeping with the physical modelling studies on which the numerical work presented herein is based. It is assumed that the vegetation is submerged and can be modelled effectively using strip-like geometry. These are core assumptions of the model being used.

This paper is structured as follows: the fundamental equations and the turbulence model for fluid used in REEF3D are first are presented. The modelling of plant based on the theoretical formulation from Tschisgale & Fröhlich (2020) is then described, including its basic assumptions. In order to validate the model performances, two experimental programs are then discussed; the first testing the drag force response, based on a simple case presented in Tschisgale & Fröhlich (2020) and the second, testing motion response, based on the work of Markov et al. (2023). The latter paper is presented in Appendix A of this thesis. Convergence analyses for fluid grid size and number of elements on the flexible structure are then presented. The simulation results for each of the experimental test cases are provided. These are discussed, conclusions are drawn from the work with the future research directions.

3.2.2. Methodology

3.2.2.1. REEF3D

REEF3D is an open-source computational fluid dynamics (CFD) software developed at NTNU. It is governed by the continuity and momentum equations, as shown in Eqn. (2) and (3) (Bihs et al., 2018), respectively:

$$\frac{\partial u_i}{\partial x_i} + \frac{\partial u_j}{\partial x_j} + \frac{\partial u_k}{\partial x_k} = 0 \tag{2}$$

$$\frac{\partial u_i}{\partial t} + u_j \frac{\partial u_i}{\partial x_j} = -\frac{1}{\rho}\frac{\partial p}{\partial x_i} + \frac{\partial}{\partial x_j}\left[\nu\left(\frac{\partial u_i}{\partial x_j} + \frac{\partial u_j}{\partial x_i}\right) - \overline{u_i u_j}\right] + g_i \tag{3}$$

where u_i, u_j and u_k are the velocity averaged over time t in x, y and z respectively, x is the grid size, ρ is the water density, ν is the kinematic viscosity, p is the pressure, g is the gravity with $\overline{u_i u_j}$ representing the Reynolds stresses.

Due to the relatively low fluid velocities encountered in the areas of focus of REEF3D, namely hydraulic and marine engineering, the influence of velocity on fluid compressibility can be assumed to be negligible. Therefore, the governing equations can be simplified as the incompressible RANS and continuity equations. A RANS-based CFD model was chosen for this work because, given the scale of saltmarsh vegetation, the primary drivers of its behaviour are assumed to be larger time-averaged hydrodynamics, as opposed to, e.g., the smaller turbulent structures of large eddy simulation.

While several turbulence models are available in REEF3D, it has been found that, for transient and complex flows, such as those employed in the present study, the *k-ω* model provides the most accurate results (Martin et al., 2020; Miquel et al., 2018; Bihs et al., 2018). The governing equations of the *k-ω* turbulence model are presented in Eqn. 4-7. The Reynolds stress term is replaced in the RANS equations with the Boussinesq approximation:

$$-\overline{u_i u_j} = \nu_t\left(\frac{\partial u_j}{\partial x_i} + \frac{\partial u_i}{\partial x_j}\right) - \frac{2}{3}k\delta_{ij} \tag{4}$$

with

$$\nu_t = c_\mu \frac{k}{\omega} \tag{5}$$

where k is the turbulent kinetic energy and ω is the specific turbulent dissipation. These parameters determine the eddy viscosity, ν_t, and their solution is found using the following transport equations:

$$\frac{\partial k}{\partial t} + u_j \frac{\partial k}{\partial x_j} = \frac{\partial}{\partial x_j}\left[\left(\nu + \frac{\nu_t}{\sigma_k}\right)\frac{\partial k}{\partial x_j}\right] + P_k - \beta_k k\omega \tag{6}$$

$$\frac{\partial \omega}{\partial t} + u_j \frac{\partial \omega}{\partial x_j} = \frac{\partial}{\partial x_j}\left[\left(\nu + \frac{\nu_t}{\sigma_\omega}\right)\frac{\partial \omega}{\partial x_j}\right] + \frac{\omega}{k}\alpha P_k - \beta\omega^2 \tag{7}$$

where P_k is the turbulent production rate and the coefficients have values of α = 5/9, β_k = 9/100, β = 3/40, σ_k = 2 and σ_ω = 2.

In REEF3D, the rough and solid boundaries are accounted for by using Schlichting's rough wall law:

$$u^+ = \frac{1}{\kappa}\ln\left(\frac{30D}{k_s}\right) \tag{8}$$

where u^+ is the dimensionless wall velocity, κ is a constant of 0.4, D is the water depth and k_s is the equivalent sand roughness. It is assumed that the turbulent production near the wall is equal to the dissipation k. The wall function for a specific turbulent dissipation ω for a bed cell of distance Δy_p from the wall is:

$$\omega_{wall} = -\frac{c_\mu^{\frac{3}{4}} k_w^{\frac{1}{2}} U_w^+}{\Delta y_p} \tag{9}$$

The formula directly provides the value for ϵ. The turbulent kinetic energy k at the wall is treated by integrating the source terms of Eqn. 5 over the bed cell:

$$\int (P_k - \epsilon_{wall})\rho = \left[\frac{\tau_w u_w}{\Delta y_p} - \frac{\rho c_\mu^{\frac{3}{4}} k_w^{\frac{3}{2}} u_w^+}{\Delta y_p}\right] \tag{10}$$

The rough wall law is used to determine the wall shear stress τ_w and the dimensionless velocity u^+. The terms from Eqn. 10 are discretized as source terms in the transport equation for k.

3.2.1.1. Flexible FSI Module

The flexible Fluid-Structure Interaction (FSI) module implemented in REEF3D was described in detail by Martin & Bihs (2021). This model is based on Cosserat rod theory because it can replicate both rigid body motion and modes of deformation common to rods accurately, particularly for the slender structures as considered in the present study (Tschisgale & Fröhlich, 2020). The motion of the rod is described by $\underline{r}(X,t)$, with X being the Lagrangian coordinates along the structure. The conservation of angular momentum is expressed through the propagation of the rotation matrices of the cross sections $\underline{\underline{R}}(X,t)$ in time. The translational and rotational accelerations are given below:

$$\rho_s A \underline{\ddot{r}} = \frac{\partial \underline{\underline{f}}}{\partial X} + \underline{f}_{ext} \tag{11}$$

$$\rho_s \underline{\underline{I}} \underline{\dot{\omega}} + \underline{\omega} \times \rho_s \underline{\underline{I}} \underline{\omega} = \frac{\partial \underline{\underline{m}}}{\partial X} + \frac{\partial \underline{r}}{\partial X} \times \underline{f} + \underline{m}_{ext} \tag{12}$$

where ρ_s is the rod material density, A is the cross-sectional area of the rod and $\underline{f}_{ext}$ and $\underline{m}_{ext}$ are the external forces and moments. The internal forces and moments, $\underline{f}$ and $\underline{m}$, are defined under the linear viscoelastic material assumption as:

$$\underline{f} = \underline{R}\underline{f}_0 = \underline{\underline{R}}\underline{\underline{C}}_{\varepsilon,0} \cdot \left[\underline{\underline{R}}^T \underline{\varepsilon} - \left(\underline{\underline{R}}^T \underline{\varepsilon}\right)|_{t=0}\right] + \underline{\underline{R}}\underline{\underline{C}}_{\dot{\varepsilon},0} \cdot \left(\underline{\underline{\dot{R}}}^T \underline{\varepsilon} + \underline{\underline{R}}^T \underline{\dot{\varepsilon}}\right) \tag{13}$$

$$\underline{m} = \underline{R}\underline{m}_0 = \underline{\underline{R}}\underline{\underline{C}}_{\kappa,0} \cdot \left[\underline{\underline{R}}^T \underline{\kappa} - \left(\underline{\underline{R}}^T \underline{\kappa}\right)|_{t=0}\right] + \underline{\underline{R}}\underline{\underline{C}}_{\dot{\kappa},0} \cdot \left(\underline{\underline{\dot{R}}}^T \underline{\kappa} + \underline{\underline{R}}^T \underline{\dot{\kappa}}\right) \tag{14}$$

with the strain and curvature vectors

$$\underline{\varepsilon} = \frac{\partial \underline{r}}{\partial X}, \qquad \left[\underline{\kappa}\right]_x = \frac{\partial \underline{\underline{R}}}{\partial X} \tag{15}$$

and the constitutive matrices in the Lagrangian frame of the rod:

$$\underline{\underline{C}}_{\varepsilon,0} = \mathrm{diag}\left(EA, c_{s,Y}\, GA, c_{s,Z}\, GA\right), \;\; \underline{\underline{C}}_{\kappa,0} = \mathrm{diag}\left(\, c_t\, GI_X, EI_Y, EI_Z\right) \tag{16}$$

where E is the Youngs modulus, G is the shear modulus, $I = \mathrm{diag}(I_X, I_Y, I_Z)$ are the second moments of area and $\underline{c} = (c_t, c_{s,Y}, c_{s,Z})$ are the torsion and shear correction factors.

The above flexible FSI module currently being implemented in REEF3D quantifies the structure's behaviour in two ways: drag force and motion. To the authors' knowledge, no studies measured both simultaneously for saltmarsh vegetation in a physical modelling context; thus, these are investigated separately herein using the numerical model. Recently, Henteleff et al., (2023) has found that, under certain hydrodynamic conditions, the force response of the strip is overestimated, suggesting that this behaviour may be due to the fundamental assumptions of the model. This is further examined in hydrodynamic contexts based on Tschisgale & Fröhlich (2020) formulations. Further, the motion behaviour is investigated based on a series of physical modelling experiments performed at the INRS in 2021, as described in Markov et al. (2023).

3.2.1.2. Experimental Work

This work builds on a study published in the proceedings of the 37th International Conference on Coastal Engineering (ICCE), testing the drag force response of REEF3D's flexible FSI module to regular wave forcing (Henteleff et al., 2023). Based on a physical modelling study conducted by Paul et al. (2016), this study found that the drag was consistently overestimated despite accurate replication of the hydrodynamic conditions tested in the flume. The differences between the numerical model's output and the measured results from the physical modelling study grew with increased orbital velocity.

Drag Force Response: Tschisgale & Fröhlich (2020)

Building on the results presented in Henteleff et al. (2023), a simpler case using a variety of hydrodynamic conditions was deemed necessary to investigate how the flexible FSI module responds. These were based on a case presented in Tschisgale & Fröhlich (2020), on which the

module itself was based. While the original case in Tschisgale & Fröhlich (2020) tested only closed-channel flow (CCF), in the current study this is expanded to equivalent open-channel flow (OCF) and solitary wave (SW) conditions.

Experimental Setup of Tschisgale & Fröhlich (2020) for Drag Force Estimation

The CCF experiments were conducted in an exact replica of the domain presented in Tschisgale & Fröhlich (2020), with a streamwise length of 0.2 m (X), a width of 0.16 m (Y) and a height of 0.16 m (Z). For the OCF and SW experiments, the domain's length and height were doubled to 0.4 m and 0.32 m respectively, while the water depth was maintained at 0.16 m. The flexible strip was located 0.05 m from the start of the numerical domain in X, 0.05 m from the wall in Y and 0.08 m from the bed in Z. The strip was 0.05 m long, 0.01 m wide and 0.002 m thick, with a density of 670 kg/m^3, a Poisson ratio of 0.4 and a Young's modulus of 5e^{-4} GPa. A sketch of the numerical domain is presented in Figure 3.2-1.

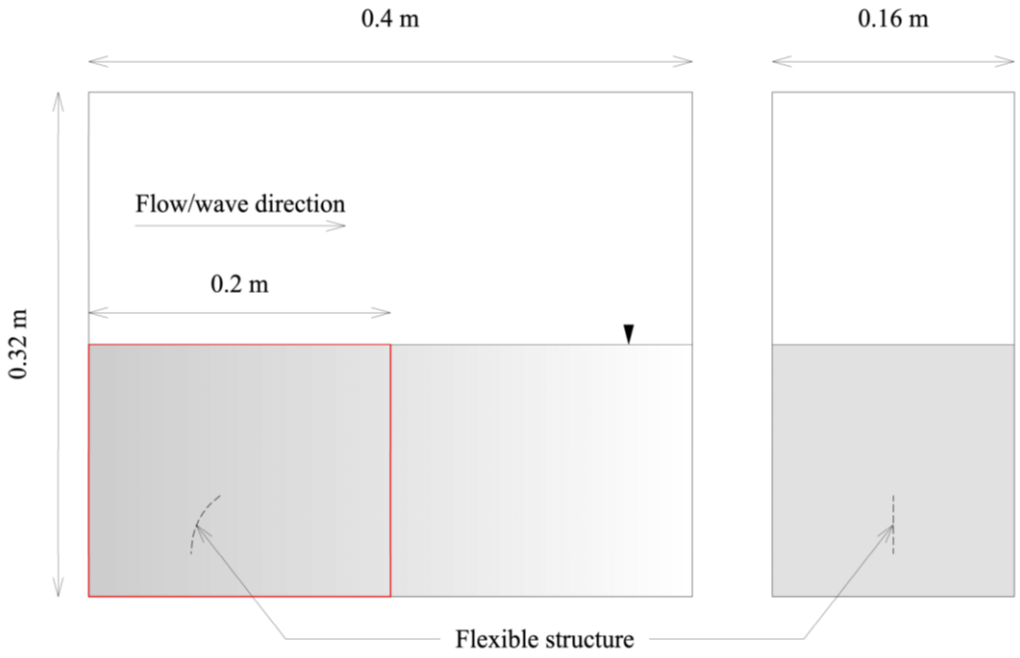

Figure 3.2-1. Sketch of Tschisgale and Fröhlich (2020) computation domain for CCF condition. The section in left and elevation in right.

A summary of the hydrodynamic conditions tested in the CCF, OCF and SW simulations is presented in Table 3.2-1.

Table 3.2-1. Tested hydrodynamic conditions for Tschisgale and Fröhlich (2020) simulations.

Case	CCF	OCF (D = 16 cm)	SW (D = 16 cm)
1	U = 0.036 m/s	U = 0.036 m/s	H = 0.009 m
2	U = 0.071 m/s	U = 0.071 m/s	H = 0.017 m
3	U = 0.11 m/s	U = 0.11 m/s	H = 0.026 m
4	U = 0.14 m/s	U = 0.14 m/s	H = 0.032 m
5	U = 0.16 m/s	U = 0.16 m/s	H = 0.036 m
6	U = 0.22 m/s	U = 0.22 m/s	H = 0.050 m
7	U = 0.27 m/s	U = 0.27 m/s	H = 0.058 m
8	U = 0.32 m/s	U = 0.32 m/s	H = 0.066 m

Experimental Setup of Markov et al. (2023) for Motion Response

The motion response of the flexible FSI module should also be investigated regarding its accuracy in representing the saltmarsh plant behaviour. To investigate this, a dataset generated by Markov et al. (2023) at the INRS was used as validation of the numerical model to quantify the movement of two common marsh plant species namely *Spartina alterniflora* and *Spartina patens*. The tests were carried out under irregular wave conditions. The plants were planted both individually and in hummocks and were subjected to various irregular wave conditions with significant wave heights between 0.1 m and 0.2 m and peak wave periods of 2.5 s or 10 s, synthesized from the JONSWAP spectra. The motion was measured using video cameras oriented to capture the wave-wise of motion of the vegetation. These videos were analyzed, and a bending angle timeseries over the course of each experimental run was produced. An example plot of the relationship between bending angle and wave conditions is presented in Figure 3.2-2.

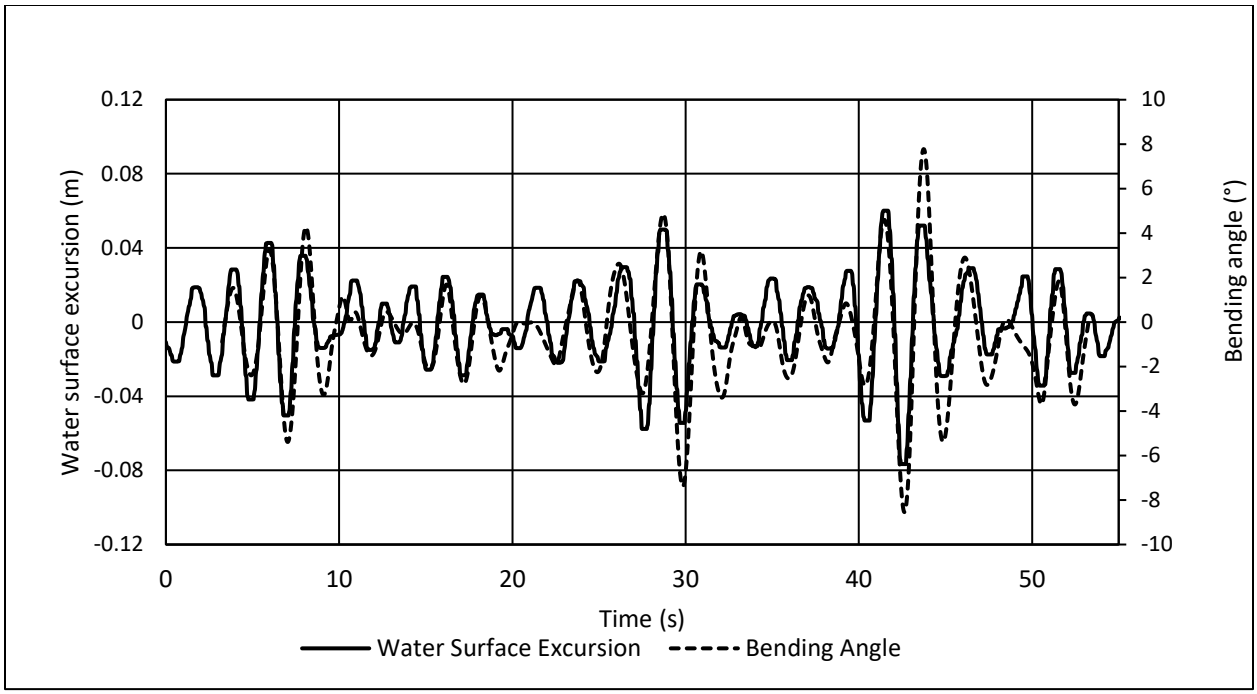

Figure 3.2-2. Bending angle of a Spartina alterniflora stem and water surface excursion over time (Markov et al., 2023).

In the experimental investigation (Markov et al., 2023) many plants of several species were measured simultaneously, however for numerical validation, a single *S. alterniflora* plant is investigated as it has a relatively simple, roughly cylindrical geometry, aligning better with the geometry imposed by the flexible FSI module being used. The domain was 4 m long in total. A fixed bed was used for the simulations with a slope of 1:18 similar to the physical model. The numerical plant surrogate considered was 0.62 m tall, 0.0045 m wide, 0.0045 m thick with a density of 900 kg/m3, a Young's modulus of 0.27 GPa and a Poisson ratio of 0.3. A sketch of the setup can be seen in Figure 3.2-3.

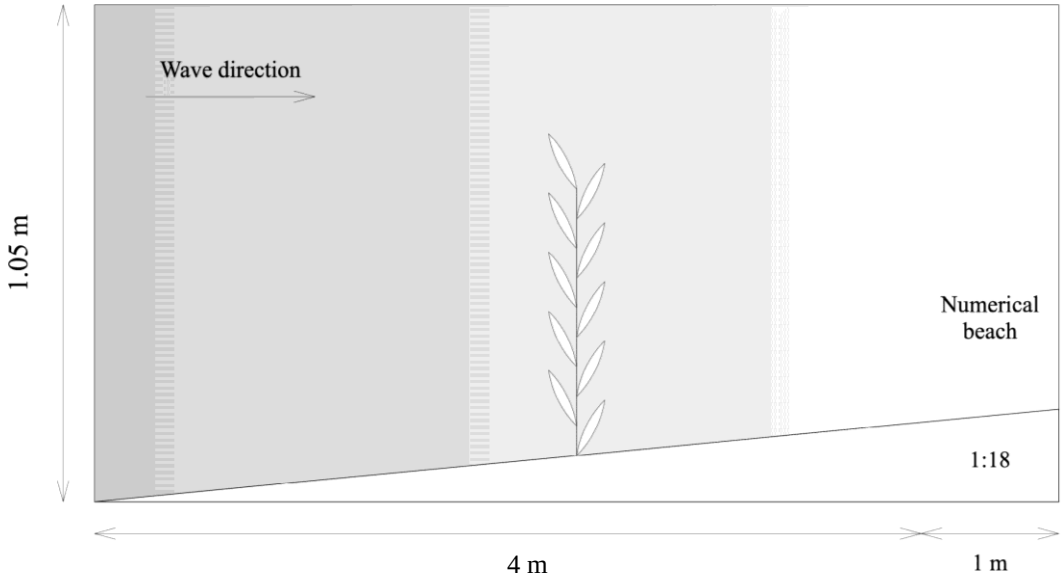

Figure 3.2-3. Numerical setup of the experimental work of Markov et al. (2023). Note: The figure is not to scale.

A variety of JONSWAP irregular wave conditions were tested in the flume study, but herein the focus is on small amplitude conditions. The significant wave height H_s = 0.1 m, and period T_p = 2.5 s were generated by a piston-type wavemaker located at one end of the flume in 2.55 m-deep water. In the numerical domain, the water depth was 1.05 m, accounting for the increased elevation of the plant on the slope, and used a measured water surface excursion timeseries at the beginning of the reduced domain as a wave generation input.

3.2.2. Results

3.2.2.1. Verification

One of the important aspects in the computational model is to investigate the convergence of the numerical model. In the present study, we have fluid domain and the elastic structure. The fluid model is discretized using finite difference method in REEF3D. Henteleff et al., (2023), using REEF3D's flexible FSI module, found that the results converge when the grid size is equal to the strip thickness. Furthermore, it requires cubic cells at the location of the strip motions (T. Martin, personal communication, March 24, 2022), limiting the possibility of flexible grid use. This leads to significant memory requirements for simulations at scales appropriate for saltmarsh vegetation, which have diameters on the order of millimetres.

Initially, the numerical results for Tschisgale & Fröhlich (2020) work has been reported for the grid convergence. Five different grid sizes corresponding to multiples of the strip thickness were investigated and the results are presented in Figure 3.2-4. The dx/t of 3 corresponds to 0.006 m and dx/t of 0.5 corresponds to 0.001 m.

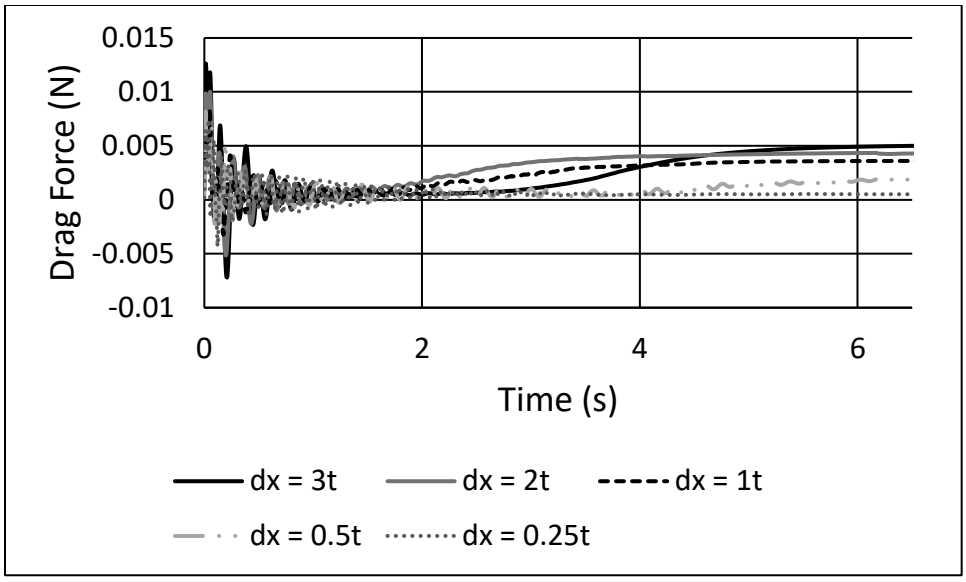

Figure 3.2-4. Convergence analysis for Tschisgale & Fröhlich (2020) grid size.

Clearly, the drag force results have not yet converged. Moreover, simulating grid resolutions below 0.001 m, i.e., 0.5 times the thickness of the strip is impossible due to computational demand. As the point of grid convergence was not found, the number of Lagrangian elements was not analyzed for convergence. Simulations were performed at dx = 0.5t, or 0.001m, and using six Lagrangian elements.

Now, the experiments from Markov et al., (2023) was analyzed for sensitivity to grid size and number of Lagrangian elements. The results are presented in Figure 3.2-5 and Figure 3.2-6, respectively.

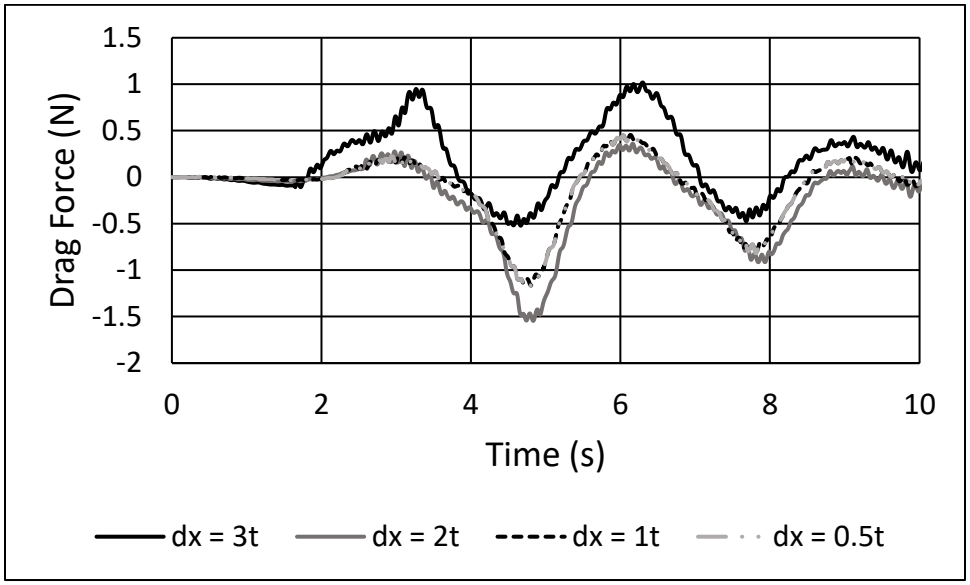

Figure 3.2-5. Convergence analysis for Markov et al. (2023) simulation grid size.

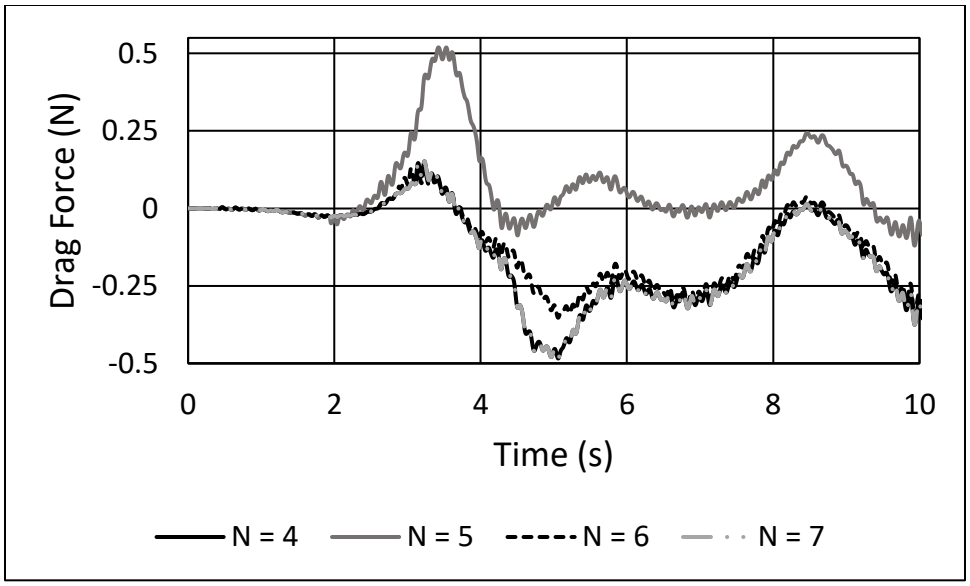

Figure 3.2-6. Convergence analysis for Markov et al. (2023) experiments with varying number of elements on the strip.

The results are seen to converge at a grid size of 4.5mm, equal to the thickness of the numerical plant surrogate, with the number of elements as 6. Thus, the verification of the numerical model has been carried out for the experimental test conditions.

3.2.1. Validation

While it was not possible to complete the convergence analysis for the Tschisgale & Fröhlich (2020) simulations, three hydrodynamic cases were investigated to obtain the response of the module for different conditions. These were performed with a grid resolution of dx = 0.001m, 0.5 x the strip thickness, and with the number of Lagrangian element on the strip as 6.

3.2.1.1. Drag Force Response Testing: Tschisgale & Fröhlich (2020)

Closed-Channel Flow

Initially, the Tschisgale & Fröhlich (2020) simulations were replicated exactly as in their paper, namely a plastic strip in a CCF system. Numerical modelling results are presented in Figure 3.2-7, compared to simulations performed by Tschisgale & Fröhlich (2020).

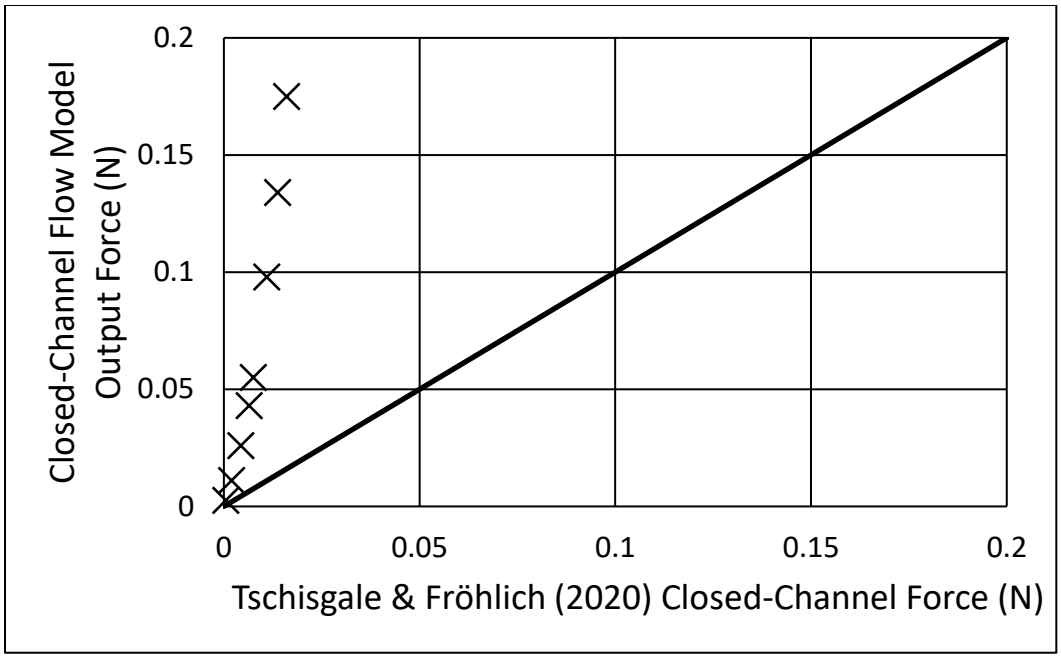

Figure 3.2-7. Comparison between present numerical model results and CCF results (Tschisgale & Fröhlich, 2020).

Similar to the results presented in Henteleff et al. (2023), the drag force response of the flexible FSI module is seen to be greatly overestimated when compared to the data from Tschisgale & Fröhlich (2020). To determine the source of this error, the module was also tested for different but equivalent flow conditions, namely OCF and SW of equivalent depth-averaged velocities. The results of these tests are presented in the following sections.

Open-Channel Flow

The model's response to the same flow velocities but in an open channel was tested. The resulting drag force from these runs is compared to the equivalent Tschisgale & Fröhlich (2020) CCF drag force in Figure 3.2-8.

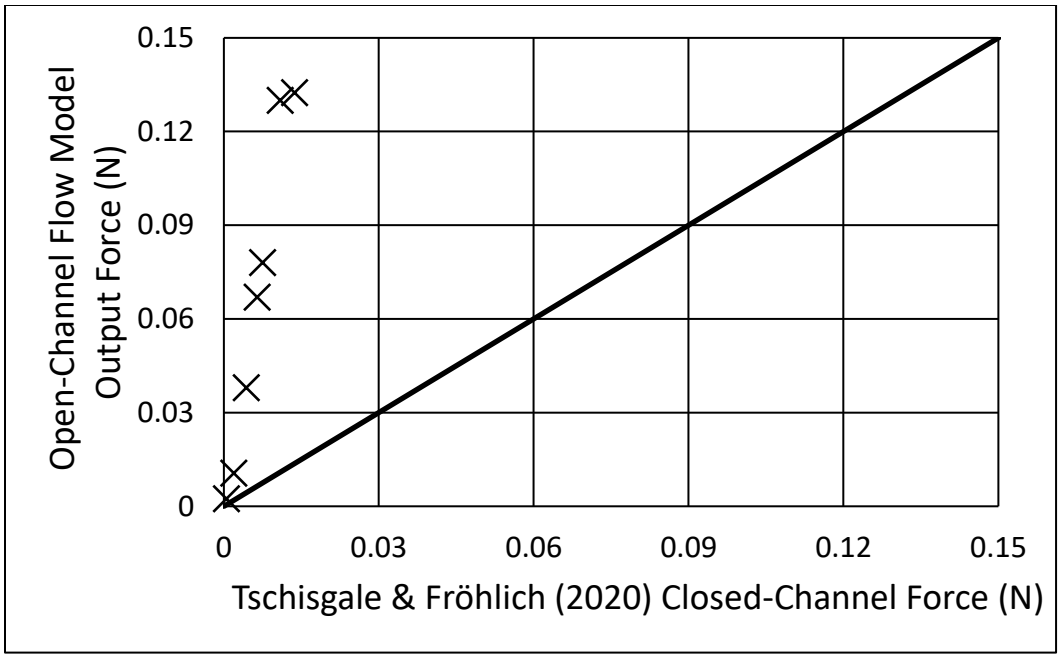

Figure 3.2-8. Comparison of OCF to published CCF results for Tschisgale & Fröhlich (2020).

Again, the CCF results and Henteleff et al. (2023), the drag force response to hydrodynamic forcing is seen to be greatly overestimated, thus showing consistency across flow conditions. The results are also similar in that the overestimation increases in magnitude as the forcing is more extreme. This notion was suggested by Henteleff et al. (2023) that the error has to do with the fundamental assumptions of the model.

Solitary Waves

Solitary Wave (SW) conditions equivalent to the CCF conditions investigated in Tschisgale & Fröhlich (2020) were carried out to confirm that the drag force response indicated by Henteleff et al. (2023) and the present study's OCF simulations was independent of hydrodynamic conditions. A screen grab of the simulation is presented in Figure 3.2-9.

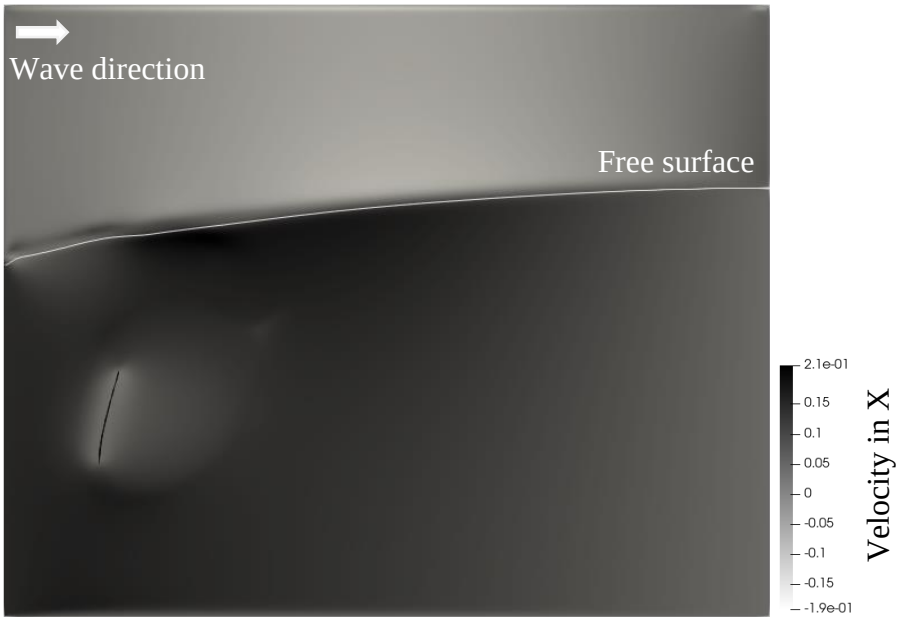

Figure 3.2-9. Screenshot of Tschisgale & Fröhlich (2020) solitary wave test.

A comparison between the depth-averaged horizontal orbital velocity of the first-order SW cases to their equivalent CCF cases is presented in Figure 3.2-10. The modelled velocities were calculated using peak velocity measured at 1cm intervals through the water column. Excellent agreement is seen between the two cases, suggesting that the results from the different versions of the Tschisgale & Fröhlich (2020) simulations should be comparable to each other.

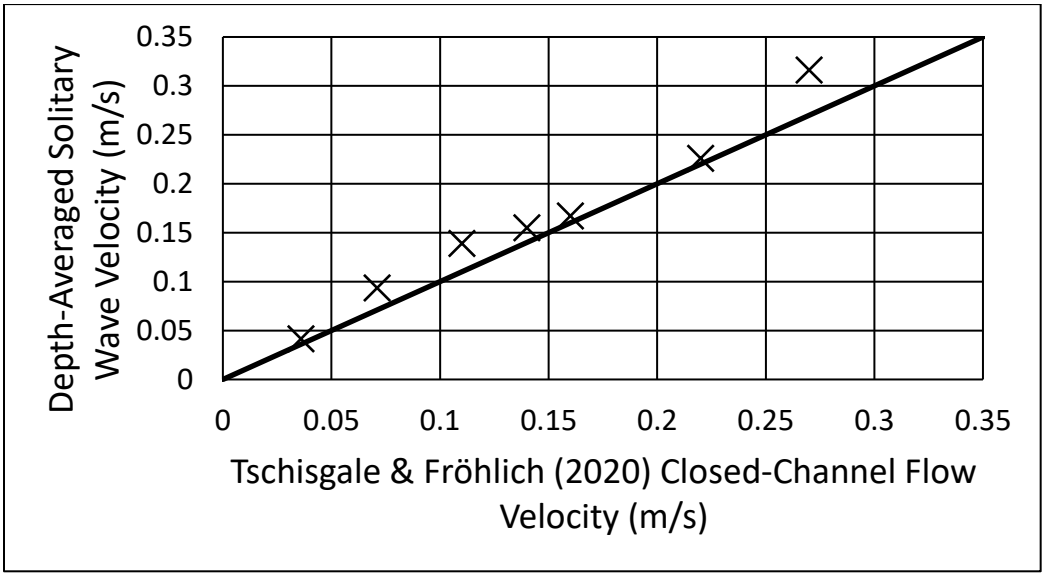

Figure 3.2-10. Depth-averaged SW velocities vs. equivalent CCF velocities.

The force responses to these waves are compared to the CCF forces in Figure 3.2-11. The drag forces shown are at their peak across the testing, consistent with the velocities above.

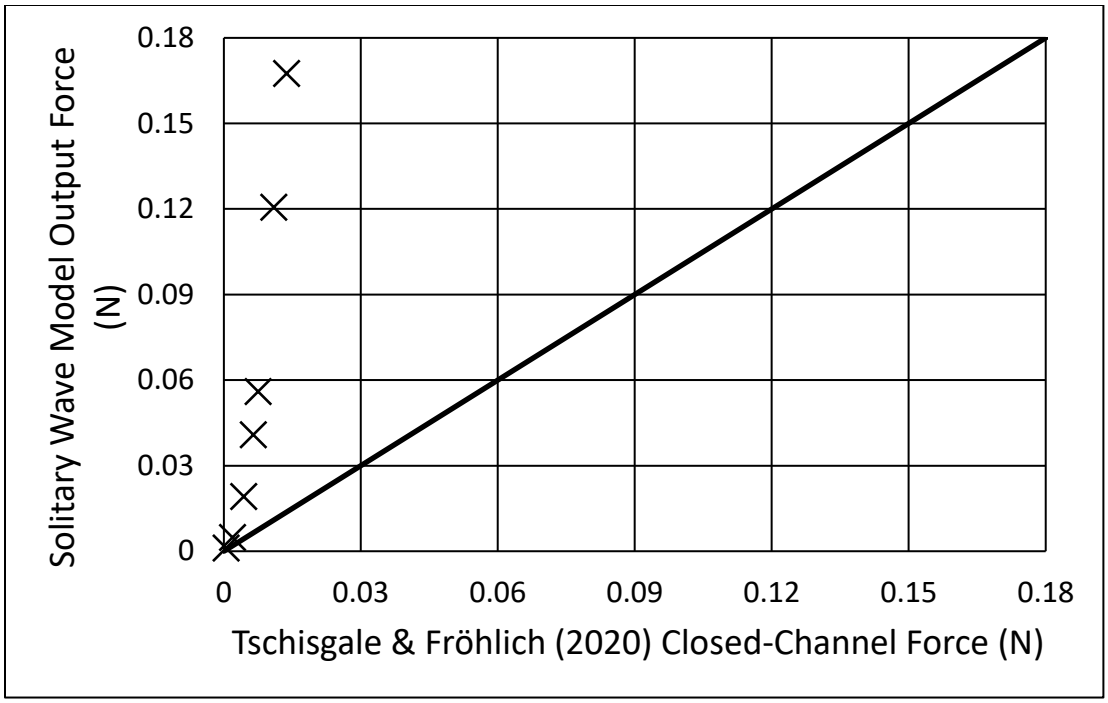

Figure 3.2-11. Comparison of SW to published CCF results for Tschisgale & Fröhlich (2020).

Again, results were consistent with both of the previous CCF and OCF simulations, as well as those of Henteleff et al. (2023). It is seen that, with more forcing, the overestimation of the drag force response increases. This further demonstrates that the behaviour shown above relates to the model itself, rather than any particular modelled condition.

It should be noted that for the OCF and SW of Tschisgale & Fröhlich (2020) tests, the numerical model was found to break down for case 8, the most energetic hydrodynamic conditions of the experimental runs and are thus not presented. This is believed to be due to the conditions that case 8 being beyond the applicable range of assumptions on which the model is based. This was further reported in the Markov et al. (2023) testing, which is described in the following section.

Motion Response Testing: Markov et al. (2023)

For the wave conditions tested from Markov et al. (2023), the flexible FSI module experienced almost immediate breakdown with the plant modelled as in-situ. A screenshot of a simulation is presented in Figure 3.2-12. This breakdown resulted in the numerical strip becoming fixed in place until the simulation was completed. Potential reasons for this failure are discussed in the following section. While this provided little insight, testing on the results' sensitivity to the flexible structure's elastic modulus resulted in greater understanding of how the flexible FSI module was behaving.

Figure 3.2-12. Experimental screenshot of Markov et al. (2023) simulation.

With an elastic modulus of 50x the in-situ value, the movement of the numerical strip was found to roughly align with the measured results, in terms of magnitude, although phase and period do not. This result can be seen in Figure 3.2-13 The movement was further damped down as the rigidity was increased. However, this result suggested that the motion response of the in-situ test would have been greatly overestimated were the module not breaking down, consistent with the force response findings described above and in previous works (Henteleff et al., 2023).

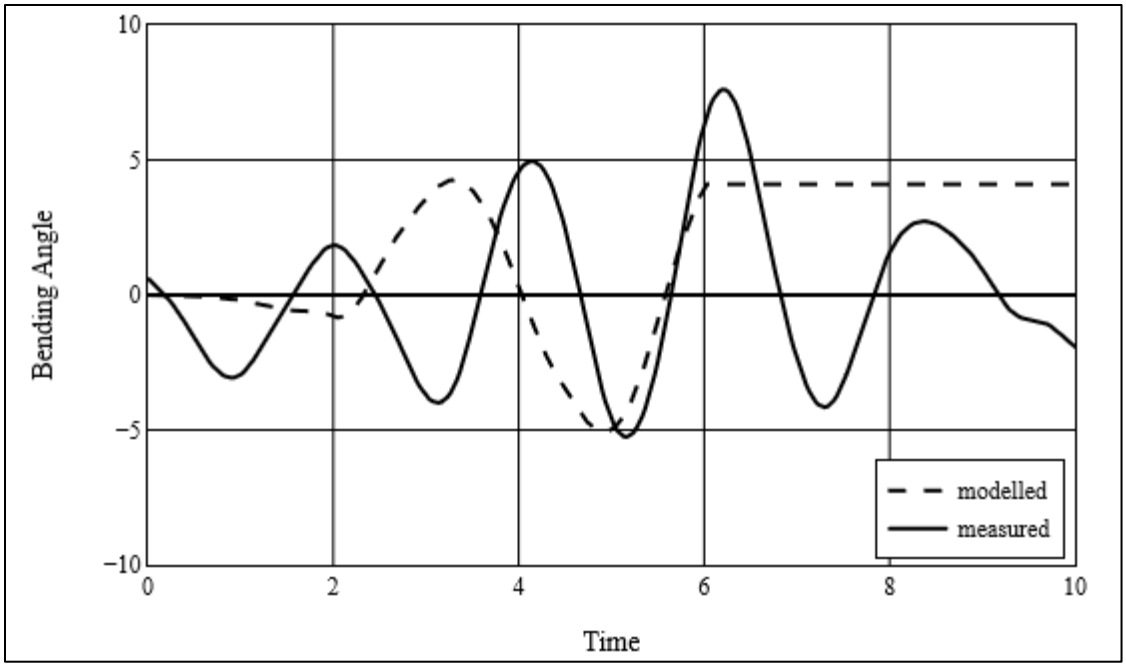

Figure 3.2-13. Modelled and measured bending angle at 50x in situ E.

3.2.1. Discussion

In the work presented herein, REEF3D's new flexible FSI module has been demonstrated to consistently overestimate the structure's response to wave action (Henteleff et al., 2023), as well as OCF conditions. Each of these sets of experiments were distinct from each other in several ways, which are worth comparing directly.

The structures tested in each of the three numerical tests varied in both geometric and mechanical properties. The smallest, lightest and most flexible of the three was the strip of the

Tschisgale & Fröhlich (2020) tests. Those of the Paul et al. (2016) tests performed in Henteleff et al. (2023) were in between the Tschisgale & Fröhlich (2020) and Markov et al. (2023) strips. However, geometrically speaking these were the most dense and rigid. Markov et al. (2023) structure was the largest by a significant margin but was in between the Tschisgale & Fröhlich (2020) and Paul et al. (2016) structures in terms of density and Young's modulus. These properties are summarized in Table 3.2-2.

Table 3.2-2. Comparison of geometric and mechanical properties of tested structures and tested velocities.

Property (unit)	**Paul et al. (2016) / Henteleff et al. (2023)**	**Tschisgale & Fröhlich (2020)**	**Markov et al. (2023)**
Length (m)	0.25	0.05	0.62
Width (m)	0.0055	0.01	0.0045
Thickness (m)	0.004	0.002	0.0045
Density (kg/m^3)	1245	670	900
Young's modulus (GPa)	3.44	0.0005	0.23
Horizontal orbital velocity range (m/s)	0.21 – 0.86	0.036 – 0.32	0.063

The hydrodynamic conditions also vary across the numerical simulations. Those of the Tschisgale & Fröhlich (2020) tests were the smallest in terms of velocity. The Markov et al. (2023) tests were in the middle, with the Paul et al. (2016) tests, as described in Henteleff et al. (2023), were the most extreme of the three.

A combination of the hydrodynamic conditions and mechanical properties of the strips resulted in the overestimation behaviour noted in the results of this study and in Henteleff et al. (2023). The longer, lighter, and more flexible structure of the Markov et al. (2023) experiments led to the breakdown of the module, whereas no such result was seen in the Henteleff et al. (2023) simulations of a shorter, denser, and more rigid body, or the light and flexible but much smaller strip of the Tschisgale & Fröhlich (2020) tests.

The new flexible FSI module in REEF3D assumes that the flexible strip is made up of a Kelvin-Voigt linearly viscoelastic material (Martin & Bihs, 2021; Tschisgale & Fröhlich, 2020). This assumption described in Meyers & Chawla (2009) as being an effective model for glassy polymers. An important aspect of this material theory is that the internal deformations must be small (Martin & Bihs, 2021; Tschisgale & Fröhlich, 2020). While this may be the case for more rigid materials, it does not appear to hold true for more flexible materials, such as those of saltmarsh vegetation. This leads to the overestimation of drag force response seen in the Tschisgale & Fröhlich (2020) tests and that of motion response seen in the Markov et al. (2023) simulations despite minor flow velocities, consistent with the findings of Henteleff et al. (2023). Both the Tschisgale & Fröhlich (2020) tests presented herein and the Henteleff et al. (2023) simulations were also conducted using significantly shorter flexible bodies than in the Markov et al. (2023) tests. The larger deformations of a longer structure of similar flexibility to the shorter ones could be another reason for the solver's breakdown.

In Meyers and Chawla (2009), soft biological material is described as exhibiting nonlinear elastic behaviour. This distinction between the sort of materials tested in this study and those of moorings, as the module was initially designed for (Martin & Bihs, 2021), show the limited range of applicability of the current state of the tool. Potential uses of the model are also limited by the geometry imposed on the structure. As tested, the model can only handle thin strips with a rectangular cross-section. While this constraint is not significant for the Tschisgale & Fröhlich (2020) tests which used this strip geometry, it is more meaningful for the Markov et al. (2023) simulations which are based on live vegetation. The structures tested in the flume, *S. alterniflora*, are more cylindrical than rectangular, and have leaves coming off the stem. Canopy and root have been demonstrated to impact hydrodynamic effect of mangroves (He et al., 2019) and can be expected to change the behaviour of marsh species as well. Furthermore, while *S. alterniflora* is relatively similar to the shape prescribed by the model, many marsh species are not. *S. patens*, for example, has many leaves of similar size to the main stem. The model tested herein is not currently equipped to effectively model such a plant. It is suggested that the model be adapted to account for more complicated structures in the future.

3.2.2. Conclusions & Next Steps

This work attempted to simplify plant behaviour using the REEF3D flexible FSI model. In this study, the new flexible FSI module being implemented in REEF3D has been demonstrated to consistently overestimate drag and motion response of in-situ saltmarsh vegetation or vegetation surrogates under wave action. It is hypothesized that this is due to the underlying assumptions regarding the material of the flexible body, namely that it demonstrates linearly viscoelastic properties. Materials that exhibit this set of properties tend to be glassy polymers, unlike the nonlinear elastic behaviour of soft biological materials, such as plants, making the attempted simplification unfeasible as tested. Without the addition of more material options for the flexible FSI module, the results presented herein suggest that the tool is not suitable for modelling saltmarsh vegetation or flexible surrogates as in-situ. Additions to the model are needed before this can be done effectively.

Even without an expanded feature set, there remains work to be done with this tool. REEF3D's new flexible FSI module may have use for other NBS methods. To the authors' knowledge, it has yet to be tested for the modelling of mangrove structures. Given that they are much more rigid, these systems are expected to be more appropriate for the tool as currently constructed. A more calibration-intensive approach may also be effective in modelling saltmarsh vegetation. While this study focussed on maintaining in-situ plants or surrogates, it is possible that physical modelling results could be replicated effectively using a flexible structure calibrated to do so, either by altering the geometric or mechanical properties of the strip.

4)Discussion

4.1. Limitations

This thesis presents the findings from a series of numerical experiments thoroughly investigating the applicability of a newly developed flexible FSI numerical model to saltmarsh vegetation in the open-source CFD software REEF3D. This was carried out using three different experimental setups designed to thoroughly test both the drag and motion response of the model to a range of hydrodynamic conditions. The model imposes certain limits on the conditions that can be tested. First, the experimental case must be such that the flexible structure remains completely submerged throughout testing. Marsh plants in the field are often emergent, thus making the conditions tested herein only partly representative of those occurring in a natural context. The model also imposes a fixed geometry on the tested structure. It must be, when upright, a rectangular prism. No change in geometry along its length is possible, nor is the use of different cross-sections. While this was not an issue for the drag force experiments, which were based on flume studies using such a structure, the motion experiments did not. The geometry of *S. alterniflora* is more cylindrical and varies along the stem. This may have introduced some error into the results, although it is assumed that it would not have prevented the breakdown noted therein. Another limitation of this study is the lack of physical modelling experiments to replicate in a numerical context. Few published studies exist quantifying an individual flexible structure's drag or motion response to any hydrodynamic condition. Furthermore, to the author's knowledge, only one exists, measuring both simultaneously, wherein the study focussed on seagrass (Luhar & Nepf, 2016) rather than saltmarsh vegetation. This, paired with the computational cost and time required to perform numerical simulations at this scale, dramatically restricts the scope of this study, and until more work is done, future research efforts in this field. It was found that, for the numerical tool used herein, the mesh resolution had to be equal to or smaller than the width of the numerical plant surrogate. As saltmarsh plants are not typically large in diameter, ranging from 0.19 – 0.43 cm per Feagin et al. (2010), this results in very fine meshes and extreme computational cost. This prevented a complete convergence analysis for grid size from being performed.

4.2. Application

As the ultimate result of the evaluation of the tool presented herein is negative, the foremost practical application of this work is that the Tschisgale & Fröhlich (2020) model, at least as implemented in REEF3D, requires more work before it can be used to model saltmarsh plant behaviour effectively. This highlights the numerical complexity of this sort of modelling. The lack of similar studies performed with other numerical tools suggests that this is the case regardless of the software used. Some suggestions on steps to take to advance the field are discussed below.

4.2.1. Proposed Physical Modelling Studies

As stated previously, the scope of this and any similar study is limited primarily by the lack of physical modelling work quantifying the drag and motion response of structures like those tested in this thesis. This is further complicated by the computational demands of replicating such studies numerically. Therefore, it is suggested that more physical modelling experiments are performed using full-scale plants, either live or surrogates. This is proposed due to the correlation between strip thickness and grid size convergence point noted above. Measuring these structures' drag and motion response to various realistic hydrodynamic conditions, i.e., 1D flow, regular/irregular waves, paired conditions, etc., would provide a strong foundation upon which future numerical studies could build.

4.2.2. Proposed Model Additions

As discussed above, the model, as tested, is rigid in the assumptions it uses for both the material and geometry of the flexible structure. The requirement of complete submergence of the structure could also be lifted. While how these foundational assumptions of the model might be expanded, and the difficulty of doing so, is outside of the scope of this work, these would make for a helpful addition in general and expand the model's applicability to more flexible, non-rectangular structures and partially submerged, such as saltmarsh vegetation. This might take the form of a set of inputs in the control file, by which the user could enter the appropriate material theory, geometry, etc., in addition to the parameters that are currently available for user editing. The limitations of the software with regard to memory-intensive simulations could also be addressed. This could be done by altering the model to work with non-cubic cells, thereby allowing for variable grid resolution. This would decrease the memory requirements for fine grids, thus expanding the model's use to smaller-diameter structures such as seagrass.

4.2.3. Future Applications

A numerical model that could accurately replicate saltmarsh plant behaviour could be used to investigate many fine-scale marsh behaviours which are difficult to measure physically. These could include:

- Determination of the fine-scale hydrodynamics surrounding moving plants. Water velocity measurement tools, such as ADVs, are limited and affect flow patterns. A numerical model can produce detailed velocity profile data without changing the behaviour of the fluid.
- Linking fine-scale hydrodynamics to marsh behaviour by investigating the effects of sheltering, flow mixing, etc., on, e.g., wave attenuation capacity.
- Comparison of motion/force response to measured breakage forces and/or positions to determine hydrodynamic conditions that could cause plant stem failure. Performing a physical modelling study would be practically extremely difficult, whereas the repeatability of numerical modelling makes it simple, with the appropriate calibration data.

5)Conclusions and Recommendations for Future Work

5.1. Conclusions

This thesis presents findings from three experimental programs designed to evaluate the accuracy of Tschisgale & Fröhlich (2020)'s flexible FSI model, as implemented in REEF3D when applied to saltmarsh vegetation. These three programs together evaluated the drag force response of the model under regular wave, closed-channel and open-channel flow and solitary wave forcing, and the motion response of the model under irregular wave forcing. These tests ultimately provide a thorough assessment of the two ways the model describes the behaviour of the flexible structure, namely drag force and motion, under various hydrodynamic conditions and with different structural geometries and materials. Key conclusions from these works are provided below:

- As tested, the Tschisgale & Fröhlich (2020)-based model in REEF3D is not capable of effectively replicating in situ saltmarsh plant behaviour. It was found to consistently overestimate the drag force response and broke down during motion response testing.
- Breakdown of the model seemed to relate to both the geometry and the material of the tested structure. However, geometry appeared to be the main driver. No breakdown was noted for the short, heavier, more rigid strips of the Paul et al. (2016) testing and only for the most extreme conditions of the Tschisgale & Fröhlich (2020) testing of the short, light, and flexible strips. However, the model broke down consistently for the Markov et al. (2023) testing, with a much longer strip with density and rigidity between those of the other two tested materials.
- The model's failure appears to be primarily related to the foundational material assumptions, namely that the structure is made up of linearly viscoelastic Kelvin-Voigt-type material. This theory is noted by Meyers & Chawla (2009) as being more appropriate for glassy polymers than soft biological materials, such as saltmarsh vegetation. These are better described, per Meyers & Chawla (2009), by nonlinear elastic material theory.

5.2. Recommendations for Future Work

The studies presented within this thesis evaluate the accuracy of a Tschisgale & Fröhlich (2020)-based flexible FSI module implemented in REEF3D for modelling saltmarsh vegetation behaviour. Considering the findings and limitations of this thesis, as well as the knowledge gaps identified in Section 2.5.3 and Sections 4.2.1 and 4.2.2, the following future work is recommended:

- As discussed above, the assumption of material on which the flexible FSI model seems to make it inapplicable to the case of saltmarsh vegetation. It is recommended that other

material theories, especially nonlinear elastic theory, is added to the model. This would broaden the applicability of this tool to saltmarsh vegetation, as well as other flexible structures.

- A significant limitation of the works presented herein is the relative lack of appropriate physical modelling studies for numerical replication. Therefore, future flume work investigating the behaviour of flexible live or surrogate saltmarsh vegetation in terms of drag force and/or motion response is recommended. This would provide opportunity for more detailed and accurate numerical modelling efforts, particularly if both drag and motion were measured simultaneously.
- The applications of a numerical modelling tool capable of replicating saltmarsh vegetation behaviour could provide significant insight into breakage conditions, if compared to the appropriate dataset, and fine-scale hydrodynamics surrounding plants in a marsh setting. Both avenues could give coastal practitioners more detailed insight into the viability of saltmarshes for coastal protection purposes.

References

"Bainbridge Island, WA." *NOAA Habitat Blueprint*, National Oceanic and Atmospheric Administration, www.habitatblueprint.noaa.gov/living-shorelines/bainbridge-island/.

"Beaufort, NC." *NOAA Habitat Blueprint*, National Oceanic and Atmospheric Administration, www.habitatblueprint.noaa.gov/living-shorelines/beaufort/.

"Coxsackie, NY." *NOAA Habitat Blueprint*, National Oceanic and Atmospheric Administration, www.habitatblueprint.noaa.gov/living-shorelines/coxsackie/.

"Ecological Restoration." *TransCoastal Adaptations*, www.transcoastaladaptations.com/ecological-restoration.

"Extreme Weather and Climate Change." *Center for Climate and Energy Solutions*, 4 Jan. 2021, www.c2es.org/content/extreme-weather-and-climate-change/.

"Green Shores | About the Program." *Stewardshipcentrebc.ca*, stewardshipcentrebc.ca/green-shores-home/gs-about/.

"Living Shorelines." *Living Shorelines | Ecology Action Centre*, Ecology Action Centre, ecologyaction.ca/livingshorelines.

"Magnolia Springs, AL." *NOAA Habitat Blueprint*, National Oceanic and Atmospheric Administration, www.habitatblueprint.noaa.gov/magnolia-springs/.

"Mangrove Ecological Restoration." *Ecopeace Asia*, www.ecopeaceasia.org/en/node/107?ckattempt=1.

"Mangrove Restoration in Haiti Moves up a Gear." *UN Environment*, 24 July 2020, www.unenvironment.org/news-and-stories/story/mangrove-restoration-haiti-moves-gear.

"Wallasea Island Wild Coast Project: Our Work." *The RSPB*, The Royal Society for the Protection of Birds, www.rspb.org.uk/our-work/our-positions-and-casework/casework/cases/wallasea-island/.

Alagan Chella, M., Bihs, H., Kamath, A., Myrhaug, D., & Arntsen, Ø. A. (2019). Breaking wave interaction with a group of four vertical slender cylinders in two square arrangements. *Journal of Offshore Mechanics and Arctic Engineering*, *141*(6), 1–10. https://doi.org/10.1115/1.4043597

Amina, & Tanaka, N. (2022). Numerical Investigation of 3D Flow Properties around Finite Emergent Vegetation by Using the Two-Phase Volume of Fluid (VOF) Modeling Technique. *Fluids*, *7*(5). https://doi.org/10.3390/fluids7050175

Anderson, M. E., & Smith, J. M. (2014). Wave attenuation by flexible, idealized salt marsh vegetation. *Coastal Engineering*, *83*, 82–92. https://doi.org/10.1016/j.coastaleng.2013.10.004

Anjum, N., & Tanaka, N. (2019). Numerical investigation of velocity distribution of turbulent flow through vertically double-layered vegetation. *Water Science and Engineering*, *12*(4), 319–329. https://doi.org/10.1016/j.wse.2019.11.001

Arunakumar, H. S., Suvarna, P., Abhijith, P. A., Prabhu, A. S., Pruthviraj, U., & Kamath, A. (2019). Effect of Emerged Coastal Vegetation on Wave Attenuation Using Open Source CFD Tool: REEF3D. *Proceedings of the Fourth International Conference in Ocean Engineering*, 591–603.

Augustin, L. N., Irish, J. L., & Lynett, P. (2009). Laboratory and numerical studies of wave damping by emergent and near-emergent wetland vegetation. *Coastal Engineering*, *56*(3), 332–340. https://doi.org/10.1016/j.coastaleng.2008.09.004

Bayraktarov, E., Saunders, M. I., Abdullah, S., Mills, M., Beher, J., Possingham, H. P., Mumby, P. J., & Lovelock, C. E. (2015). The cost and feasibility of marine coastal restoration. *Ecological Applications*, *26*(4), 1055–1074. https://doi.org/10.1890/15-1077.1

Bendoni, M., Georgiou, I. Y., Roelvink, D., & Oumeraci, H. (2019). Numerical modelling of the erosion of marsh boundaries due to wave impact. *Coastal Engineering*, *152*(May), 103514. https://doi.org/10.1016/j.coastaleng.2019.103514

Best, S. N., Van der Wegen, M., Dijkstra, J., Willemsen, P. W. J. M., Borsje, B. W., & Roelvink, D. J. A. (2018). Do salt marshes survive sea level rise? Modelling wave action, morphodynamics and vegetation dynamics. *Environmental Modelling and Software*, *109*(September 2017), 152–166. https://doi.org/10.1016/j.envsoft.2018.08.004

Bihs, H., Kamath, A., Chella, Mayilvahanan Alagan Ahmad, N., Aggarwal, A., Wang, W., Martin, T., & Fornes, P. (2018). *REEF3D :: User Guide 18.01*. NTNU: Norwegian University of Science and Technology.

Bilkovic, D. M., Mitchell, M. M., La Peyre, M. K., & Toft, J. D. (Eds.). (2017). *Living Shorelines: The Science and Management of Nature-Based Coastal Protection*. CRC Press.

Borsje, B. W., van Wesenbeeck, B. K., Dekker, F., Paalvast, P., Bouma, T. J., van Katwijk, M. M., & de Vries, M. B. (2011). How ecological engineering can serve in coastal protection. *Ecological Engineering*, *37*(2), 113–122. https://doi.org/10.1016/j.ecoleng.2010.11.027

Bryant, D. B., Anderson Bryant, M., Sharp, J. A., Bell, G. L., & Moore, C. (2019). The response of vegetated dunes to wave attack. *Coastal Engineering*, *152*(October 2018), 103506. https://doi.org/10.1016/j.coastaleng.2019.103506

Burden, A., Garbutt, A., & Evans, C. D. (2019). Effect of restoration on saltmarsh carbon accumulation in Eastern England. *Biology Letters*, *15*(1), 0–3. https://doi.org/10.1098/rsbl.2018.0773

Bureau of Reclamation and U.S. Army Engineer Research and Development Center (USBR and ERDC). 2016. National Large Wood Manual: Assessment, Planning, Design, and Maintenance of Large Wood in Fluvial Ecosystems: Restoring Process, Function, and Structure. 628pages + Appendix. Available: www.usbr.gov/pn/ and http://cw-environment.usace.army.mil/restoration.cfm (click on “River Restoration,” then “Techniques”)

Chakrabarti, A., Brandt, S. R., Chen, Q., & Shi, F. (2017). Boussinesq modeling of wave-induced hydrodynamics in coastal wetlands. *Journal of Geophysical Research: Oceans*, *122*, 3861–3883. https://doi.org/10.1002/2016JC012264

Chakrabarti, A., Brandt, S. R., Chen, Q., & Shi, F. (2017). Boussinesq modeling of wave-induced hydrodynamics in coastal wetlands. *Journal of Geophysical Research: Oceans*, *122*, 3861–3883. https://doi.org/10.1002/2016JC012264

Davis, J. L., Currin, C. A., O’Brien, C., Raffenburg, C., & Davis, A. (2015). Living shorelines: Coastal resilience with a blue carbon benefit. *PLoS ONE*, *10*(11), 1–18. https://doi.org/10.1371/journal.pone.0142595

Davis, J. L., Currin, C. A., O’Brien, C., Raffenburg, C., & Davis, A. (2015). Living shorelines: Coastal resilience with a blue carbon benefit. *PLoS ONE*, *10*(11), 1–18. https://doi.org/10.1371/journal.pone.0142595

Deltares Systems. (2014). *Delft3D User Manual*.

Eyquem, J. (2021). *Rising Seas and Shifting Sands Combining Natural and Grey Infrastructure To Protect Canada'S Eastern and Western Coastal Communities*. *December*. www.intactcentreclimateadaptation.ca

Feagin, R. A., Irish, J. L., Möller, I., Williams, A. M., Colón-Rivera, R. J., & Mousavi, M. E. (2011). Short communication: Engineering properties of wetland plants with application to wave attenuation. *Coastal Engineering*, *58*(3), 251–255. https://doi.org/10.1016/j.coastaleng.2010.10.003

Fisheries, NOAA. "Coastal Wetlands: Too Valuable to Lose." *NOAA*, National Oceanic and Atmospheric Administration, 5 Aug. 2020, www.fisheries.noaa.gov/national/habitat-conservation/coastal-wetlands-too-valuable-lose.

Foster-Martinez, M. R., Lacy, J. R., Ferner, M. C., & Variano, E. A. (2018). Wave attenuation across a tidal marsh in San Francisco Bay. *Coastal Engineering*, *136*(October 2017), 26–40. https://doi.org/10.1016/j.coastaleng.2018.02.001

Garzon, J. L., Maza, M., Ferreira, C. M., Lara, J. L., & Losada, I. J. (2019). Wave Attenuation by Spartina Saltmarshes in the Chesapeake Bay Under Storm Surge Conditions. *Journal of Geophysical Research: Oceans*, *124*(7), 5220–5243. https://doi.org/10.1029/2018JC014865

Garzon, J. L., Miesse, T., & Ferreira, C. M. (2019). Field-based numerical model investigation of wave propagation across marshes in the Chesapeake Bay under storm conditions. *Coastal Engineering*, *146*(November 2018), 32–46. https://doi.org/10.1016/j.coastaleng.2018.11.001

Greenshields, C. J. (2020). *OpenFOAM* (Issue July).

Hardaway Jr., C. S., & Duhring, K. A. (2010). *Design and Construction of Living Shorelines: A course for living shorelines professionals*. Center for Coastal Resources Management.

Hartmann, K., & Stock, M. (2019). Long-term change in habitat and vegetation in an ungrazed, estuarine salt marsh: Man-made foreland compared to young marsh development. *Estuarine, Coastal and Shelf Science*, *227*(July), 106348. https://doi.org/10.1016/j.ecss.2019.106348

He, F., Chen, J., & Jiang, C. (2019). Surface wave attenuation by vegetation with the stem, root and canopy. *Coastal Engineering*, *152*(December 2017), 103509. https://doi.org/10.1016/j.coastaleng.2019.103509

Henteleff, R.; Markov, A.; Stolle, J.; Sriram, V. and Nistor, I. (2023). Flexible Fluid-Structure Interaction of a Flexible Plant Model for Nature-Based Solutions. *International Conference on Coastal Engineering (ICCE) 2022*, Sydney, Australia.

Hoque, A., Husrin, S., & Oumeraci, H. (2018). Laboratory studies of wave attenuation by coastal forest under storm surge. *Coastal Engineering Journal*, *60*(2), 225–238. https://doi.org/10.1080/21664250.2018.1486268

IUCN (2020). *Global Standard for Nature-Based Solutions: A User-Friendly Framework for the Verification, Design and Scaling up of NbS.* First edition. Gland, Switzerland: IUCN. https://doi.org/10.2305/iucn.ch.2020.08.en

Jadhav, R. S., Chen, Q., & Smith, J. M. (2013). Spectral distribution of wave energy dissipation by salt marsh vegetation. *Coastal Engineering*, *77*, 99–107. https://doi.org/10.1016/j.coastaleng.2013.02.013

Johannessen, J., MacLennan, A., Blue, A., Waggoner, J., Williams, S., Gerstel, W., Barnard, R., Carman, R., & Shipman, H. (2014). *Marine Shoreline Design Guidelines*. https://wdfw.wa.gov/publications/01583

Johnson, M. F., Thomas, R. E., Dijkstra, J. T., Paul, M., Penning, W. E., & Rice, S. P. (2014). Using surrogates, including scaling issues, in laboratory flumes and basins. In *Users Guide to Ecohydraulic Modelling and Experimentation: Experience of the Ecohydraulic Research Team (PISCES) of the HYDRALAB Network* (Issue 1978, pp. 23–39).

Kim, H. S., Nabi, M., Kimura, I., & Shimizu, Y. (2015). Computational modeling of flow and morphodynamics through rigid-emergent vegetation. *Advances in Water Resources*, *84*, 64–86. https://doi.org/10.1016/j.advwatres.2015.07.020

Lara, J. L., Maza, M., Ondiviela, B., Trinogga, J., Losada, I. J., Bouma, T. J., & Gordejuela, N. (2016). Large-scale 3-D experiments of wave and current interaction with real vegetation. Part 1: Guidelines for physical modeling. *Coastal Engineering*, *107*, 70–83. https://doi.org/10.1016/j.coastaleng.2015.09.012

Le Minor, M., Bartzke, G., Zimmer, M., Gillis, L., Helfer, V., & Huhn, K. (2019). Numerical modelling of hydraulics and sediment dynamics around mangrove seedlings: Implications for mangrove establishment and reforestation. *Estuarine, Coastal and Shelf Science*, *217*(October 2018), 81–95. https://doi.org/10.1016/j.ecss.2018.10.019

Lei, J., & Nepf, H. (2019). Wave damping by flexible vegetation: Connecting individual blade dynamics to the meadow scale. *Coastal Engineering*, *147*(October 2018), 138–148. https://doi.org/10.1016/j.coastaleng.2019.01.008

Leonardi, N., Carnacina, I., Donatelli, C., Ganju, N. K., Plater, A. J., Schuerch, M., & Temmerman, S. (2018). Dynamic interactions between coastal storms and salt marshes: A review. *Geomorphology*, *301*, 92–107. https://doi.org/10.1016/j.geomorph.2017.11.001

Leonardi, N., Ganju, N.K., Fagherazzi, S., 2016. A linear relationship between wave power and erosion determines salt-marsh resilience to violent storms and hurricanes. Proc. Natl. Acad. Sci. U. S. A. 113, 64–68.

MAINE DEPARTMENT OF ENVIRONMENTAL PROTECTION. (2016). *Erosion and Sediment Control Best Management Practices Manual* (Issue August).

Marjoribanks, T. I., Hardy, R. J., Lane, S. N., & Parsons, D. R. (2017). Does the canopy mixing layer model apply to highly flexible aquatic vegetation? Insights from numerical modelling. *Environmental Fluid Mechanics*, *17*(2), 277–301. https://doi.org/10.1007/s10652-016-9482-z

Markov, A., Stolle, J., Henteleff, R., Nistor, I., Van, D. P., Murphy, E., & Cornett, A. (2023). Deformation of Spartina Patens and Spartina alterniflora stems under irregular wave action. *Coastal Engineering Journal*, *00*(00), 1–22. https://doi.org/10.1080/21664250.2023.2195030

Martin, T., & Bihs, H. (2021). A numerical solution for modelling mooring dynamics, including bending and shearing effects, using a geometrically exact beam model. *Journal of Marine Science and Engineering*, *9*(5), 1–27. https://doi.org/10.3390/jmse9050486

Martin, T., Tsarau, A., & Bihs, H. (2020). A numerical framework for modelling the dynamics of open ocean aquaculture structures in viscous fluids. *Applied Ocean Research*, *1*. https://doi.org/10.1016/j.apor.2020.102410

Mattis, S. A., Kees, C. E., Wei, M. V., Dimakopoulos, A., & Dawson, C. N. (2019). Computational model for wave attenuation by flexible vegetation. *Journal of Waterway, Port, Coastal and Ocean Engineering*, *145*(1), 1–23. https://doi.org/10.1061/(ASCE)WW.1943-5460.0000487

Maza, M., Lara, J. L., Losada, I. J., Ondiviela, B., Trinogga, J., & Bouma, T. J. (2015). Large-scale 3-D experiments of wave and current interaction with real vegetation. Part 2: Experimental analysis. *Coastal Engineering*, *106*, 73–86. https://doi.org/10.1016/j.coastaleng.2015.09.010

Mei, C. C., Chan, I. C., Liu, P. L. F., Huang, Z., & Zhang, W. (2011). Long waves through emergent coastal vegetation. *Journal of Fluid Mechanics*, *687*, 461–491. https://doi.org/10.1017/jfm.2011.373

Meyers, M., & Chawla, K. (2009). *Mechanical Behavior of Materials* (Second). Cambridge University Press.

Miquel, A. M., Kamath, A., Chella, M. A., Archetti, R., & Bihs, H. (2018). Analysis of different methods for wave generation and absorption in a CFD-based numerical wave tank. *Journal of Marine Science and Engineering*, *6*(2), 1–21. https://doi.org/10.3390/jmse6020073

Möller, I., Kudella, M., Rupprecht, F., Spencer, T., Paul, M., Van Wesenbeeck, B. K., Wolters, G., Jensen, K., Bouma, T. J., Miranda-Lange, M., & Schimmels, S. (2014). Wave attenuation over coastal salt marshes under storm surge conditions. *Nature Geoscience*, *7*(10), 727–731. https://doi.org/10.1038/NGEO2251

Murphy, E., Boisvert, J., McLean, R., Pilechi, V., Cousineau, J., Sushama, L., & Liang, Z. (2019). Wave run-up contributions to coastal flood hazards in New Brunswick. *Proceedings, Annual Conference - Canadian Society for Civil Engineering*, *2019-June*(Figure 1).

Osorio-Cano, J. D., Osorio, A. F., & Peláez-Zapata, D. S. (2019). Ecosystem management tools to study natural habitats as wave damping structures and coastal protection mechanisms. *Ecological Engineering*, *130*, 282–295. https://doi.org/10.1016/j.ecoleng.2017.07.015

Ozeren, Y., Wren, D. G., & Wu, W. (2014). Experimental investigation of wave attenuation through model and live vegetation. *Journal of Waterway, Port, Coastal and Ocean Engineering*, *140*(5), 1–12. https://doi.org/10.1061/(ASCE)WW.1943-5460.0000251

Paul, M., Bouma, T. J., & Amos, C. L. (2012). Wave attenuation by submerged vegetation: Combining the effect of organism traits and tidal current. *Marine Ecology Progress Series*, *444*, 31–41. https://doi.org/10.3354/meps09489

Paul, M., Kerpen, N. B., & Kerpen, N. B. (2021). Erosion protection by winter state of salt marsh vegetation Erosion protection by winter state of salt marsh vegetation. *Journal of Ecohydraulics*, *0*(0), 1–10. https://doi.org/10.1080/24705357.2021.1938252

Paul, M., Rupprecht, F., Möller, I., Bouma, T. J., Spencer, T., Kudella, M., Wolters, G., van Wesenbeeck, B. K., Jensen, K., Miranda-Lange, M., & Schimmels, S. (2016). Plant stiffness and biomass as drivers for drag forces under extreme wave loading: A flume

study on mimics. *Coastal Engineering*, *117*, 70–78. https://doi.org/10.1016/j.coastaleng.2016.07.004

Pinsky, M. L., Guannel, G., & Arkema, K. K. (2013). Quantifying wave attenuation to inform coastal habitat conservation. *Ecosphere*, *4*(8). https://doi.org/10.1890/ES13-00080.1

Placek, M. (2022, November 29). *Worldwide Maritime Trade - Transport Volume 2021*. Statista. Retrieved January 5, 2023, from https://www.statista.com/statistics/264117/tonnage-of-worldwide-maritime-trade-since-1990/

Ramsayer, K. (2022, December 7). *NASA scientists map global salt marsh losses and their carbon impact*. NASA. Retrieved February 1, 2023, from https://www.nasa.gov/feature/esnt/2022/nasa-scientists-map-global-salt-marsh-losses-and-their-carbon-impact

Readshaw, J. (2018). *Design Basis for the Living Dike Concept* (Issue July).

Reclamation, B. of. (2016). *National Large Wood Manual* (Issue January).

Reef, R., Schuerch, M., Christie, E. K., Möller, I., & Spencer, T. (2018). The effect of vegetation height and biomass on the sediment budget of a European saltmarsh. *Estuarine, Coastal and Shelf Science*, *202*, 125–133. https://doi.org/10.1016/j.ecss.2017.12.016

Roelvnik, D., van Dongeren, A., McCall, R., Hoonhout, B., van Rooijen, A., van Geer, P., de Vet, L., & Nederhoff, K. (2015). *XBeach Manual*.

Rupprecht, F., Möller, I., Paul, M., Kudella, M., Spencer, T., van Wesenbeeck, B. K., Wolters, G., Jensen, K., Bouma, T. J., Miranda-Lange, M., & Schimmels, S. (2017). Vegetation-wave interactions in salt marshes under storm surge conditions. *Ecological Engineering*, *100*, 301–315. https://doi.org/10.1016/j.ecoleng.2016.12.030

Sauvé, P., Bernatchez, P., & Glaus, M. (2022). Multicriteria Decision Analysis to Assist in the Selection of Coastal Defence Measures: Involving Coastal Managers and Professionals in the Identification and Weighting of Criteria. *Frontiers in Marine Science*, *9*(April). https://doi.org/10.3389/fmars.2022.845348

Scheres, B., & Schüttrumpf, H. (2019). Enhancing the ecological value of sea dikes. *Water (Switzerland)*, *11*(8). https://doi.org/10.3390/w11081617

Schoutens, K., Heuner, M., Fuchs, E., Minden, V., Schulte-Ostermann, T., Belliard, J. P., Bouma, T. J., & Temmerman, S. (2020). Nature-based shoreline protection by tidal marsh plants depends on trade-offs between avoidance and attenuation of hydrodynamic forces. *Estuarine, Coastal and Shelf Science*, *236*(December 2019), 106645. https://doi.org/10.1016/j.ecss.2020.106645

Shepard, C. C., Crain, C. M., & Beck, M. W. (2011). The protective role of coastal marshes: A systematic review and meta-analysis. In *PLoS ONE* (Vol. 6, Issue 11). https://doi.org/10.1371/journal.pone.0027374

Stewardship Centre for British Columbia. (2020). *GREEN SHORES FOR SHORELINE DEVELOPMENT CREDITS AND RATINGS GUIDE*. www.stewardshipcentrebc.ca

Suzuki, T., Hu, Z., Kumada, K., Phan, L. K., & Zijlema, M. (2019). Non-hydrostatic modeling of drag, inertia and porous effects in wave propagation over dense vegetation fields. *Coastal Engineering*, *149*(135), 49–64. https://doi.org/10.1016/j.coastaleng.2019.03.011

SWAN: Scientific and Technical Documentation. (2020). Delft University of Technology.

Taillardat, P., Friess, D. A., & Lupascu, M. (2018). Mangrove blue carbon strategies for climate change mitigation are most effective at the national scale. *Biology Letters*, *14*(10). https://doi.org/10.1098/rsbl.2018.0251

TELEMAC-2D Software User Manual (Issue December). (2014). EDF-R&D.

Temmerman, S., Meire, P., Bouma, T. D., Herman, P. M., Ysebaert, T., & De Vriend, H. J. (2013). Ecosystem-based coastal defence in the face of global change. *Nature*, *504*(7478).

Thomas, R. E., Johnson, M. F., Frostick, L. E., Parsons, D. R., Bouma, T. J., Dijkstra, J. T., Eiff, O., Gobert, S., Henry, P. Y., Kemp, P., McLelland, S. J., Moulin, F. Y., Myrhaug, D., Neyts, A., Paul, M., Penning, W. E., Puijalon, S., Rice, S. P., Stanica, A., … Vousdoukas, M. I. (2014). Physical modelling of water, fauna and flora: Knowledge gaps, avenues for future research and infrastructural needs. *Journal of Hydraulic Research*, *52*(3), 311–325. https://doi.org/10.1080/00221686.2013.876453

Tschisgale, S., & Fröhlich, J. (2020). An immersed boundary method for the fluid-structure interaction of slender flexible structures in viscous fluid. *Journal of Computational Physics*, *423*, 109801. https://doi.org/10.1016/j.jcp.2020.109801

USACE. (2002). *Coastal Engineering Manual*. *Coastal Engineering Manual*. https://doi.org/10.1093/intimm/dxs026

USER MANUAL SWAN Cycle III version 41.31A. (n.d.). Delft University of Technology.

USER MANUAL SWASH version 7.01. (2020). Delft University of Technology.

van Loon-Steensma, J. M. (2014). *Salt marshes for flood protection (Summary Thesis)*.

van Loon-Steensma, J. M. (2015). Salt marshes to adapt the flood defences along the Dutch Wadden Sea coast. *Mitigation and Adaptation Strategies for Global Change*, *20*(6), 929–948. https://doi.org/10.1007/s11027-015-9640-5

Van Loon-Steensma, J. M., Hu, Z., & Slim, P. A. (2016). Modelled Impact of Vegetation Heterogeneity and Salt-Marsh Zonation on Wave Damping. *Journal of Coastal Research*, *32*(2), 241–252. https://doi.org/10.2112/JCOASTRES-D-15-00095.1

van Veelen, T. J., Karunarathna, H., & Reeve, D. E. (2021). Modelling wave attenuation by quasi-flexible coastal vegetation. *Coastal Engineering*, *164*, 103820. https://doi.org/10.1016/j.coastaleng.2020.103820

Vouk, I., Pilechi, V., Proval, M., & Murphy, E. (2021). *Nature-Based Solutions for Coastal and Riverine Flood and Erosion Risk Management* (Issue October).

Vousdoukas, M. I., Paul, M., Penning, W. E., & Dijkstra, J. T. (2013). Plants, hydraulics and sediment dynamics. *Critical Review of Ecohydraulic Experiments*, *JANUARY*, 25–69.

Vuik, V., Borsje, B. W., Willemsen, P. W. J. M., & Jonkman, S. N. (2019). Salt marshes for flood risk reduction: Quantifying long-term effectiveness and life-cycle costs. *Ocean and Coastal Management*, *171*(January), 96–110. https://doi.org/10.1016/j.ocecoaman.2019.01.010

Vuik, V., Jonkman, S. N., Borsje, B. W., & Suzuki, T. (2016). Nature-based flood protection: The efficiency of vegetated foreshores for reducing wave loads on coastal dikes. *Coastal Engineering*, *116*, 42–56. https://doi.org/10.1016/j.coastaleng.2016.06.001

Vuik, V., van Vuren, S., Borsje, B. W., van Wesenbeeck, B. K., & Jonkman, S. N. (2018). Assessing safety of nature-based flood defenses: Dealing with extremes and uncertainties. *Coastal Engineering*, *139*(April), 47–64. https://doi.org/10.1016/j.coastaleng.2018.05.002

Whitworth, Andrew. "Mangrove Forest Restoration Boosts Costa Rica Communities (Commentary)." *Mongabay Environmental News*, 24 July 2020, news.mongabay.com/2020/07/mangrove-forest-restoration-boosts-costa-rica-communities-commentary/.

Willemsen, P. W. J. M., Borsje, B. W., Vuik, V., Bouma, T. J., & Hulscher, S. J. M. H. (2020). Field-based decadal wave attenuating capacity of combined tidal flats and salt marshes.

Coastal Engineering, *156*(December 2019), 103628. https://doi.org/10.1016/j.coastaleng.2019.103628

Wollenberg, J. T., Biswas, A., & Chmura, G. L. (2018). Greenhouse gas flux with reflooding of a drained salt marsh soil. *PeerJ*, *2018*(11), 1–20. https://doi.org/10.7717/peerj.5659

Wu, W. C., & Cox, D. T. (2016). Effects of vertical variation in vegetation density on wave attenuation. *Journal of Waterway, Port, Coastal and Ocean Engineering*, *142*(2), 1–9. https://doi.org/10.1061/(ASCE)WW.1943-5460.0000326

Yang, Y., Irish, J. L., & Weiss, R. (2017). Impact of patchy vegetation on tsunami dynamics. *Journal of Waterway, Port, Coastal and Ocean Engineering*, *143*(4), 1–16. https://doi.org/10.1061/(ASCE)WW.1943-5460.0000380

Zelo, I., & Shipman, H. (2000). *Alternative Bank Protection Methods for Puget Sound Shorelines*.

Zhu, L., & Chen, Q. (2019). Discussion of "Field-based numerical model investigation of wave propagation across marshes in the Chesapeake Bay under storm conditions" by Juan L. Garzon, Tyler Miesse and Celso M. Ferreira. *Coastal Engineering*, *149*(February), 1–3. https://doi.org/10.1016/j.coastaleng.2019.03.005

Zuzek, P. J. (2016). Natural and Nature Based Features Workshop. *Coastal Zone Canada Conference*.

Appendix A: Physical Modelling of NBS for Coastal Protection

A. Deformation of *Spartina patens* and *Spartina alterniflora* stems under wave action

Pre-print of an article published in the Coastal Engineering Journal, *Taylor & Francis*.

A.1. Contribution

As a co-author of the following work, the author of this thesis contributed to it in a number of ways. He assisted the lead author in experimental design and execution, both during the flume experiments and afterwards in the measurement of the reported biophysical parameters of the vegetation. He also provided input to the data analysis which contributed to the numerical modelling outlined in the body of the thesis.

A.2. Introduction

Globally, coastal flood and erosion risk is increasing in the context of climate change, including the effects of sea level rise (IPCC 2022; Muis et al. 2020; Vitousek et al. 2017). Conventionally, "hard" engineering structures such as seawalls and breakwaters have been used to protect developed shorelines (Temmerman et al. 2013; Wu et al. 2011). However, the static nature of these structures means they are limited in their capacity for adaptation under changing hydrodynamic conditions, and thus less resilient in a changing climate (Gracia et al. 2017; Temmerman et al. 2013). Additionally, hard coastal infrastructure is known to produce potential adverse environmental effects, including loss of intertidal habitat, sediment supply disturbances, and accelerated erosion of the structure periphery (Gracia et al. 2018; Bilkovic et al. 2017; Temmerman et al. 2013). The limitations associated with hard infrastructure have thus encouraged more multi-disciplinary approaches to coastal erosion and flood risk management. Nature-based solutions (NBS) are one such approach, providing promising strategies for protecting vulnerable coasts in the context of climate change through utilizing the natural ability of ecosystems to self-repair and dynamically respond to changing external stressors (Piercy et al. 2021; Spalding et al. 2014). The coastal protection capabilities of natural environments such as reefs, sea grass meadows, salt marshes, mangrove forests and gravel beaches have been acknowledged for decades (Manca et al. 2012; Komar 2007; Fonseca & Cahalan 1992), however their consideration for use in engineered coastal protection strategies is presently limited, particularly in Canada where there have been few studies performed to address the distinct regional climates and native fauna (Rahman et al. 2019; Tschirky et al. 2000).

Coastal marsh vegetation delivers numerous positive ecosystem services related to coastal flood and erosion risk management in low- and medium-energy wave climates, with performance under high-energy wave climates still under investigation (Rupprecht et al. 2017; Moller et al.

2014). The coastal protection capacity of marsh vegetation is strongly tied to flow-stem interactions, including wave attenuation associated with vegetation-induced flow resistance and erosion protection resulting from reduced bed shear stresses within vegetated canopies and stabilization by plant roots (Wang et al. 2021). Physical and numerical modeling efforts have endeavored to quantify the coastal protection capacity of various coastal marsh species to inform nature-based design practices. Previous physical modeling studies have investigated the relative influence of various plant biophysical parameters (stem flexibility, stem width and height) and hydrodynamics (wave height, wave period period) on coastal protection function, particularly wave attenuation (Anderson & Smith 2014; Augustin et al. 2009; Paul et al. 2016; Moller et al. 2014; Ozeren et al. 2014; Wu & Cox 2016; Blackmar et al. 2014; Lima et al. 2006; Tschirky et al. 2000; van Veelen et al. 2020; Mendez & Losada 2004). Most of these studies yielded an estimate of the canopy bulk drag coefficient ($C_{D,canopy}$) to characterize wave energy dissipation and parameterize wave attenuation at canopy scales in numerical models (Augustin et al. 2009; Anderson & Smith 2014; Ozeren et al. 2014; van Veelen et al. 2020; Wang et al. 2021; Moller et al. 2014; Wu & Cox 2016).

To date, few experimental studies have been conducted with live vegetation due to plant husbandry challenges in laboratory settings and significant facility requirements. Alternatively, the majority have used surrogate elements of various materials and complexities to represent live vegetation. Augustin et al. (2009) investigated the effect of water depth on the wave attenuation capacity of *Spartina alterniflora* utilizing prototype-scale model vegetation. This study utilized both rigid and flexible elements to represent *S. alterniflora*: cylindrical wooden dowels and polyethylene foam tubing, respectively (Augustin et al. 2009). Wu et al. (2011) and Ozeren et al. (2014) compared the performance of live plants to vegetation surrogates using rigid birch dowels, flexible EDPM foam-rubber cords and live *S. alterniflora* and *Juncus roemarianus* plants, and found that the surrogate elements did not accurately capture the vertical variation in vegetation properties present in live vegetation. Anderson & Smith (2014) investigated the wave attenuation capacity of *Spartina alterniflora* using semi-flexible cross-linked polyolefin (XLPO) tubing. Surrogate vegetation was tested with various irregular wave configurations, through varying submergence ratio (or relative depth – stem length divided by water depth, *l/d*), wave height, wave period and stem densities (Anderson & Smith 2014). Wu & Cox (2016) investigated the impacts of water depth on irregular wave attenuation through homogeneous versus heterogeneous stands of salt marsh vegetation, utilizing zip ties to model *Schoenoplectus pungens* at small-scale (1:4). Other flexible or semi-flexible elements that have been used include braided nylon rope, used by Lima et al. (2006) to represent *Brachiaria subquadripara*, strips of plastic Lexaan plates and silicon sealants (Paul et al. 2016; van Veelen et al. 2020).

To address the limited number of live vegetation studies, Lara et al. (2016) and Maza et al. (2015) conducted a full-scale experimental program with live *Puccinellia maritima* and *Spartina anglica* plants. Their study yielded an assessment of the comparative wave damping capacity of *P. maritima* and *S. anglica*, as well as guidelines for physical modeling with live vegetation,

providing recommendations for plant sourcing and plant husbandry (Lara et al. 2016; Maza et al. 2015). Overall, experimental wave studies using live coastal marsh vegetation have been limited to few salt marsh species, including *P. maritima* (Rupprecht et al. 2017; Lara et al. 2016; Maza et al. 2015; Moller et al. 2014), *S. anglica* (Paul & Kerpen 2021; Poppema et al. 2019), *Elymus athericus* (Paul & Kerpen 2021; Rupprecht et al. 2017; Moller et al. 2014), *Atriplex prostrata* (Moller et al. 2014), *Spartina alterniflora* and *Juncus roemarianus* (Wu et al. 2011).

Vegetation flexibility has been found to have a significant impact on wave attenuation, particularly when hydrodynamic conditions are high enough that wave-induced vegetation motion occurs (Luhar & Nepf 2016; Rupprecht et al. 2017; Lei & Nepf 2019). Mullarney & Henderson (2010) investigated the influence of vegetation flexibility on wave attenuation, deriving an analytical model for wave-induced single-stem motion that was validated against field observations of *Schoenoplectus americanus* stems. The model developed in their study yielded that moderately flexible salt marsh species stems, such as *S. americanus*, provide approximately 30% of the wave damping capacity of equivalent rigid stems (Mullarney & Henderson 2010). van Veelen et al. (2020) further investigated the influence of vegetation flexibility on wave attenuation through a combined physical and numerical study. This study found that the drag coefficient for flexible vegetation had consistent correlations with stem Reynolds number, Re (**Eq. A-1**), relative wave height (wave height/water depth), Froude number, Fr (**Eq. A-2**) and Keulegan-Carpenter number, KC (**Eq. A-3**). Conversely, it was found that the drag coefficient of rigid vegetation was only strongly correlated to parameters that incorporated stem diameter (Re and KC) (van Veelen et al. 2020). This indicates that attenuation by rigid vegetation is dictated primarily by vegetation physical properties and not flow conditions, whereas the attenuation by flexible vegetation is more dependent on hydrodynamic conditions (van Veelen et al. 2020; Bradley & Houser 2009).

$$Re = \frac{U_c b_v}{\nu} \quad \textbf{(A-1)}$$

$$F_r = \frac{U_c}{\sqrt{gd}} \quad \textbf{(A-2)}$$

$$KC = \frac{U_c T}{b_v} \quad \textbf{(A-3)}$$

In which U_c is the characteristic velocity acting on the plant stem (m/s), b_v = plant stem width (m), ν = kinematic viscosity of water (m^2s^{-1}), g = gravitational constant (9.81 ms^{-2}), d = water depth (m) and T = wave period (s). The definition of characteristic velocity varies across studies in literature. For the present study, the characteristic velocity is defined as the incident maximum horizontal orbital velocity (in the direction of wave propagation), measured 10 cm above the flume bed and adjacent to the plant stem.

This dependence of flexible vegetation drag on hydrodynamic conditions is in-part due to induced vegetation motion. Vegetation motion alters the relative velocity between the fluid and vegetation, consequently impacting drag forces and wave energy dissipation (van Veelen et al.

2020; Bradley & Houser 2009). Two primary mechanisms of wave-induced vegetation motion have been identified in literature: swaying motion and whip-like motion (Ghisalberti & Nepf 2002; Losada et al. 2016; Rupprecht et al. 2017). Swaying motion is characterized by symmetry in the forward (the direction of wave travel) and backward bending angles, whereas whip-like motion is characterized by an extended, wider-angled forward bend, followed by a rapid, small-angled backward bend (Bradley & Houser 2009; Paul et al. 2012; Rupprecht et al. 2017). Whip-like movement can cause a flattening of the vegetation canopy for an extended portion of the wave cycle - resembling that of vegetation under unidirectional current flow, with wide stem extension in the direction of wave travel - resulting in a reduction in vegetative resistance to flow (Rupprecht et al. 2017; Gosselin 2019). Additionally, the asymmetry of motion in whip-like states alters the relative plant-fluid velocity (u_r), which should be used to estimate the drag force induced by flexible stems (**Eq. A-4**):

$$F_x = \frac{1}{2}\rho C_D A_p u_r |u_r| \quad \textbf{(A-4)}$$

In which F_x = horizontal drag force (N), ρ = water density (kgm^{-3}), C_D = depth-averaged stem drag coefficient, A_p = frontal area of the plant (m^2) and u_r = the relative velocity between fluid and plant (Zhang & Nepf 2021; Mendez & Losada 2004).

Rupprecht et al. (2017) investigated wave-induced live vegetation reconfiguration using live *Elymus athericus* and *Puccinellia maritima*, two salt marsh species of significantly different flexural rigidities, under increasing hydrodynamic conditions (regular, non-breaking waves). Rupprecht et al. (2017) correlated the onset of motion, and transition between motion states (swaying to whip-like), to the wave Cauchy number (*Ca*) - the ratio of drag forces to restoring forces due to material stiffness (**Eq. A-5**) - and to the ratio of plant stem height to wave orbital excursion (*L*, **Eq. A-6**):

$$Ca = \frac{\rho b_v U_c^2 l^3}{EI} \quad \textbf{(A-5)}$$

$$L = \frac{l}{A}, A = \frac{U_c}{\omega} \quad \textbf{(A-6)}$$

In which *EI* = stem flexural rigidity (Nm^2), defined by the product of *E* = elastic modulus (Nm^{-2}) and *I* = 2nd moment of inertia (m^4), *l* = plant stem height (m), *A* = wave orbital excursion (m), and ω = wave angular frequency (ω=2π/*T*, rads^{-1}) (Rupprecht et al. 2017; Luhar & Nepf 2016). These dimensionless variables have been identified as the most important parameters governing vegetation motion (Luhar & Nepf 2016). For highly flexible aquatic vegetation, the buoyancy parameter (*B*), which considers restoring forces due to buoyancy, is also significant for stem reconfiguration (Rupprecht et al. 2017; Luhar & Nepf 2016). However, *B* can be neglected in the case of salt marsh plants, which exhibit relatively high stiffness versus other flexible aquatic vegetation such as seagrasses (Rupprecht et al. 2017, Luhar & Nepf 2016). For large values of *Ca*, significant deformation of flexible elements is expected, and the relative velocity (u_r) becomes very different from the fluid velocity, *U*. Rupprecht et al. (2017) also recorded stem

bending angles in and counter to the direction of wave travel to assess transitions between motion states and thresholds of irreversible deformation (i.e., stem folding).

There are uncertainties surrounding the reliability and accuracy of data pertaining to wave-vegetation interactions captured by studies using vegetation surrogates, which exhibit morphological and biomechanical simplifications in comparison to their live counterparts and thus may not accurately mimic live vegetation flexibility or motion (Vettori & Nikora 2020; Zhang & Nepf 2021; Blackmar et al. 2014; Tempest et al. 2015; Ozeren et al. 2014). Based on the findings of Rupprecht et al. (2017) and van Veelen et al. (2020), among others, it is evident that characterization of wave-induced flexible vegetation motion is integral for understanding and quantifying the wave attenuation capacity of coastal marsh vegetation. However, due to a lack of experimental studies with live vegetation this knowledge gap has remained largely unaddressed, even more-so neglected in a Canadian context. To address this, prototype-scale experiments were conducted with live vegetation in the large wave canal at the Institut National de la Recherche Scientifique (INRS) in Quebec, Canada. Two salt marsh species native to the Canadian coastline were selected: smooth cordgrass (*Spartina alterniflora*) and salt marsh hay (*Spartina patens*). These are the dominant coastal marsh species within the Bay of Fundy, in Nova Scotia and New Brunswick (Gordon et al. 1985; Wu et al. 2011). *S. patens* are also found on the west (Pacific) coast of Canada, whereas the native distribution of *S. alterniflora* in Canada is primarily limited to the east (Atlantic) coast (Natural Resources Conservation Service 2021). Presently, few comprehensive wave-vegetation motion studies for *S. alterniflora* have been performed (Zhang & Nepf 2021) and, to the authors' knowledge, *S. patens* has not been studied in this context.

The objectives of the experimental program were to investigate irregular wave-induced motion of the two selected plant species (*S. patens* and *S. alterniflora*), using the stem bending angle to characterize motion type and quantify stem deformation. Various wave heights, wave periods and water depths were considered to investigate the influence of hydrodynamic conditions and relative stem submergence on flexible vegetation motion. *S. patens* and *S. alterniflora* have distinct morphologies and stiffness characteristics, allowing for investigation of the role of plant biophysical and biomechanical parameters on stem deformation and motion. An additional novel aspect of this study was the use of live vegetation in an outdoor flume facility for an extended period, yielding practical insight to support plant husbandry practices in controlled experimental settings.

A.3. Experimental Program

A.3.1. Flume Setup

Experiments were conducted in the Large Wave Canal of the Laboratoire Hydraulique Environnemental (LHE) at the Institut National de la Recherche Scientifique (INRS) located in Quebec City, Canada (**Figure A-1**Error! Reference source not found.). The wave flume measures 120 m long by 5 m wide and 5 m deep, and utilizes a piston-type wave generator with a 4 m stroke.

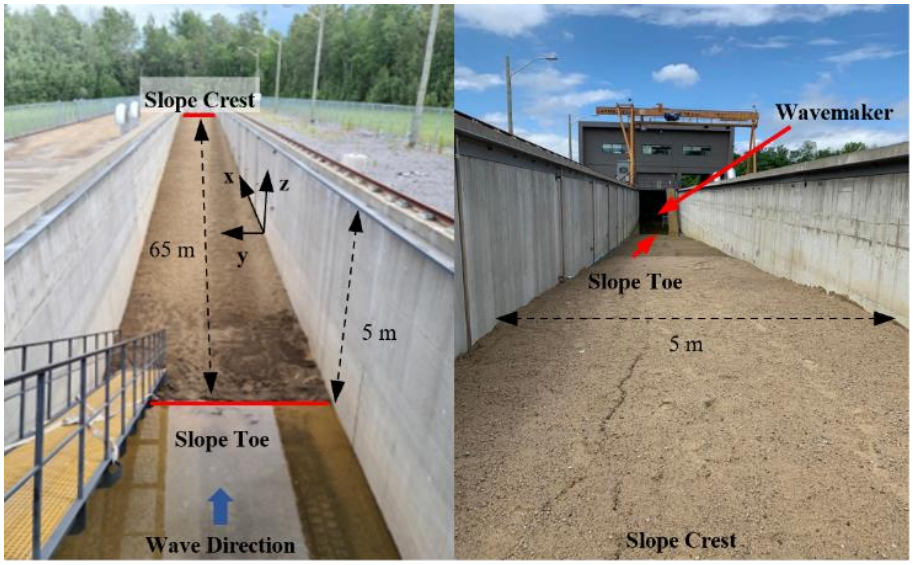

Figure A-1. View away from (left) and towards (right) the wavemaker in the large wave canal, LHE (Institut National de la Recherche Scientifique, Quebec).

A 1:18 (vertical: horizontal) sand slope (median grain diameter, D_{50} = 285.9 μm) was installed in the canal, with its toe located at a distance of 27 m from the wave paddle. To avoid significant influences of bed morphology changes during experimentation, the slope was first subjected to 16-hours of moderate wave action (JONSWAP spectrum; zero-moment wave height, H_{m0} = 0.5 m; peak wave period, T_p = 3.5 s; water depth, d = 2.5 m). Slope morphology changes during subsequent tests with smaller waves and vegetation were negligible and did not influence observed wave-vegetation interactions. The cross-shore profiles of the sand slope before and after the 16-hour exposure to H_{m0} = 0.5 m waves are compared in **Figure A-2**; some sorting of sediments in the cross-shore direction were observed, but no large morphological changes occurred.

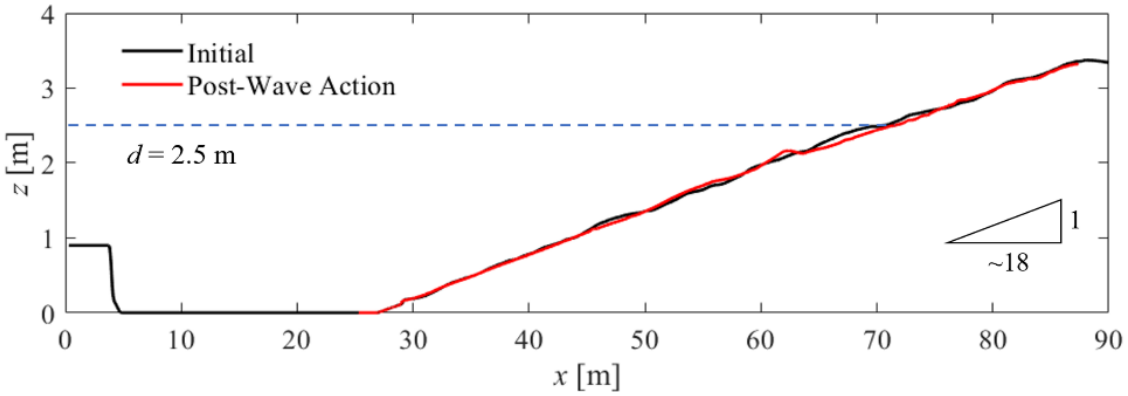

Figure A-2. Constructed sandy slope (1:18), before (black) and after (red) 16-hours of moderate wave action (JONSWAP, Hm0 = 0.5 m, Tp = 3.5 s, d = 2.5 m). Still water level is indicated by the blue dotted line.

A.3.2. Plant husbandry and installation

Plants were sourced from a natural marsh located in Trois-Pistoles, Quebec, Canada, either as juvenile plants or as seeds that were subsequently grown in a local greenhouse. Plants were installed in rows with each row containing two plots (**Figure A-3**). Their spatial organization was selected such that there would be very little interaction between plots, allowing independent observations of wave-vegetation interactions for individual plots.

Live plants were transplanted directly into the sandy slope. The first row was placed 15.3 m from the slope toe (42.2 m from the wave paddle) at an elevation of 0.96 m above the flume bottom. Five rows of each *S. alterniflora* and *S. patens* were installed, with *S. alterniflora* populating the lower elevation section. Within each row, two plots of vegetation were installed 1 m apart laterally: (1) an individual stem, and (2) an adjacent cluster of 8 stems. Stems planted in the cluster had a 15-cm spacing, and a 3-2-3 staggered row arrangement as shown in Error! R eference source not found.. Rows were spaced 3 m apart in the cross-shore direction, so that the elevation range for each species spanned ~0.7 m.

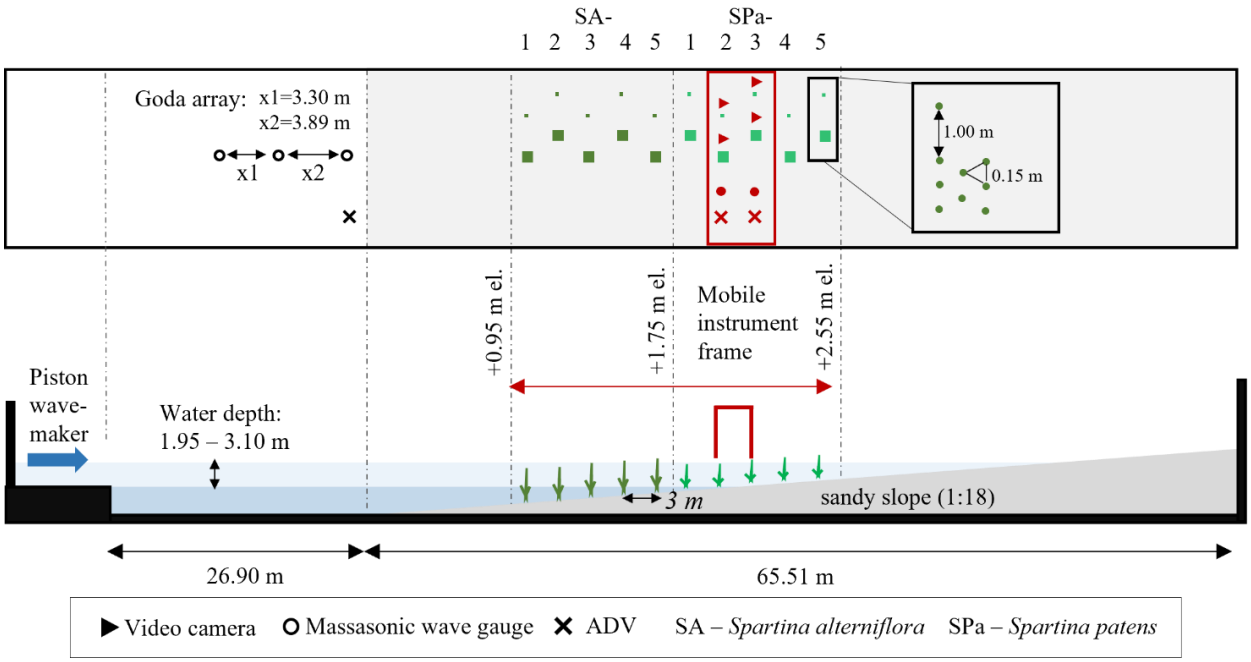

Figure A-3. Instrumentation and vegetation set-up in the large wave canal at LHE, INRS. Instruments installed on the frame (red) were moved along the flume length indicated by the red arrow.

All plants were transplanted into the wave canal between July 6-8, 2021. For each individual plant, a hole was dug approximately 20 cm deep, approximately three quarters filled with potting soil (Microrhizae ProMix BX General Purpose, commercially available) and topped with approximately 1 teaspoon of fertilizer (Botanika Green annual & perennial flowers fertilizer). Individual plants were planted in the potting soil, with an approximate planting depth of 10 cm, and then the remainder of the hole was filled in with sand and compacted manually (body weight). Each plot was watered immediately after planting. A similar planting methodology was

used for the cluster plots, except the initial hole was dug wider to accommodate 8 plants at 15-cm spacing (~0.5 m diameter hole). Plants were left to grow in the flume for 3 weeks before testing began on July 28, 2021. During this period, plants were watered every 2-3 days. *S. patens* plants were hand-watered, whereas *S. alterniflora* plants were fully inundated by raising the water level in the flume for 6-8 hours. Soil was sufficiently compacted around each plant plot such that there were no observed impacts to soil levels following significant rainfall events. Error! Reference source not found. compares the plant husbandry methods used in this study w ith those used in previous experimental programs with live vegetation. The guidelines for physical modeling with live vegetation by Lara et al. (2016) were considered in the development of the experimental program and plant care techniques.

Table A-1. Summary of plant husbandry methodologies for physical modeling with live vegetation.

Study	Test Species	Source	Geography	Watering method	Fertilizer	Storage/ Growth Setting
Poppema et al. (2019)	• *Spartina anglica*	From seed (growing)	Western Scheldt Estuary, the Netherlands	Tidal mesocosms (semi-diurnal, 2-hour inundation, 23 ppt salinity)	No	Indoor
Moller et al. (2014)	• *Elymus athericus*, • *Puccinellia maritima*, • *Atriplex prostrata*	Excavated marsh blocks (collecting)	German Wadden Sea	Drained every 2 days for 12-hours of open-air gas exchange	No	Outdoor
Wu et al. (2011)	• *Spartina alterniflora*, • *Juncus roemarianus*	Outdoor nursery (growing)	Louisiana	Fully inundated for 30 days	No	Indoor
Maza et al. (2015), Lara et al. (2016)	• *Spartina anglica*, • *Puccinellia maritima*	From seed (growing) and collecting	Scheldt Estuary, the Netherlands	Primarily watered with freshwater, occasionally saltwater	Yes	Outdoor
Silinski et al. (2015)	• *Scirpus maritimus*	From seed (growing) and collecting	Scheldt Estuary, the Netherlands	n/a	No	Outdoor
Paul & Kerpen (2021)	• *Spartina anglica*, • *Elymus athericus*	Sod (collecting)	The Netherlands	Watered and occasionally inundated with freshwater	No	Outdoor

A.3.3. Instrumentation

A mobile frame was constructed such that instruments could be deployed simultaneously along two plant rows during each test, monitoring four plant plots per wave test. The frame was designed to support two acoustic Doppler velocimeters (ADVs) and two acoustic wave gauges, one of each in line with each row of plants to provide reference incident velocities and wave height measurements. Adjustable mounts were installed on the frame in line with each of the four plant plots for deployment of GoPro HERO8 cameras. The mobile frame setup is shown in **Figure A-4**, which also shows the instrument positioning relative to the plants. The frame was moved along the length of the flume to capture data from multiple plant rows under repeated wave conditions. At each new location, the ADVs were adjusted to maintain a position 10-cm above the slope surface.

In addition to the mobile instrumentation, three fixed acoustic wave gauges were deployed between the wavemaker and the slope toe. These wave gauges formed a Goda-type array (x_1 =

3.30 m, x_2 = 3.89 m) for estimation of wave reflection during testing (Lin & Huang 2004). Wave gages obtained water surface elevation at a sampling rate of 50 Hz, and ADVs obtained velocity in the *x*, *y* and *z*-direction also at a rate of 50 Hz. GoPro cameras obtained video footage in rectangular mode (to minimize impacts of fisheye distortion) at a rate of 30 frames per second (fps). The experimental setup (instrumentation and plant arrangement) in the Large Wave Canal is shown in **Figure A-4.**

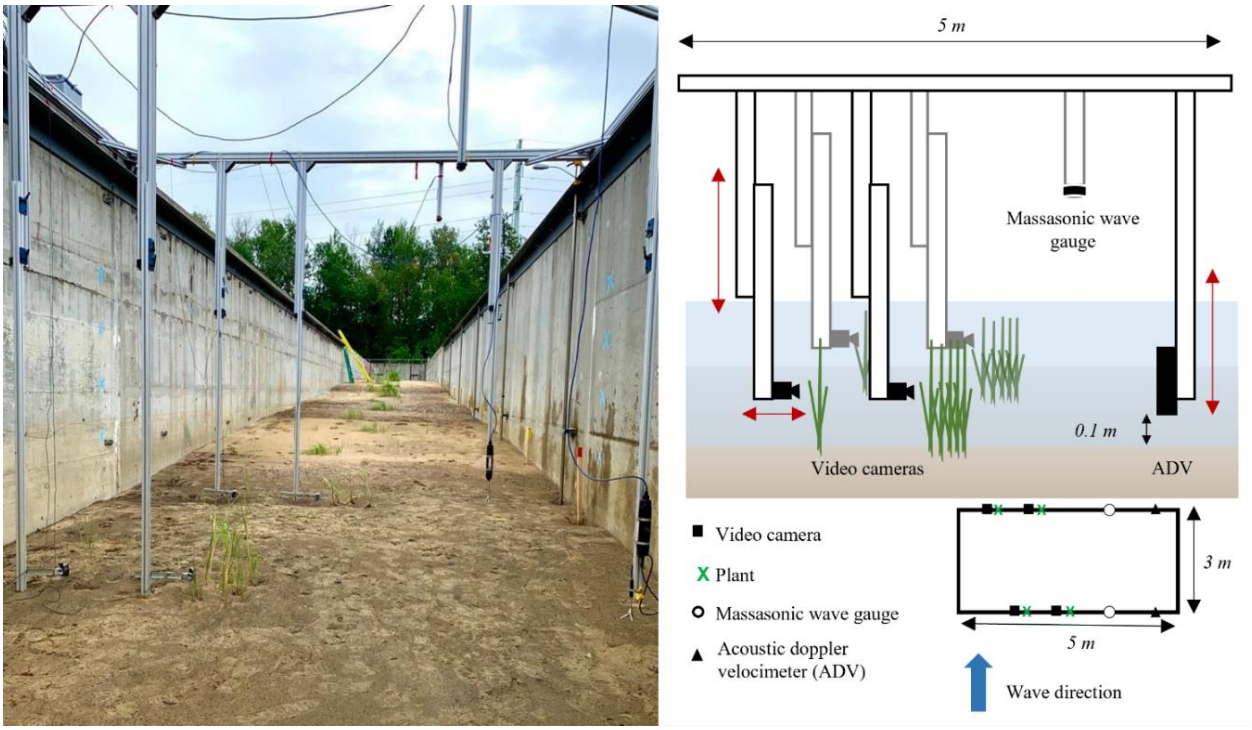

Figure A-4. Mobile instrumentation frame: photo from within the canal [left] and schematic of frame setup [right]; not drawn to scale. The individual plant plots are closest to the flume wall, with plant clusters closer to the flume center. Instrumentation deployed on the frame consisted of GoPro HERO8s (4), acoustic wave gauges (2) and Acoustic Doppler Velocimeters (2).

A.3.4. Wave and Water Level Conditions

A series of experiments were conducted to investigate wave-induced vegetation motion under irregular wave action. Mild wave conditions, with incident offshore wave heights ranging from 0.1 m < H_{m0} < 0.2 m at two different peak wave periods (T_p = 2.5 s and 10 s) were used to capture the comparative response of vegetation to small, short period seas and longer period swells. All wave conditions were synthesized from JONSWAP spectra (peak enhancement factor, γ = 3.3; number of wave components, *nc* = 100). The active wave absorption function was used for all experiments considering the water depth at the face of the wavemaker. Three water depths (*d* =1.95 m, 2.55 m, 3.10 m, measured at the wavemaker) were selected to represent a range of submergence ratios for each plant species (*S. alterniflora*: 0.60 < *l*/*d* < 2.52, *S. patens*: 0.58 < *l*/*d* < 2.04). At each water depth, the motion of several rows of plants was captured. This required incrementally moving the instrumentation frame along the slope profile as it was only

equipped to record two rows at a time. The hydrodynamic conditions and plant motion at each station were recorded for five minutes before moving the frame to the next station.

A.3.5. Video Analysis of Stem Deformation

A frame-by-frame analysis of the GoPro camera video footage was performed using Matlab, with two main steps: (1) frame pre-processing (contrast enhancement) and (2) manual stem bending angle tracking. Prior to analysis, potential lens distortion was quantified using *estimateFisheyeParameters* (MATLAB 2021). Polynomial distortion coefficients were negligible for all cameras (average a_2=1.3x10-4, a_3=-5.2x10-7, a_4=3.78x10-10); thus, no correction was applied to minimize the already high computational requirements for video processing. For video observations of clustered plant plots, a single stem from the cluster was selected for stem deformation tracking.

(1) Contrast enhancement

Video frames were pre-processed to enhance contrast and improve plant structure visibility despite the underwater setting. This was done through conversion of the image from RGB to LAB colour spaces (*rgb2lab*) and applying a contrast-limited adaptive histogram equalization function (*adapthisteq*) along the Red/Green and Blue/Yellow axes in Matlab (MATLAB 2021). The corrected image was then converted back to RGB format before continuing with bending analysis.

(2) Stem bending angle tracking

Manual stem tracking consisted of frame-by-frame image analysis performed in Matlab. The videos of stem motion were resampled at a frame rate between 1 and 3 Hz, selected to optimize computation time and tracking accuracy, while considering the magnitude and period of motion. For the first frame, the stem base was selected, and for every proceeding resampled frame the distal end of the stem was selected. In instances where the stem base moved throughout the video, translational corrections were applied to the selected distal stem locations. The selected coordinate pairs were then converted to angles (degrees) and adjusted for initial plant posture. Finally, a linear interpolation function was applied to compute a continuous time series of bending angle. Due to the significant time requirements associated with the video analysis described herein, bending angle tracking was completed for approximately 20 waves per wave condition. Automated stem tracking was attempted to amend analysis requirements; however, the tested methods were unsuccessful due to stem interactions and crossover. A description of the attempted automated stem tracking analysis is provided in Section 3.1.4.4.

A.4. Results

A.4.1. Plant Husbandry

The live plants used for experimentation remained in the outdoor wave canal for 6 weeks (July 6-August 17, 2021), during which temperatures in the region (Quebec City, Canada) ranged from 9.3°C to 31.5°C, with a mean temperature of 20°C and total precipitation of 133.2 mm

(Government of Canada 2021). Plots of daily precipitation and temperature data for the entire duration are provided in **Figure A-5**.

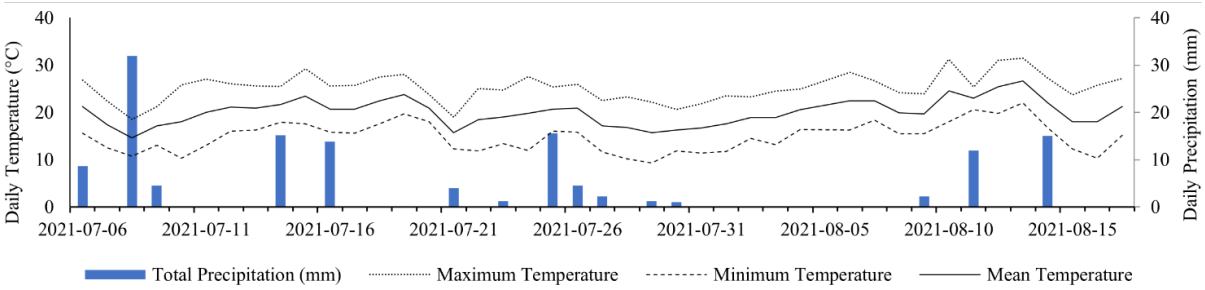

Figure A-5. Temperature fluctuations and total precipitation during period of outdoor experimentation with live vegetation. Data was obtained from the Government of Canada Historical Climate Data portal (Government of Canada 2021).

Minimal plant loss was observed during this period, demonstrating success of the implemented plant installation and maintenance techniques. New growth was identified at several plots, particularly for the *S. alterniflora*, after as few as 19 days (**Figure A-6**). Following experimentation, selected plant plots were harvested from the flume, maintaining intact root structures. Significant root growth was observed for both *S. patens* and *S. alterniflora* amongst the harvested plants (**Figure A-6**), with root interactions between individual plants particularly prominent between the *S. patens* clusters. This further demonstrates the potential value of outdoor experimental programs with live vegetation, particularly for investigating the erosion control benefits of vegetation, which depend on soil-root interactions and thus cannot be tested accurately with vegetation surrogates.

Figure A-6. Successful establishment of transplanted vegetation, demonstrated through the growth of new shoots adjacent to planted Spartina alterniflora stems [top, circled], and development of significant root structures [bottom left – S. patens; bottom right – S. alterniflora]; 1 m ruler used for scale. The dotted lines delineate aboveground biomass from belowground biomass (roots). Average root length post-experimentation was 28 +/- 9.9 cm for S. patens (n = 24), and 19 +/- 5.5 cm for S. alterniflora (n = 22).

A.4.2. Plant Bio-Physical Parameters

Stem Height, Width, and Morphology

S. alterniflora plants were characterized by a single semi-rigid stem, with several thinner, flexible blades. The blades were arranged uniformly around the stem, at the same approximate angle from the vertical (~ +/- 15°). Average stem length for the sampled *S. alterniflora* plants was 62 +/- 18 cm (n=18), with an average stem width of 4.47 +/- 0.89 mm (n=18), measured 10 cm from the stem base (point of stem-soil intersection). *S. patens* plants were characterized by a collection of several flexible, narrow stems, with long flat blades extending orthogonally from the main stems. Average stem length for the sampled *S. patens* plants was 55 +/- 10 cm (n=24), with an average stem width of 1.36 +/- 0.29 mm (n=21). Stem lengths were taken as the full stretched length from blade tip to the base of the stem (aboveground matter only – i.e., above the dotted line, Error! Reference source not found.), using the longest stem in the case of the multi-s temmed *S. patens* plants. Stem tapering of both species was also measured and is plotted in **Figure A-7**. Stem tapering measurements were terminated at a height of 50 cm above the stem base for both species, as stem widths were < 0.1 mm at this point and above. Statistically, the *S. patens* stems were narrower than the *S. alterniflora* stems (t-test; $p < 0.05$). *S. alterniflora* also demonstrated stronger stem tapering than *S. patens*, as shown in **Figure A-7**.

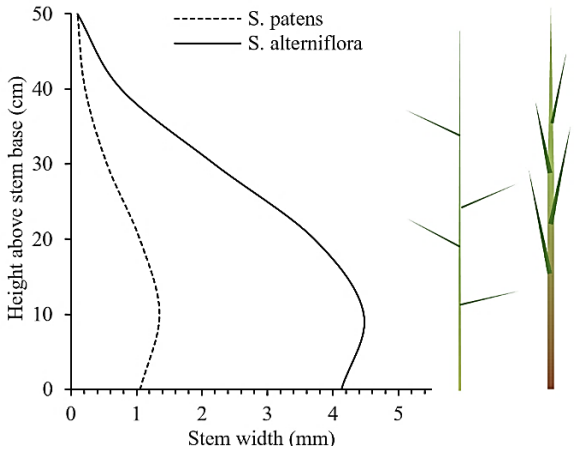

Figure A-7. Variation in stem width with increasing height above the stem base (stem tapering) for S. patens (left) and S. alterniflora (right). Reported values are averages of the measured widths at each height, considering 18 samples of S. alterniflora and 20 samples of S. patens. The stem base can be taken as analogous with the sediment surface. Stem tapering measurements were terminated at a height of 50 cm above the stem base for both species, as stem widths were < 0.1 mm at this point and above.

All of the above-mentioned plant parameters were measured immediately following wave testing. There were no appreciable changes in stem width for either species between the time of planting and the final post-testing measurements. However, stem heights increased, on average, approximately 26% for *S. patens* and 27% for *S. alterniflora* over the six-week growth and testing period, to the final average values reported in **Table A-2**. Inter-species differences in root structure were also observed for the cluster plots upon harvesting the plants after testing. The

roots of *S. alterniflora* generally grew vertically (Error! Reference source not found.), and there w as minimal interaction between the roots of individual plants. The roots of *S. alterniflora* extended through the potting soil and into the underlying sand media. Conversely, the roots of *S. patens* developed horizontally, with significant root interaction between individual plants. The roots of *S. patens* did not grow below the potting soil, but instead extended laterally beyond the radius of the soil and into the adjacent sand.

Table A-2. Summary of biophysical parameters of S. patens and S. alterniflora used for experimentation. Differences in plant parameters were statistically significant for stem width, flexural rigidity and normalized frontal area (t-test; $p < 0.05$).

Parameter		***S. patens***	***S. alterniflora***
Stem width, b (mm)		1.36 +/- 0.29 (n=21)	4.47 +/- 0.89 (n=18)
Stem height, h (cm)		55 +/- 10 (n=24)	62 +/- 18 (n=16)
Frontal area, FA (cm^2)	*Cluster:* *Individual:*	976.5 +/- 265.6 (n=5) 157.2 +/- 69.2 (n=1)	899.9 +/- 175.3 (n=5) 138.9 +/- 28.3 (n=1)
Normalized FA (cm^2/cm)	*Cluster:* *Individual:*	24.3 +/- 7.5 (n=5) 6.0 +/- 2.3 (n=1)	12.6 +/- 1.7 (n=5) 2.2 +/- 0.5 (n=1)
Young's modulus (MPa)		1140 +/- 460 (n=21)	230 +/- 40 (n=18)
Flexural rigidity, EI (Nm^2)		0.0015 +/- 0.0002 (n=21)	0.051 +/- 0.015 (n=18)

Frontal Area and Biomass Distribution

Average frontal area and vertical biomass distributions were quantified for each plant plot using the binary image analysis technique of Neumeier et al. (2005). A colour image of each individual plant and plant cluster was captured using a whiteboard and a tilted mirror to minimize background interference. The Matlab *ColorThresholder* application was used to convert the RGB image to a binary image with the background removed (MATLAB 2021). A scale was applied based on control points of known distance on the whiteboard background, allowing conversion of pixel count to units of frontal area. Values of frontal area, as well as normalized frontal area (divided by the maximum plant height) are provided in **Table A-2**. Vertical biomass distribution and percent lateral obstruction were also quantified for each plant plot (**Figure A-8**), following the methods of Neumeier et al. (2005).

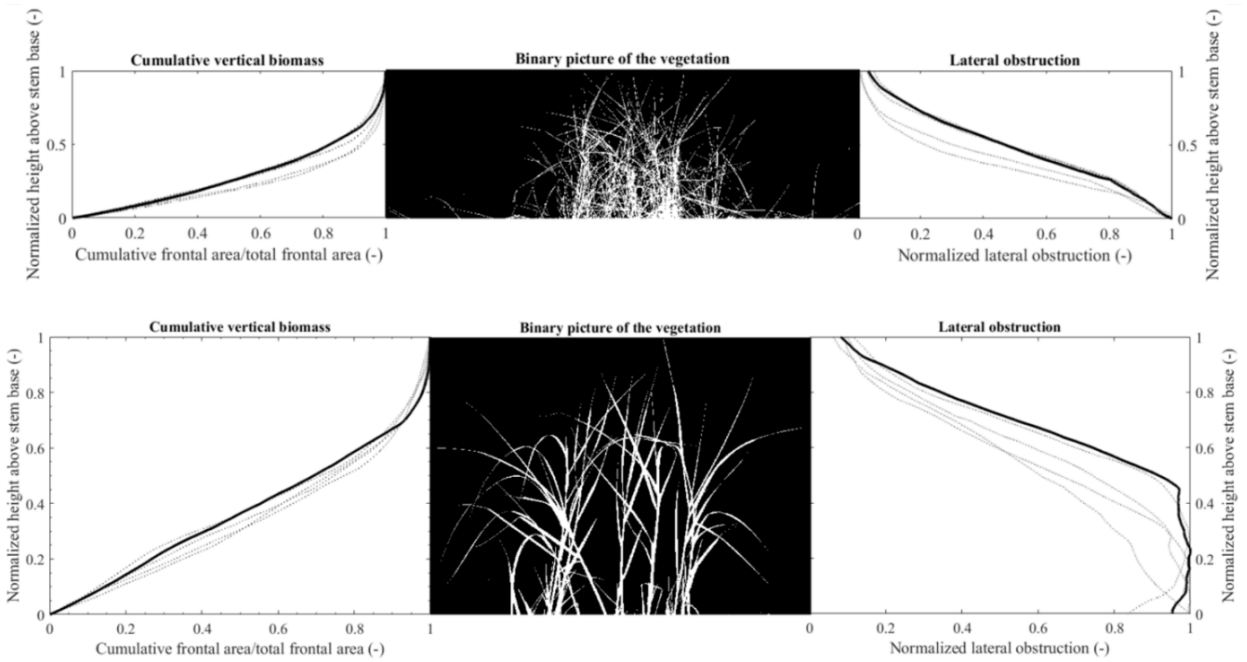

Figure A-8. Vertical variation in vegetation biomass for S. patens [top] and S. alterniflora [bottom]. Solid lines show the distributions for the displayed binary images, dashed lines provide the distribution of the other plots of the same species. Values on the y-axis (height above stem base) have been normalized by the height of each individual plant. Lateral obstruction was also normalized by the maximum percent obstruction for each plant plot.

Biomechanical Testing

Elastic modulus (*E*) and flexural rigidity (*EI*) were estimated for each of the species using the field method described in Feagin et al. (2011). Stems of *S. patens* and *S. alterniflora* were subjected to a three-point bending test immediately upon harvesting. Sections 20 cm in length were cut starting from the base of the stem (one test section per stem) and laid across a beam loading apparatus consisting of two 10 cm wooden dowels spaced 10 cm apart. The stems were loaded at their midpoint with a string-supported plastic cup of known weight and volume, with incremental additions of water. GoPro cameras were mounted in front of the beam loading apparatus, and an image of stem deflection was captured following each addition of water. Image post-processing to quantify maximum deflection per incremental load required georectification to the local coordinate system (using control points stationed behind the beam loading apparatus), and conversion to a binary image based on colour thresholding. Maximum deflection for each captured image was selected as the mid-point of the binary image pixels with values of 1 (i.e., stem pixels), at the intersection point of the applied load. Results from the three-point bending test yielded estimates of elastic modulus for the harvested samples of *S. patens* and *S. alterniflora*: E_{pat} = 1140 +/- 460 MPa and E_{alt} 230 +/- 40 MPa. Flexural rigidity was also estimated for each species through the product of elastic modulus and the 2nd moment of inertia ($I = (\pi/4)b_v^4$). The average diameter of the 20 cm stem segment subjected to bending was taken as b_v in the determination of *I*, based upon three evenly spaced measurements across the sample span (at 0 cm, 10 cm and 20 cm). *S. alterniflora* exhibited a significantly higher flexural rigidity (0.0730 +/- 0.03 Nm^2) than *S. patens* (0.0015 +/- 0.0002 Nm^2) (t-test; $p < 0.05$). Existing studies

of the biomechanical properties of *S. alterniflora* report elastic moduli differing across an order of magnitude, with *E* estimated as 1410+/- 710 MPa by Feagin et al. (2011) and 159.8 MPa by Chatagnier (2012). Estimates of elastic modulus for *S. alterniflora* in the present study fall within the range of Feagin et al. (2011) and Chatagnier (2012). Chatagnier (2012) also performed biomechanical testing on *S. patens* samples, yielding E = 2950 MPa and EI = 0.0028 Nm^2, on the same order of magnitude as the estimates for *S. patens* samples tested herein. **Table A-2** provides a summary of the measured and calculated plant biophysical parameters, including biomechanical properties, for the sampled *S. patens* and *S. alterniflora* plants used in this study.

A.4.3. Hydrodynamic Conditions

The zero-upcrossing method was used to obtain summary statistics for all wave gauges deployed in the Large Wave Canal during testing. Fifty-four wave tests were completed in total (6 different wave conditions at 3 water depths, and 3 replicates of each to account for movement of the instrument frame), however, the video quality for 26 of these tests was insufficient for performing bending angle analysis. A summary of the incident offshore hydrodynamic conditions (as measured by the Goda array, Error! Reference source not found.) for the tests that a llowed bending angle analysis (28 total) is provided in **Table A-3.** Significant wave heights ($H_{s,o}$) were determined through time domain analysis (zero-upcrossing) of the water surface oscillations recorded by the offshore wave gauges, where $H_{s,o}$ was calculated as the average of the highest one-third of the recorded waves. Insufficient video quality was a result of poor underwater visibility in turbid waters, from algae growth and/or sediment re-suspension. This led to a loss of several replicate tests, as reflected by the respective column in **Table A-3.** Values of the Iribarren parameter (ξ), calculated using **Eq. A-7**, are also provided in **Table A-3** along with classification of wave breaker type.

$$\xi = \frac{\tan\alpha}{\sqrt{\frac{H_o}{L_0}}}, L_0 = \frac{9.81T_{s,o}^2}{2\pi}\tanh\frac{2\pi d}{L_0} \quad \textbf{(A-7)}$$

In which $\tan\alpha$ = beach slope (1/18), H_0 = offshore wave height (m) and L_0 = offshore wavelength (m). The offshore significant wave heights ($H_{s,o}$), calculated as described in the paragraph above, were used for H_0, and the corresponding wave periods ($T_{s,o}$), along with offshore water depths (d), were used in the estimation of L_0.

Table A-3. Summary statistics for incident waves, measured offshore of the vegetated slope. Only tests where subsequent bending angle analysis was performed are included. For tests with replicates, the reported parameters are average values. Significant wave height is defined as the average of the largest one-third of the recorded waves, and the reported values present an average of the three offshore wave gauges.

Water depth, d (m)	Offshore significant wave height, $H_{s,o}$ (m)	Offshore significant wave period, $T_{s,o}$ (s)	Iribarren number, ξ (-)	Breaker type	Number of waves	Number of replicates	Plant species captured
1.95	0.075	2.37	0.57	Plunging	133	3	*S. alterniflora, S. patens*
	0.060	10.87	1.55	Plunging	28	1	*S. alterniflora*
	0.114	2.35	0.46	Spilling	138	2	*S. alterniflora*
	0.144	2.42	0.42	Spilling	125	2	*S. alterniflora*
2.55	0.080	2.35	0.57	Plunging	128	3	*S. alterniflora, S. patens*
	0.060	9.77	1.57	Plunging	29	2	*S. alterniflora, S. patens*
	0.118	2.43	0.48	Spilling	131	3	*S. alterniflora, S. patens*
	0.088	9.58	1.29	Plunging	31	1	*S. alterniflora*
	0.164	2.38	0.40	Spilling	124	3	*S. alterniflora, S. patens*
	0.125	9.99	1.10	Plunging	32	1	*S. alterniflora,*
3.10	0.079	2.41	0.59	Plunging	122	1	*S. patens*
	0.062	9.72	1.62	Plunging	33	1	*S. patens*
	0.122	2.42	0.47	Spilling	124	1	*S. patens*
	0.078	10.50	1.51	Plunging	29	1	*S. patens*
	0.164	2.44	0.41	Spilling	132	1	*S. patens*
	0.108	10.08	1.25	Plunging	30	1	*S. patens*

A.4.4. Plant Motion Response to Wave Forcing

Eighty-seven videos of plant motion were analyzed, each capturing stem bending oscillations over a cycle of approximately 20 waves. This corresponded to 40 videos of *S. alterniflora* and 47 videos of *S. patens*. **Figure A-9** provides a sample of the output data from manual stem tracking for both *S. patens* and *S. alterniflora*, with the results overlaid on water surface oscillations recorded by adjacent wave gauges in **Figure A-9 C) and D)**.

Significant wave heights ($H_{s,i}$) and their associated periods ($T_{s,i}$) were extracted from the water surface elevation time series measured by the wave gauges directly in-line with the tracked plants (mobile frame wave gauges, Error! Reference source not found.) using the zero-u pcrossing method. This method was also applied to the bending angle data to allow comparisons between stem extension and hydrodynamic summary statistics, extracting the significant bending angle (average of the highest one-third angles) in the forward and backward directions (F_s, B_s, respectively). Error associated with manual stem bending angle tracking was quantified through duplicate analysis of a random sample of six videos, for which estimates of F_s and B_s were compared pairwise. An approximate error of +/- 0.80 degrees in bending angle estimates was determined from the mean difference between replicate data pairs at the 95% confidence level.

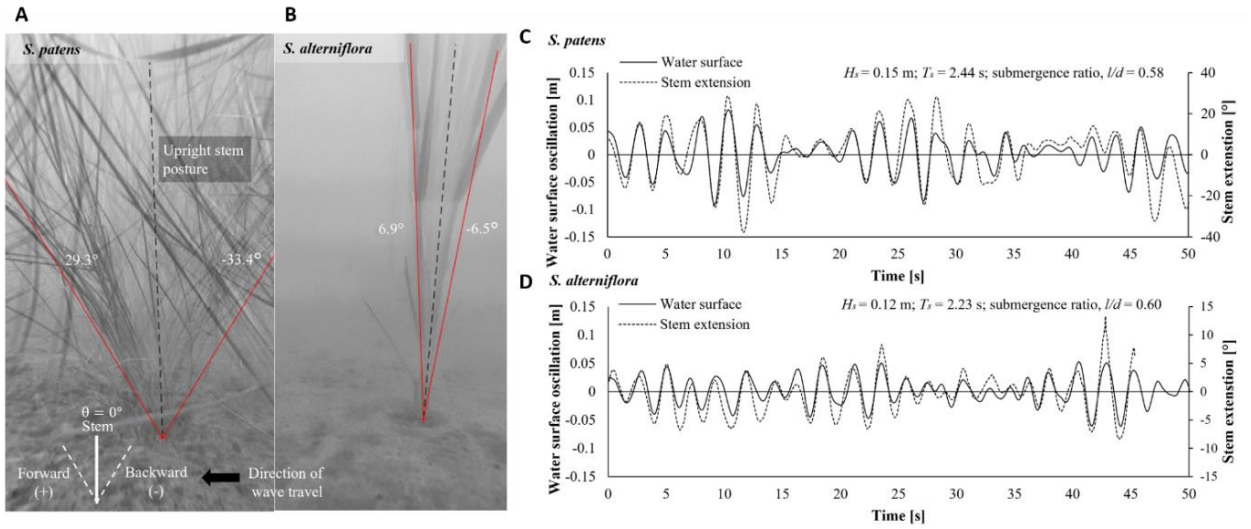

Figure A-9. Wave-induced vegetation motion for S. alterniflora and S. patens under similar hydrodynamic conditions: 0.12 m < Hs < 0.15 m, 2.23 s < Ts < 2.44 s, 0.12 m < h/d < 0.15 m (as measured at the plant location). A) Visual representation of stem tracking for with overlaid image frames for one wave cycle for S. patens and B) S. alterniflora. C) Comparison of stem extension timeseries (manual tracking) with water surface oscillations as recorded by wave gauges at the plant location for S. patens, and D) S. alterniflora.

Stem deformation results were compared between adjacent individual and clustered plant plots observed under the same wave test conditions. There were 34 instances (pairs) where bending angle analysis could be performed on adjacent individual and clustered plant plots (68 video records total). Summary bending angle statistics (F_s and B_s) were compared between the individual and clustered plants for each of these instances yielding two difference datasets: F_s(individual) – F_s(cluster) = F_s(difference), and $|B_s|$(individual) – $|B_s|$(cluster) = B_s(difference), for each *S. alterniflora* and *S. patens*. F_s(difference) and B_s(difference) datasets were subjected to pairwise t-tests for both *S. alterniflora* individual vs. cluster and *S. patens* individual vs. cluster (four statistical tests total). Results from statistical comparison indicated that there was a significant difference ($p < 0.05$) between the forward bending response of *S. patens* stems planted individually versus within a cluster, with the individual stems exhibiting higher degrees of forward bending. There was also a statistically significant difference between the backward bending response of *S. alterniflora* for clustered versus individual stems, with the clustered stems exhibiting a higher degree of bending in the backward direction. Boxplots that display the differences between F_s and B_s estimates for stems within adjacent individual and clustered plant plots are provided in **Figure A-10.** Note that the absolute values of B_s(individual) and B_s(cluster) were used to calculate the difference dataset, B_s(difference), such that a positive difference in both **Figure A-10 A)** and **Figure A-10 B)** indicates that stem bending was more significant for the individual stem than for the stem within the cluster.

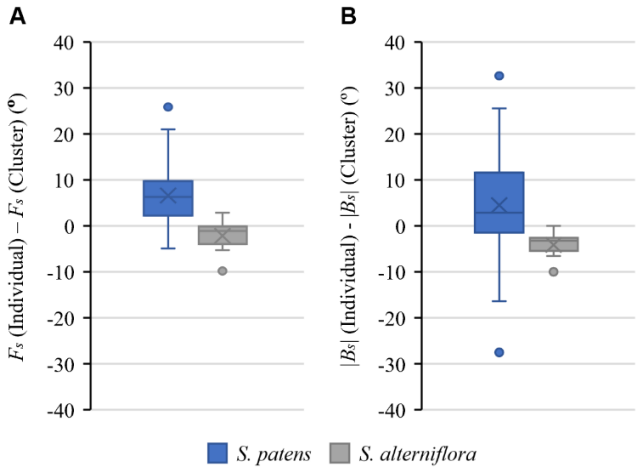

Figure A-10. Boxplots demonstrating the differences in bending angle response between tracked stems planted individually (i.e., in isolation) and those planted within a cluster of eight stems for S. patens (23 paired data sets) and S. alterniflora (11 paired datasets). A) Differences in significant forward bending angles (Fs) between paired tests, where differences were calculated as Fs (Individual) – Fs (Cluster). A positive difference indicates that the forward bending of individual plants was greater than the cluster. B) Differences in significant backward bending angles (Bs) between paired tests, where differences were calculated as |Bs| (Individual) – |Bs| (Cluster). As absolute values were used, a positive difference also indicates that the magnitude of backward bending for individual plants was greater than the cluster. The X on each boxplot indicates the mean of the dataset.

Table A-4. Results from stem bending analysis of S. patens and S. alterniflora. The significant wave heights and periods reported in this table were measured by wave gauges positioned in variable cross-shore locations on the slope, in line with the target plant stems.

Plant species	Stem incident $H_{s,i}$ (m)	Stem incident $T_{s,i}$ (s)	F_s (°)	$-B_s$ (°)	U_c (m/s)	U_{max} (m/s)	l/d (-)	Re	KC	Ca	L
S. patens	0.07-0.28	2.2-10.0	11-63	14-76	0.10-0.27	0.12-0.37	0.58-2.04	132-367	171-1925	1.4-11.0	1.3-14.9
S. alterniflora	0.03-0.10	2.0-10.4	4-32	4-32	0.08-0.22	0.11-0.28	0.60-2.52	339-1239	35-603	0.02-1.1	2.0-25.2

Stem deformation results were also compared with the non-dimensional parameters Re, KC, *Ca* and *L*. Peak forward horizontal velocities (in the direction of wave travel) were extracted from the velocity records measured by the ADVs positioned adjacent to the plant plots (z = 10 cm above the bed). The average of the highest one-third of these peak velocities (over the 20-wave cycle for which bending analysis was performed) was taken as the characteristic velocity ($U_c = U_{1/3}$) in the calculations of all non-dimensional parameters (Re, KC, *Ca* and *L*). The wave period $T_{s,i}$ was used for estimations of KC and *L*. The maximum peak forward velocity (U_{max}) for each wave test was also obtained from the velocity records but was not used for further calculations. The range of conditions for which bending analysis was conducted for each species is provided in **Table A-4**, along with a summary of the resulting magnitudes of stem extension. Stem bending was not plotted against the Froude number, as it is less relevant for characterization of flexible plant motion. For the experiments presented here, Fr = $O(10^{-1} - 10^{-2})$.

Error! Reference source not found. summarizes the results for stem bending angle tracking for all t ests. Submergence ratio was not found to have a significant influence on stem bending within the ranges investigated (*S. alterniflora:* 0.60 < *l/d* < 2.52, *S. patens*: 0.58 < *l/d* < 2.04) and

considering the data sample size. Emergent and submerged tests are distinguished in **Figure A-11 A)**, which compares stem bending with significant incident wave height ($H_{s,i}$), but are combined thereafter. The results of stem bending analysis were also plotted against *Ca* and *L*, the primary non-dimensional parameters that govern flexible stem motion (**Figure A-11 B), C), and D)**). Results from linear regression for the relationships plotted in **Figure A-11** are provided in **Table A-5**.

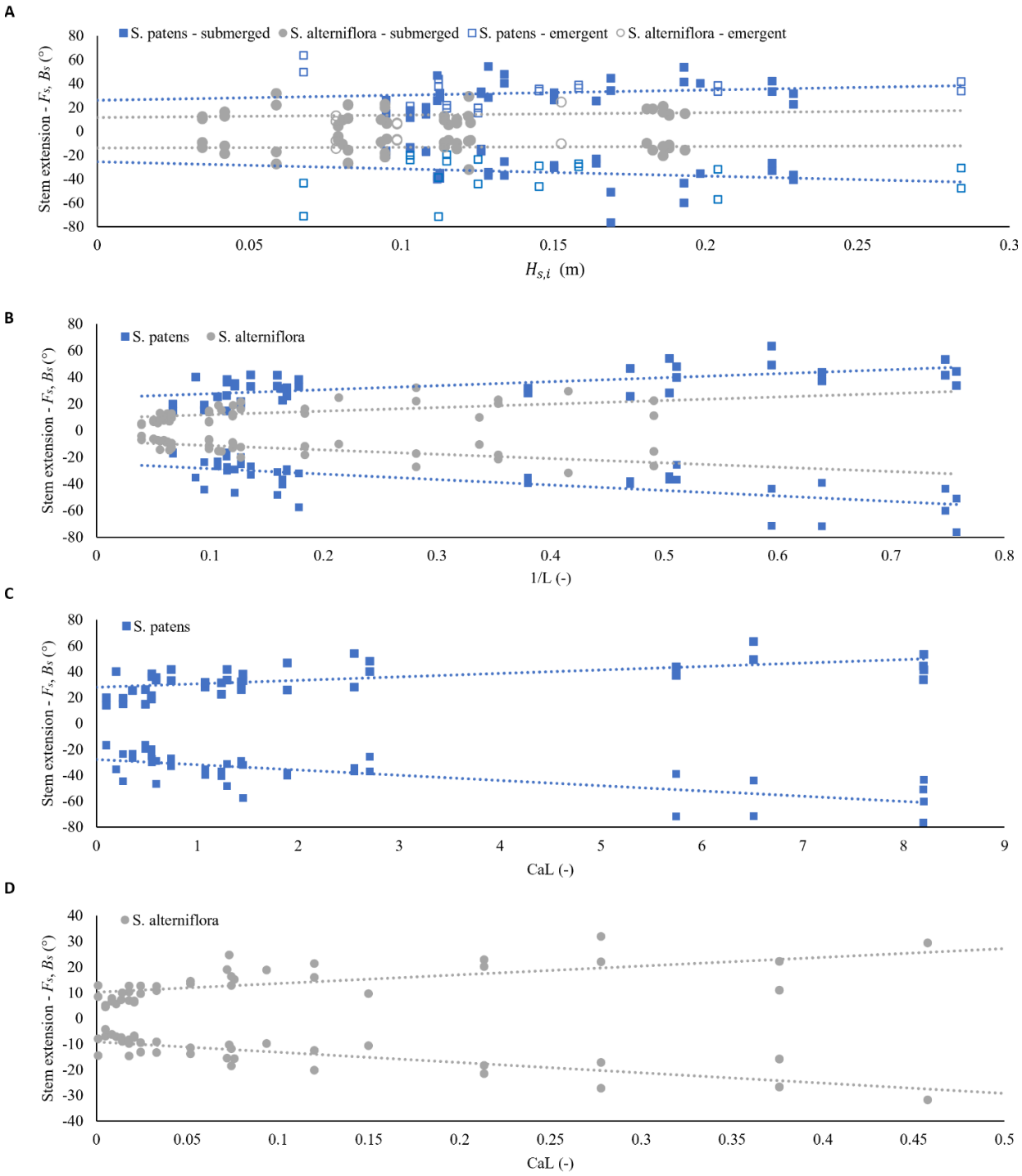

Figure A-11. Stem extension (bending angle) in the forward (Fs) and backward (Bs) directions as a function of A) Significant stem incident wave height for Spartina alterniflora and Spartina patens (Hs,i), B) 1/L for S. patens and S. alterniflora, C) CaL for S. patens and D) CaL for S. alterniflora. Bending angles are reported with an uncertainty of +/- 0.80 degrees associated with manual stem tracking analysis (95% confidence level).

Table A-5. Linear regression results for the relationships between stem extension and the various non-dimensional parameters shown in **Error! Reference source not found.**.

Figure	Plant Species	Forward	Backward
3-11 A) - F_s, B_s vs. $H_{s,i}$	*S. patens*	y = (43.56 ± 68.01)X + (25.9 ± 10.6), R^2 = 0.04	y = (-58.78 ± 88.27)X - (25.7 ± 13.7), R^2 = 0.04
	S. alterniflora	y = 20.63 ± 49.24)X + (11.6 ± 5.7), R^2 = 0.02	y = (6.05 ± 47.47)X - (14.1 ± 5.5), R^2 = 0.00
3-11 B) - F_s, B_s vs. 1/L	*S. patens*	y = (30.06 ± 12.18)X + (24.8 ± 4.7), R^2 = 0.39	y = (-41.11 ± 15.00)X - (24.4 ± 5.7), R^2 = 0.44
	S. alterniflora	y = (26.54 ± 12.45)X + (9.3 ± 2.8), R^2 = 0.33	y = (-32.32 ± 9.92)X - (8.0 ± 2.2), R^2 = 0.53
3-11 C) - F_s, B_s vs. CaL	*S. patens*	y = (2.67 ± 1.13)X + (27.9 ± 3.8), R^2 = 0.37	y = (-4.06 ± 1.27)X - (27.7 ± 4.3), R^2 = 0.52
3-11 D) - F_s, B_s vs. CaL	*S. alterniflora*	y = (33.98 ± 12.75)X + (9.8 ± 2.1), R^2 = 0.47	y = (-40.12 ± 9.42)X - (9.1 ± 1.6), R^2 = 0.63

A.5. Discussion

Few experimental studies have been conducted to date that investigate the dynamic response of live vegetation to wave forcing at prototype scale, limiting the development, optimization, and ultimately practical application of coastal nature-based solutions incorporating vegetation. The studies that have previously been performed with live vegetation have considered only a limited number of coastal marsh species, and often use intrusive methods of plant sourcing (i.e., excavation) (Paul & Kerpen 2021; Rupprecht et al. 2017; Moller et al. 2014) that may be damaging to the source environment or not feasible in regions with strict environmental regulations. In this study two live salt marsh species (S. alterniflora and S. patens) were planted in a large-scale outdoor flume and after three weeks of establishment, exposed to a wide range of irregular wave conditions throughout three weeks of testing. This experimental program allowed for novel collection of plant biophysical parameters for both species, particularly S. patens which, to the authors' knowledge, has never been studied in this context. In addition, measures of plant health throughout and after testing indicate that the plant husbandry techniques used herein were successful, providing significant support for future large-scale experiments with live vegetation. Stem dynamics were recorded using submerged cameras for comparison of plant motion response between species and under varying hydrodynamic conditions. A manual stem tracking algorithm was implemented to generate stem bending time series, and summary statistics for the reconfiguration response of S. patens and S. alterniflora to a range of hydrodynamic (wave and water depth) conditions.

A.5.1. Plant Physical Properties and Stem Deformation

There is significant natural variation in the physical and biomechanical properties of salt marsh plants, with different species exhibiting contrasting plant morphologies, stem widths, stem heights, and elastic moduli (Zhang & Nepf 2021; Zhu et al. 2020; Rupprecht et al. 2017; Puijalon et al. 2011). This diversity can contribute to distinct dynamic responses to wave forcing, with species adopting what has been classified as either "avoidance" or "resistance" strategies to withstand hydrodynamic forces (Schoutens et al. 2020; Vuik et al. 2018; Puijalon et al. 2011). Morphological adaptations that typically favor resistance to hydrodynamic stress include larger frontal areas (more leaves, wider and longer stems), and greater rigidity (Schoutens et al. 2020;

Puijalon et al. 2011). By contrast, avoidance species are characteristically more flexible with smaller frontal areas (shorter, thinner stems), and higher capacities to reconfigure (Schoutens et al. 2020; Puijalon et al. 2011). Hydrodynamic drag forces exerted on avoidance species are typically much lower. Consequently, they do not attenuate waves as effectively as resistance species, which experience higher drag forces and hence yield greater wave energy dissipation (Schoutens et al. 2020). However, resistant species are more susceptible to damage under increasingly severe hydrodynamic conditions (Rupprecht et al. 2017; Vuik et al. 2018). This was demonstrated by Rupprecht et al. (2017), where the more rigid *Elymus athericus* species exhibited irreversible stem deformation (folding or breakage) at lower orbital velocities than *Puccinellia maritima,* resulting in a rapid decline in flow resistance. At similar orbital velocities, extreme bending of the more flexible ("avoidance") *P. maritima* canopy was observed, but not breakage, thus the plants still provided some wave energy dissipation as well as erosion protection in the form of shielding (Rupprecht et al. 2017). It has since been proposed in Schoutens et al. (2020) that there are benefits to combining both types of species in coastal protection strategies, as the resistance species provide greater protection below their threshold for breakage, and avoidance species may provide prolonged protection with a greater chance of survival. In their study, Schoutens et al. (2020) demonstrated this through the complementary functioning of two *Scirpus* species: the presence of a band of *Scirpus tabernaemontani* ("avoidance" traits) placed at the marsh edge could dissipate enough wave energy to create a favorable environment for *Scirpus maritimus,* a plant with a greater frontal area that experiences higher drag forces ("resistance" traits).

Based on the measured plant parameters reported herein, *Spartina patens* presents traits typical of an "avoidance" strategy species with thinner, more flexible stems and leaves, whereas *S. alterniflora* exhibits more of a "resistance" strategy. This is further supported by the present observations of stem deformation under wave action. *Spartina patens* appeared to move more passively with the waves, with greater ranges of total stem extension ($25° < F_s - B_s < 121°$) than *S. alterniflora* ($9° < F_s - B_s < 61°$) under similar wave action. Drag forces were not directly measured in this study, however stem deformation observations indicate that drag on the *S. patens* stems would be lower due to reductions in frontal area over a large portion of the wave cycle, as well as low relative stem-flow motion. The inter-species contrast in response to wave action suggests that the two plants could be used to provide complementary flood and erosion control benefits within nature-based hazard management strategies, capitalizing on the cooperative feedback discussed in Schoutens et al. (2020). However, the ecological niche of each species must be considered when designing such strategies, as the optimal elevation zone for providing flood and erosion control may not align with the species' optimal elevation for growth. *S. alterniflora* typically dominates low marsh habitats as it thrives in anoxic environments (Wu et al. 2011; Augustin et al. 2009; Bertness 1991). Contrastingly, *S. patens* frequently colonizes mid- to high marsh habitats, due to its limited ability to oxygenate its rhizosphere in anoxic soils (Bertness 1991). Bertness (1991) investigated species zonation of *S. patens* and *S. alterniflora* in a New England salt marsh, experimenting with transplanting each species to different elevation

zones and observing growth and survival. Their study found that *S. patens* that were transplanted to low marsh environments either exhibited significantly stunted growth or died (Bertness 1991). They also found that *S. alterniflora* was restricted from high marsh zones, as a result of interspecies competition rather than physical constraints (Bertness 1991). Ultimately, more research is needed to investigate the feasibility of utilizing *S. patens* and *S. alterniflora* in complementary roles as part of nature-based coastal protection strategies, optimizing their placement for hydrodynamic resistance while balancing ecological constraints.

A.5.2. Factors Influencing Motion Response

The influence of planting configuration on live vegetation motion response was investigated in this study through pairwise comparison of bending angles observed between stems planted in isolation and within clusters (planting configurations are shown in Error! Reference source not f ound.). Statistical analyses indicated that there was a significant difference in forward stem bending between individual and clustered stem configurations for *S. patens*, and in backward stem bending between individual and clustered stems for *S. alterniflora*. Error! Reference source n ot found. demonstrates that there was overall more variability in stem bending between individual and clustered stem configurations for *S. patens*, particularly that the stems planted in isolation tend to bend more in both the forward and backward directions in comparison to their clustered counterpart. Some of the variability in bending between stems in isolation versus planted in clusters can be attributed to differences in plant properties between the two tracked stems. As demonstrated in **Table A-2**, there was more variability in plant properties within the sampled *S. alterniflora* stems, which could account for a large proportion of the variability in stem bending response between the individual and clustered stem observations. For *S. patens* the reduced bending observed for the stems planted in clusters is likely attributed to stem interactions, which could consequently obstruct deformation of adjacent stems or reduce hydrodynamic forces within the cluster. The morphology and flexibility of *S. patens* favors inter-plant interactions within clustered configurations, with many slender stems per plant versus the rigid single-stem morphology of *S. alterniflora*. Stem interactions were observed in the video footage of *S. patens* clusters, but not in the *S. alterniflora* clusters.

The magnitude of stem bending was generally found to increase with wave height for both *S. patens* and *S. alterniflora* (Error! Reference source not found.**A)**). However, wave height alone w as not an effective relative predictor of stem extension. Stem dynamics demonstrated a strong dependence on wave period with longer period waves consistently generating larger bending angles in the forward and backward direction for the same wave height, across both species. This aligns with existing theory that suggests stem motion is dependent on wave excursion, which is a function of both wave period and wave amplitude (*A*, **Eq. 3-6**) (Luhar & Nepf 2016).

Luhar & Nepf (2016) have proposed the parameter *L* to characterize stem reconfiguration in consideration of the ratio of stem length to wave excursion. For small wave excursions ($L > 1$), the linear stem bending angle (θ) is proportional to the ratio of wave excursion to blade length, $\theta \sim A_w/l$ (or $1/L$) (Lei & Nepf 2019). Error! Reference source not found. **B**) demonstrates that this a

pproximation holds well for the blade length ratio range investigated in this study ($L > 1.3$). As L approaches 1, theoretically a transition from swaying to whip-like stem motion is expected to occur (Rupprecht et al. 2017; Luhar & Nepf 2016). The experimental results of Rupprecht et al. (2017) indicated that this motion transition may occur at a range of L values, dependent on plant properties, with the more rigid *P. maritima* first exhibiting whip-like behavior at $L = 0.6$, and the more flexible *E. athericus* at $L = 1.8$ in their study. The symmetry of forward and backward bending angles was used to deduce motion type (swaying vs. whip-like) in the present study, with asymmetry that favors forward bending indicating whip-like motion. Ratios of forward to backward stem extension were compared against the hydrodynamic setting for all tests, however consistently remained close to unity for both species. This indicates that the hydrodynamic forcing was not sufficient to induce whip-like motion in any of tests presented herein, potentially a result of the limited number of tests conducted with L near or less than 1.

To incorporate the effects of stem flexibility, stem bending was also plotted against the combined non-dimensional parameter, *CaL*. A value of $Ca < 1$ indicates that the restoring forces due to plant stiffness exceed hydrodynamic forcing, and the plant should remain primarily upright. As values of *Ca* increase to $Ca > 1$, hydrodynamic forces overpower the restoring forces, and initiation of stem bending is expected. Above this threshold for motion, stem bending can be expected to intensify with increasing hydrodynamic forces (increasing *Ca*), however bending will still be limited by the wave excursion (Gosselin 2019). Using the combined parameter *CaL*, the influence of the magnitude of hydrodynamic forces and wave excursion with respect to stem reconfiguration can be examined simultaneously. Error! Reference source not f ound. **C)** demonstrates this relationship for *S. patens*, with $Ca > 1$ in all cases, and bending angles $\propto CaL$.

S. alterniflora still showed a strong correlation between stem bending and *CaL* (Error! Reference s ource not found. **D)**) despite being primarily in the range of $Ca < 1$. The flexural rigidity value used to calculate *Ca* for *S. alterniflora* was based on an average of the harvested stem samples that underwent biomechanical testing. Variations in flexural rigidity were observed between the sampled stems of *S. alterniflora* ($EI_{S.alt} = 0.051 +/- 0.015$ Nm^2, **Table A-2**), indicating that the range of *Ca* is likely wider than reported in **Table A-4,** and thus more of the tests may fall in the range of $Ca > 1$, where increased stem bending is expected. Furthermore, the *S. alterniflora* stems exhibited a high degree of stem tapering, which is expected to be associated with decreasing flexural rigidity along the stem's length. Considering this, the *Ca* values reported for *S. alterniflora* may be an underestimation for upper sections of the tracked stems, where most deformation occurred. Furthermore, Zhang & Nepf (2022) demonstrate that the drag on *S. alterniflora* leaves may contribute to a large portion of the overall drag forces acting on the plant, and that stem motion can be enhanced by leaf drag (Zhang & Nepf 2022; Zhang & Nepf 2021). Consequently, Zhang & Nepf (2022) propose the use of a modified stem Cauchy number that incorporates an additional term inclusive of drag forces acting on the leaves. The neglect of these forces in the *Ca* estimates presented herein could contribute to the discrepancies between the

expected theoretical thresholds for stem motion ($Ca > 1$), and the degree of stem bending observed for *S. alterniflora* in this study ($Ca < 1$). Ultimately, testing under a wider range of hydrodynamic conditions could elucidate if the reported relationship between bending and *CaL* for *S. alterniflora* changes significantly as *Ca* increases further above 1, or as more complex plant biomechanics (i.e., height-varying properties) and morphologies (leaves) are considered.

A.5.3. Stem Deformation and Wave Attenuation

This study represents a first step towards addressing the logistical challenges and viability of outdoor wave experimental programs with live vegetation, and as such, a full marsh canopy was not planted. Consequently, wave attenuation was not directly measured, and instead this study focused on observations of individual plant motion as a means to infer wave attenuation capacity based on drag force theory and previous experimental studies. Considering the formulation of drag forces acting on plant stems (**Eq. 3-4**), wave energy dissipation is expected to be proportional to plant frontal area, and decrease with increasing plant deflection (i.e., extreme bending in phase with wave action) (Wang et al. 2021; Lei & Nepf 2019; Paul et al. 2016). Thus, it may be possible to correlate the magnitude of stem deformation to relative wave attenuation capacity.

Based upon measures of stem deformation, it is expected that drag forces on *S. alterniflora* plants would be greater than on *S. patens* under comparable hydrodynamic conditions and canopy densities, and thus *S. alterniflora* could provide greater wave attenuation. However, it should be noted that the attenuation capacity of the two species could be comparable given a high enough density of *S. patens* stems. This was demonstrated in Bouma et al. (2010), who found that wave attenuation was remarkably similar for *S. anglica* and *P. maritima* when compared per unit biomass, despite significant differences in plant morphology and flexibility, similar to that of *S. alterniflora* versus *S. patens.*

Wave period was also found to have a significant influence on the degree of stem bending, with the largest stem excursions recorded for both *S. patens* and *S. alterniflora* attributed to the long-period waves ($T_{s,i} > 9$ s). This observed influence of wave period is particularly significant as previous physical modeling studies have yielded inconsistent results with respect to the influence of wave period on wave attenuation by vegetation surrogates (Maza et al. 2019; Anderson & Smith 2014). Contrastingly, reductions in frontal area due to extreme bending under longer period waves, as observed in this study, indicate that for flexible vegetation wave attenuation may be limited by wave period, or more accurately, large wave orbital excursions. Overall, this highlights the importance of using surrogates with realistic stiffness characteristics or live vegetation when using physical modeling techniques to assess the performance of vegetation as part of nature-based solutions, ensuring effects that are linked to plant biomechanical properties are captured.

Wave attenuation by flexible vegetation may also rapidly decrease as material thresholds for deformation are exceeded. Irreversible stem deformation (folding or severing) causes a rapid

decrease in wave attenuation due to a reduction in plant height (Rupprecht et al. 2017; Vuik et al. 2018), thus, there is an interest in determining these species-specific thresholds for damage. This has previously been investigated by Rupprecht et al. (2017) and Vuik et al. (2018), for *Puccinellia maritima, Elymus athericus, Spartina anglica* and *Scirpus maritimus*. The critical velocity thresholds that result in stem breakage for these species (U_{crit}), as determined by Rupprecht et al. (2017) and Vuik et al. (2018), are: $U_{crit} > 0.90$ m/s (*P. maritima*), $U_{crit} = 0.42$ m/s (*E. athericus*) (Rupprecht et al. 2017), $U_{crit} = 0.86$ +/- 0.28 m/s (*S. anglica*), and $U_{crit} = 0.59$ +/- 0.22 m/s (*S. maritimus*) (Vuik et al. 2018). The critical velocities determined by Rupprecht et al. (2017) were calculated according to linear wave theory, corresponding to a height 15-cm above the bed. Only regular, non-breaking waves were considered in their study (Rupprecht et al. 2017). The values presented by Vuik et al. (2018) were determined from a stem breakage numerical model, that utilized linear wave theory for predictions of critical orbital velocity. No stem folding or breakage was observed during the present experiments, indicating that thresholds for irreversible deformation exceed the maximum velocity conditions presented in **Table A-4.** This yields $U_{crit} > 0.37$ m/s for *S. patens* and $U_{crit} > 0.28$ m/s for *S. alterniflora.* Future experiments with *S. patens* and *S. alterniflora* should attempt to identify the exact thresholds through experimental programs with more extreme waves.

A.5.4. Stem Tracking Methodologies

Automated stem tracking was initially attempted using the Matlab-based tool *CytoSpectre* (Kartasalo et al. 2015). This tool was previously developed for quantification of orientation and size distributions of cell structures in microscopy images (Kartasalo et al. 2015). The *CytoSpectre* tool was configured to load in an image frame, compute the power spectral density (PSD) using Welch's method (also referred to as the Weighted Overlapped Segment Averaging method), convert the PSD to polar coordinates, and output the complete orientation distribution of identified spectral components (Kartasalo et al. 2015). Peaks of the spectral distribution (i.e., dominant stem orientation angles) were then identified for each frame using *findpeaks* and stored for post-processing. Unfortunately, multiple stems of different orientation (i.e., in the case of the *S. patens*), or the presence of prominent angled blades (*S. alterniflora*) frequently interfered with the analysis, and the tool was unable to consistently identify the peak from the spectral distribution that corresponded to the dominant stem orientation. As a result, stem tracking analysis was performed manually for the experiments presented herein. However, with further development, spectral analysis tools such as *Cytospectre* could yield effective automation of stem bending angle tracking, particularly within vegetation canopies where it is difficult to distinguish individual stems.

A.6. Conclusions

This paper presents the findings of a large-scale experimental program that investigated the bending response of live salt marsh vegetation to irregular waves. While the data presented in this study, based on individual plants and plant groupings, is not sufficient to derive quantitative relationships for wave attenuation by marsh vegetation at meadow-scale, it directly supports the

development of these relationships by providing a validation dataset for future physical and numerical modeling. This study contributes novel quantitative knowledge of plant physical characteristics for two salt marsh species native to the Canadian coast, *S. patens* and *S. alterniflora*, and lays the groundwork for future large-scale experimental programs with live vegetation. The results demonstrate that plant morphology and biomechanical differences between *S. patens* and *S. alterniflora* have an influence on the magnitude of stem deformation under wave action. The more flexible *S. patens* plants consistently exhibited greater stem bending than the more rigid *S. alterniflora* under comparable incident wave conditions (0.03 m < $H_{s,i}$ < 0.28 m, $T_{s,i}$ ≈ 2 and 10 s). Neither *S. alterniflora* or *S. patens* exhibited irreversible stem deformation (folding or breakage) during the experiments conducted, indicating that the species are resilient under hydrodynamic forces up to, at minimum, U_c = 0.37 m/s for *S. patens* and U_c = 0.28 m/s for *S. alterniflora*. The measured plant physical properties, combined with observations of dynamic reconfiguration, indicate that *S. alterniflora* adopts more of a "resistance" strategy when faced with hydrodynamic stress, versus the "avoidance" strategy of *S. patens.* These distinct behaviors suggest that the two species could work together effectively in nature-based coastal protection strategies, capitalizing simultaneously on the attenuative capacity associated with resistance species and the resilience of avoidance species (Schoutens et al. 2020; Rupprecht et al. 2017; Puijalon et al. 2011). It is recommended that future studies focus on the optimal way of combining these two species, particularly considering their unique ecological requirements.